

Dissertation zur Erlangung des Doktorgrades
der Fakultät für Biologie
der Ludwig-Maximilians-Universität München

**Engineered extracellular vesicles
for immunotherapy of
chronic lymphocytic leukemia (CLL)**



Kathrin Christina Gärtner

2016

Eidesstattliche Erklärung

Ich versichere hiermit, dass die vorliegende Arbeit mit dem Titel

**„Engineered extracellular vesicles for immunotherapy of
chronic lymphocytic leukemia (CLL)“**

von mir eigenständig und ohne unerlaubte Hilfe angefertigt wurde, und ich mich dabei nur der ausdrücklich bezeichneten Quellen und Hilfsmittel bedient habe. Die Arbeit wurde weder in der jetzigen noch in einer abgewandelten Form einer anderen Prüfungskommission vorgelegt.

München, den 15.11.2016

Kathrin Gärtner

Dissertation eingereicht am 15. November 2016.

1. Gutachter: PD Dr. Josef Mautner

2. Gutachter: Prof. Dr. Rainer Glaß

Tag der mündlichen Prüfung: 19. Juni 2017

„So eine Arbeit wird eigentlich nie fertig, man muss sie für fertig erklären, wenn man nach Zeit und Umständen das Möglichste getan hat.“

Johann Wolfgang von Goethe

List of contents

1 Abstract	1
1.1 Zusammenfassung	2
2 Introduction	4
2.1 Extracellular vesicles	4
2.1.1 Definition and biogenesis	4
2.1.2 The biochemical composition of EVs	5
2.1.3 The methodology of EV isolation and characterization	6
2.1.4 The biological functions of EVs	8
2.2 EVs in the immune system	8
2.2.1 EVs are a source of antigens	9
2.2.2 EVs as suppressors of immune responses	10
2.2.3 EVs and disease	10
2.3 EV-based therapeutics	11
2.4 Chronic lymphocytic leukemia (CLL)	14
2.4.1 Phenotype, origin and diagnosis	14
2.5 Immunological situation in CLL	15
2.5.1 CLL and infection	17
2.5.2 Cytomegalovirus infection influences the T-cell repertoire in CLL	17
2.6 Treatment of CLL	18
2.6.1 CD40L-based therapy in CLL	19
2.7 Aim of the current study	20
3 Material	21
3.1 Eukaryotic cells	21
3.2 Mice	22
3.3 Viruses	22
3.4 Cell culture	22
3.4.1 Media and solutions	22
3.4.2 Consumables	23
3.4.3 Equipment	23
3.5 Antibodies	24
3.5.1 Antibodies for flow cytometry, electron microscopy and NTA	24
3.5.2 Beads for flow cytometry and NTA	25
3.5.3 Antibodies for dot blot, Western blot and ELISA	25
3.6 Kits	26
3.7 Enzymes	26
3.8 Oligonucleotides	277
3.9 Plasmids	27
3.10 Peptides, peptide mixes and recombinant proteins	27
3.11 General equipment	28
3.12 General consumables	28
3.13 Chemicals and reagents	29
3.14 Buffers and solutions	30
3.15 Software	31

4	Methods	32
4.1	Cell culture	32
4.1.1	Cultivation of stable cell lines	32
4.1.2	Cultivation of T-cell clones	32
4.1.3	Freezing and thawing of cells	33
4.1.4	Transfection of HEK293 cells	33
4.1.5	Lentivirus transduction of BJAB cells	34
4.1.6	Electroporation of BJAB cells	34
4.1.7	Isolation of PBMCs from CLL blood samples by Ficoll gradient	35
4.1.8	Isolation of primary B lymphocytes from human adenoids	35
4.1.9	Detection of EBV in primary B cells by PCR	35
4.1.10	Virus production and titration	36
4.1.11	Limiting dilution assay and MTT assay	37
4.2	Antibody staining and analysis of cells by flow cytometry	37
4.2.1	Staining of cells with CFSE	38
4.3	Purification and characterization of EVs	38
4.3.1	Generation of EV-depleted medium	38
4.3.2	Isolation of EVs by serial centrifugation and iodixanol density gradient	38
4.3.3	Determining the buoyant density of each fraction	39
4.3.4	Electron microscopy analysis of EVs	39
4.3.5	Nanoparticle tracking analysis (NTA)	40
4.3.6	Flow cytometry analysis of EVs bound to beads	40
4.4	Immunoblotting	40
4.4.1	Preparation of cell lysates and EVs for Western blotting	40
4.4.2	Bis-Tris PAGE and protein transfer	41
4.4.3	Protein detection	42
4.4.4	Staining of acrylamide gels with Coomassie protein dye	42
4.4.5	Dot blot	42
4.5	Labeling of EVs with PKH26 membrane dye	42
4.6	Isolation and analysis of vesicular and cellular RNA	43
4.6.1	RNA quality assessment	44
4.6.2	Reverse Transcription	44
4.7	T-cell assays	44
4.7.1	ELISA	44
4.7.2	ELISPOT	45
4.8	CLL <i>in vivo</i> model	46
5	Results	47
5.1	Generation of extracellular vesicles (EVs) in HEK293 cells	47
5.2	Stimulatory effect of EV-associated CD40L on B lymphocytes	49
5.2.1	CD40L+ EVs enhance EBV-mediated transformation of human B lymphocytes	51
5.3	Engineered EVs for immunotherapy of chronic lymphocytic leukemia	55
5.3.1	EV-associated gp350 confers tropism for B lymphocytes	55
5.3.2	Interaction of engineered EVs with CLL cells	57
5.3.3	EV-mediated delivery of functional <i>Cre</i> mRNA to B lymphocytes	61
5.3.4	CD40L+ EVs protect CLL cells transiently from undergoing spontaneous apoptosis <i>in vitro</i>	66
5.3.5	CD40L+ EVs induce upregulation of immune accessory molecules	68
5.3.6	CLL cells stimulated with CD40L+ EVs become efficient APCs	71
5.4	Redirection of CMV-specific immunity towards CLL cells	73
5.4.1	EV-associated pp65 stimulates CMV-specific T cells	73
5.4.2	EV-associated pp65 stimulates autologous pp65-specific T cells in CLL	77

5.4.3	Enrichment of CLL-derived T-cell populations by EV stimulation	78
5.5	Development of an <i>in vivo</i> model to evaluate an EV-based immunotherapy for CLL	82
5.5.1	Humoral immune responses against mCD40L+/gp350+ & mCD40L+/pp65+ EVs	83
5.5.2	Engraftment and proliferation of murine CLL cells	84
5.5.3	Analysis of immune cell subsets in murine splenocytes	85
5.6	Characterization of EVs by Nanoparticle Tracking Analysis (NTA)	88
5.6.1	Evaluation of NTA performance	89
5.6.2	Detection of fluorescent PS beads	95
5.6.3	Characterization of HEK293-derived EVs by NTA	97
5.6.4	Fluorescent labeling of CD40L+ EVs	98
6	Discussion	102
6.1.	Isolation and characterization of EVs	102
6.1.1	NTA technology: A reliable method for EV characterization?	104
6.2	EV-based therapeutics	105
6.2.1	Engineered EVs for immunotherapy of CLL	107
6.2.2	Activation of CMV-specific T cells as effector cells in CLL	108
6.2.3	Preliminary <i>in vivo</i> evaluation of an EV-based immunotherapy for CLL	110
6.3	Concluding remarks and outlook	112
7	References	113
8	Abbreviations	125
9	Presentations	126
10	Acknowledgment	127

1 Abstract

Extracellular vesicles (EV) are membrane-enclosed nanoparticles and important mediators of cell-cell communication. They are released by all kinds of cells and participate in both physiological and pathological processes by transferring functional proteins and nucleic acids to recipient cells. Over the last decade EVs have, therefore, gained increasing attention as potential gene vectors, vaccine candidate, or immunotherapeutic agents in various clinical applications.

Despite therapeutic progress chronic lymphocytic leukemia (CLL) continues to be an incurable disease that is characterized by progressive accumulation of malignant B cells that possess a poor antigen-presenting capacity. However, the dysfunction of malignant CLL cells can be restored by CD40 stimulation via its ligand, CD40L. Interestingly, although CLL patients suffer from progressive general immunodeficiency, immunity against the widespread human herpesvirus 5, also known as Cytomegalovirus (CMV), is retained.

The present work aimed at the generation of engineered EVs in order to transfer functional CD40L together with immunodominant herpesviral proteins to CLL cells, thus specifically redirecting the strong preexisting CMV-specific immunity in CLL patients to these cells. Engineered EVs were successfully isolated from cell culture supernatants of HEK293 cells overexpressing the proteins of interest by differential centrifugation and density gradient fractionation. EV preparations were characterized by Western blot and electron microscopy. Since gold standards for EV characterization are still lacking, the suitability of Nanoparticle Tracking Analysis (NTA), a new technology for enumeration and sizing of EVs, was furthermore critically evaluated.

CD40L, the Epstein-Barr virus (EBV) glycoprotein gp350 and the CMV protein pp65 were efficiently incorporated into HEK293-derived EVs and retained their functionality. Gp350 conferred B-cell tropism to EVs. EV-associated CD40L reactivated the antigen-presenting capacity by inducing expression of costimulatory surface molecules, not only in directly bound CLL cells but also in malignant bystander cells. CLL cells treated with CD40L+/gp350+/pp65+ EVs induced activation of pp65-specific T cells and subsequently became targets for autologous cytolytic T-cell responses. Furthermore, a

novel murine model system was developed and represents a first proof-of-concept for the *in vivo* evaluation of an EV-based CLL immunotherapy.

In essence, the present study showed that engineered EVs are promising tools for the specific transfer of functional proteins to recipient cells and trigger HLA-independent immune responses. This may facilitate the development of new immunotherapeutic strategies for treatment of CLL and other B-cell malignancies.

1.1 Zusammenfassung

Extrazelluläre Vesikel (EV) sind membranumschlossene Nanopartikel und dienen der zellulären Kommunikation. Sie werden von allen lebenden Zellen in den Extrazellulärraum abgegeben und sind sowohl an physiologischen, als auch pathologischen Prozessen beteiligt, indem sie funktionelle Proteine und Nukleinsäuren an Empfängerzellen übertragen. Seit einigen Jahren besteht daher großes wissenschaftliches Interesse an der genauen Erforschung von EVs und ihrer Einsatzmöglichkeiten als Genvektoren, Impfstoff-Kandidaten oder als Werkzeuge zur Entwicklung neuer immuntherapeutischer Konzepte.

Trotz therapeutischer Fortschritte bleibt die chronisch-lymphatische Leukämie (CLL) eine unheilbare Erkrankung, die sich durch eine starke Vermehrung maligner B-Zellen auszeichnet. Diese Zellen weisen eine stark geschwächte Fähigkeit zur Antigenpräsentation auf, die jedoch durch eine Simulation von zellulärem CD40 mit seinem Liganden, CD40L, aufgehoben werden kann. Obwohl CLL Patienten unter einer ausgeprägten allgemeinen Immunschwäche leiden, ist die Immunität gegen das weitverbreitete Humane Herpesvirus 5, auch bekannt als Zytomegalovirus (CMV), in CLL-Patienten interessanterweise weitestgehend intakt.

Das Ziel der vorliegenden Arbeit war die Generierung modifizierter EV, um funktionellen CD40L, sowie immundominante herpesvirale Proteine an CLL-Zellen zu transportieren. Dadurch sollte die bereits vorhandene Immunität gegen CMV auf CLL-Zellen dirigiert werden.

EV wurden erfolgreich durch differentielle Zentrifugation und Dichtegradient aus HEK293-Zellkulturüberständen isoliert. Aufgereinigte EV wurden darüber hinaus per Immunoblot und Elektronenmikroskopie charakterisiert. Da es derzeit noch an

standardisierten Methoden zur EV-Charakterisierung mangelt, wurde außerdem die Tauglichkeit einer neuen Technologie, genannt NTA („Nanoparticle Tracking Analysis“), näher untersucht. CD40L, das EBV-Glykoprotein gp350, sowie das CMV-Protein pp65 wurden erfolgreich in modifizierte HEK293 EV eingebaut und behielten ihre Funktionalität. Gp350 verlieh einen zellulären Tropismus und erhöhte die Bindungskapazität von EVs an CD21-exprimierende CLL-Zellen erheblich. EV-assoziiertes CD40L induzierte die Expression kostimulatorischer Moleküle auf der Zelloberfläche und verbesserte so die Fähigkeit Antigene zu präsentieren, nicht nur in direkt gebundenen CLL Zellen, sondern auch in benachbarten Zellen. CLL-Zellen, die mit CD40L+/gp350+/pp65+ EV inkubiert worden waren, aktivierten schließlich pp65-spezifische T-Zellen und wurden so zum Ziel autologer zytotoxischer T-Zellantworten. Darüber hinaus wurde im Rahmen dieser Arbeit ein neues Tiermodell entwickelt, welches in Zukunft die in-vivo-Analyse einer EV-basierten CLL-Immuntherapie ermöglichen könnte.

Zusammenfassend konnte die vorliegende Arbeit demonstrieren, dass modifizierte EV vielversprechende Werkzeuge sind, um intakte Proteine spezifisch an Empfängerzellen zu transportieren und HLA-unabhängige Immunantworten auszulösen. Dies könnte die Entwicklung neuer immuntherapeutischer Ansätze für die Behandlung von CLL und anderer B-Zell-Lymphome erleichtern.

2 Introduction

2.1 Extracellular vesicles

2.1.1 Definition and biogenesis

Extracellular vesicles (EVs) are membrane-enclosed vesicles released by all kinds of cells ranging from prokaryotes to higher eukaryotes and plants. EVs are widely distributed and are found in many body fluids, such as blood, urine, breast milk, saliva, semen or ascites, and also in the extracellular space of cells in tissue culture [1–4].

Three main types of vesicles differing in their size and biogenesis pathway can be distinguished: apoptotic bodies (0.5 – 3 μm) released by cells undergoing apoptosis, microvesicles (100 nm – 1 μm), which directly bud from the plasma membrane, and exosomes (50 – 150 nm), which are generated in cellular endosomal compartments and are released upon fusion of multivesicular bodies (MVBs) with the cell membrane (Fig. 2.1). Due to the variety of vesicles released from different cell types, also other terms for EVs referring to their size (e.g. nanoparticles, microparticles) or their origin (e.g. ectosomes, oncosomes, virosomes, outer membrane vesicles) have spread through the literature and are still causing confusion [3,5]. Until now, there is no technology available that allows separation and purification of EV subpopulations. It is therefore recommended to use the collective term ‘extracellular vesicles’, which comprises all types of cell-derived vesicles.

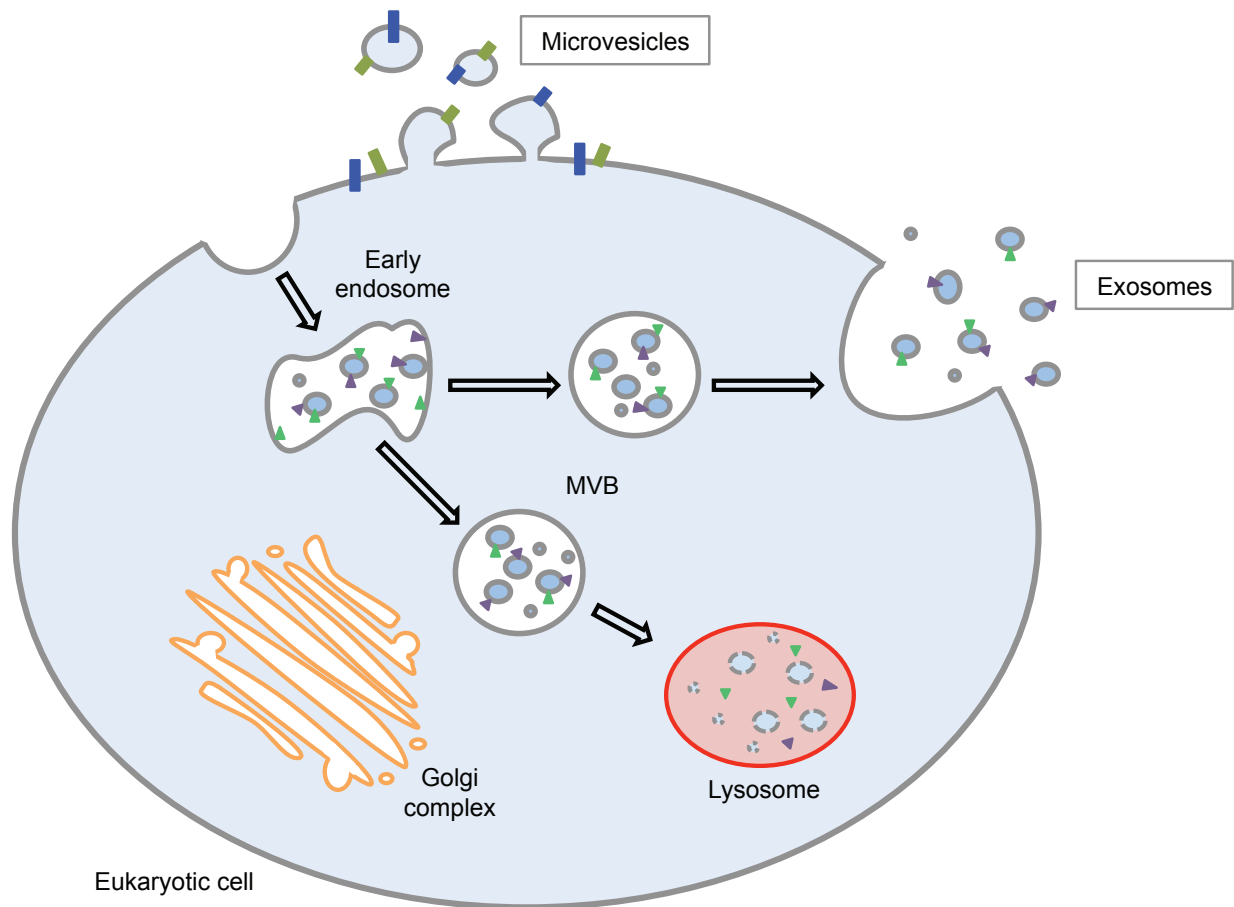


Fig. 2.1: Biogenesis of extracellular vesicles in eukaryotic cells

Microvesicles are released by direct budding from the plasma membrane, whereas exosomes are formed by budding into early endosomes and multi-vesicular bodies (MVBs). MVBs either direct their content for lysosomal degradation or release it into the extracellular space by fusion with the plasma membrane. Triangles and rectangles represent membrane-associated and transmembrane proteins. (*adapted from M. Colombo et al., 2014 [3]*)

2.1.2 The biochemical composition of EVs

At the present day it is common knowledge that the features of EVs are very diverse; their function and composition is directly linked to the type and physiological state of the parental cell. EVs contain many different proteins, lipids and nucleic acids. Especially the protein content has been extensively investigated, initially by classical antibody-based techniques (immunoelectron microscopy, immunoblotting), and later by large-scale proteomic analysis [3,6,7]. These investigations revealed that EVs carry on the one hand a set of conserved proteins found in most cell types, such as tetraspanins (e.g. CD63, CD9, CD81), integrins, cytoplasmic enzymes, cytokines and proteins involved in

EV biogenesis (e.g. actin, tubulin), while lacking proteins from the cell nucleus, endoplasmic reticulum or mitochondria [7–9]. Due to their endosomal origin, exosomes contain endosome-associated proteins (e.g. annexins, flotillin, Rab GTPases, SNAREs) and proteins contributing to the formation of MVBs (e.g. Alix, TSG101) [9–12]. Furthermore, also proteins involved in cell signaling pathways, as for instance interleukins and Wnt/ β -catenin or Notch signaling proteins have been detected in EVs [13–16]. On the other hand EVs also harbor cell type-specific proteins and thus mimic some biological functions of the producer cell. EVs secreted from dendritic cells (DCs) for example have been shown to express MHC molecules and costimulatory molecules, such as CD54, CD80 and CD86, and as a result have antigen-presenting features [6,7,17]. Following this, it has been postulated for the first time in 2001 that EVs secreted by tumor cells are a source of tumor-associated antigens [18].

The lipid composition of EVs has been poorly investigated on a molecular level, however several studies reported differences between the lipid composition of EVs and producer cells. EV membranes are often enriched in cholesterol, glycosphingolipids, sphingomyelin and phosphatidylserine, supporting the hypothesis that lipids are selectively sorted into EVs [19–21]. EVs mediate trafficking of lipids, fatty acids, lipid binding proteins and lipid related enzymes between cells and are thus able to interfere with the lipid metabolism of a target cell [22].

A major breakthrough in the EV research field was the discovery that EVs also harbor nucleic acids including DNA, mRNA, ribosomal RNA and non-coding RNAs like microRNAs (miRNAs) [23]. EVs transport these nucleic acids to recipient cells, where they are translated into functional protein or interact with their target sequence. As with proteins or lipids, it remains unclear how the loading of nucleic acids into EVs is regulated. It is assumed that EV biogenesis and cargo loading is not a random process, but instead regulated by sorting mechanisms, which are currently not understood. Also cellular stress, such as hypoxia, inflammation, hyperglycemia or infection, results in augmented release of EVs or influences their composition [24,25].

2.1.3 The methodology of EV isolation and characterization

EVs can be isolated from cell culture supernatants and a variety of biofluids, but due to their small size purification remains challenging. Standardization of EV isolation techniques is still lacking and improving established techniques is a major goal in the EV

field. Described methods comprise differential centrifugation steps and sedimentation of small vesicles by ultracentrifugation at 100,000 x g, filtration, density gradient fractionation using sucrose or iodixanol, size exclusion chromatography and immunoprecipitation [26–30]. Usually a combination of these methods is used in order to enrich EVs and at the same time eliminate debris, soluble proteins and larger vesicles. All EV isolation techniques depend on certain EV properties, such as floatation density or size. However, no method currently exists that allows the purification of distinct EV sub-populations, and therefore their individual origins, compositions and functions have not yet been unambiguously elucidated. Consequently, purified EVs usually represent a heterogeneous mixture of vesicles. Furthermore, different methods might enrich EV sub-populations with different properties [31]. Also commercially available kits for timesaving EV isolation have been developed, but since they usually rely on polymer-based precipitation, they do not separate EVs from macromolecular protein aggregates, thus need to be used with caution [32]. As a result, comparison of published results that do not use identical isolation procedures is questionable. Standard methods are still urgently needed, especially for the production of pure clinical grade EVs.

Just as EV purification, also characterization of isolated EVs requires a combination of different methods to determine their morphological, biochemical and functional features [30]. Characterization of EVs by transmission electron microscopy (TEM) became indispensable and is still widely used, because it allows direct inspection of the size and morphology of nanoparticles. Also analysis of EV content by Western blot is performed routinely to examine the presence of different EV protein markers.

A novel technique known as Nanoparticle Tracking Analysis (NTA) was invented to measure size distribution and concentration of nanoparticles [33,34]. NTA is a light-scattering method that tracks the movement of nanoparticles undergoing Brownian motion and calculates their size using statistical methods. Although NTA has been gathering lots of attention in the last years and was promoted as a ‘gold standard’ for characterization of EVs, the technology clearly has its limitations. E.g. it is not capable to discriminate between EVs and aggregated proteins of similar size. Vesicles larger than 300 nm can, furthermore, be analyzed by flow cytometry. One advantage of this technique is that it enables detection of specific surface markers present on cells or large vesicles by fluorescent labeling [35]. Detection of EVs smaller than 300 nm remains

challenging, but novel high-sensitive cytometers, optimized settings and specific labeling of EVs with lipid dyes currently hold a lot of promise [36–38].

2.1.4 The biological functions of EVs

Already since the late 1960s it is known that cell-derived membrane vesicles are present in body fluids, solid tissues or cell culture supernatants [39–41]. At that time these vesicles were considered to be cellular ‘garbage bags’, which help a cell to discard unnecessary protein. Consequently, EVs did not capture much attention at that time. The biogenesis of exosomes in endosomal compartments and MVBs was then discovered in 1983 [42]. A few years later, during investigations on reticulocyte maturation, Rose Johnstone and colleagues for the first time succeeded to isolate nanoparticles from cell culture supernatants of sheep reticulocytes and, furthermore, showed that these vesicles contained active enzymes [43]. It still took more than ten years to finally discover that EVs actually hold important biological functions and mediate communication between proximal and distal cells. This discovery was based on the findings that DCs and B-lymphocytes secrete endosomal vesicles, which harbor immunogenic activities [44,45]. Today the features of EVs are still not fully understood, but it is beyond dispute that they hold an important, and for a long time underestimated, role in intercellular communication. Interaction between EVs and target cells is diverse and includes a various set of mechanisms. EVs bind to the cell surface via cell surface receptors and induce intracellular signaling pathways, directly fuse with cell membranes or are engulfed by endocytotic processes, such as phagocytosis, clathrin-coated pits, pinocytosis, macropinocytosis or displacement (extrusion) through cell channels [46–49]. In either case, EVs transfer their biological content, which includes proteins, active enzymes, lipids and nucleic acids, and eventually modify the physiological state of the recipient cell.

2.2 EVs in the immune system

In 1996 Graça Raposo and colleagues published the first evidence that EVs are involved in immune regulation. They demonstrated that EVs secreted by Epstein-Barr virus (EBV)-infected cells stimulate CD4⁺ T-cell responses in an antigen-specific manner [44].

Subsequently these novel findings were expanded by demonstrating that EVs secreted by DCs have antigen-presenting capacity. Furthermore pulsing of these vesicles with tumor-derived peptides activated specific CD8⁺ T cell responses and suppressed tumor growth *in vivo* [45]. Since then many investigations confirmed the role of EVs in immunity and uniformly showed that EVs produced by both immune cells and non-immune cells participate in the regulation of immune responses. In essence, EVs play important roles in many physiological processes and pathologic conditions [4,8].

2.2.1 EVs are a source of antigens

EVs released by professional antigen-presenting cells (APCs) carry MHC class I and II molecules, adhesion and co-stimulatory molecules, like CD54, CD80 and CD86 and, therefore, possess antigen-presenting functions [50–53]. However, the capacity of EVs to directly stimulate naïve T cells is limited, probably due to their small size and inability to efficiently cross-link T-cell receptors [54,55]. In contrast, EVs exert efficient T-cell activation indirectly by transferring antigens to APCs (Fig. 2) [53]. How exactly EVs and APCs interact is still not fully understood, but it is assumed that EVs are either internalized or remain attached to the cell surface. In the first case, EVs are engulfed by APCs and their protein content is processed and presented in association with MHC molecules. In the second case, EVs directly bind to the cell surface thus ‘decorating’ the surface of APCs (a process called ‘cross-dressing’) and presenting antigens to T cells without further processing [8,56–59]. In line with this, DCs deficient for MHC class II molecules have been shown to stimulate CD4⁺ T-cell proliferation by acquiring EV-associated peptide-MHC complexes [54]. Also subsequent to transplantation DCs in the spleen are able to take up EVs, which carry alloantigens and contribute to stimulation of alloreactive T cells and, hence, graft rejection [56,60].

Also non-immune cells secrete EVs that interact with the immune system. EVs secreted by tumor cells or cells infected with pathogens carry specific antigens, which can be transferred to APCs and presented to CD4⁺ and cytotoxic CD8⁺ T cells [18,61–63].

2.2.2 EVs as suppressors of immune responses

Besides their function as a source of antigen for the promotion of immune responses, EVs may also have immunosuppressive potential. In fact, it has been demonstrated that particular EVs subsets induce immune tolerance, T-cell apoptosis, T-cell anergy, or favor immune evasion of cancer cells or viruses (Fig. 2.2) [64–67]. Immunosuppressive properties of EVs have also been described in transplant tolerance and during pregnancy [68–70].

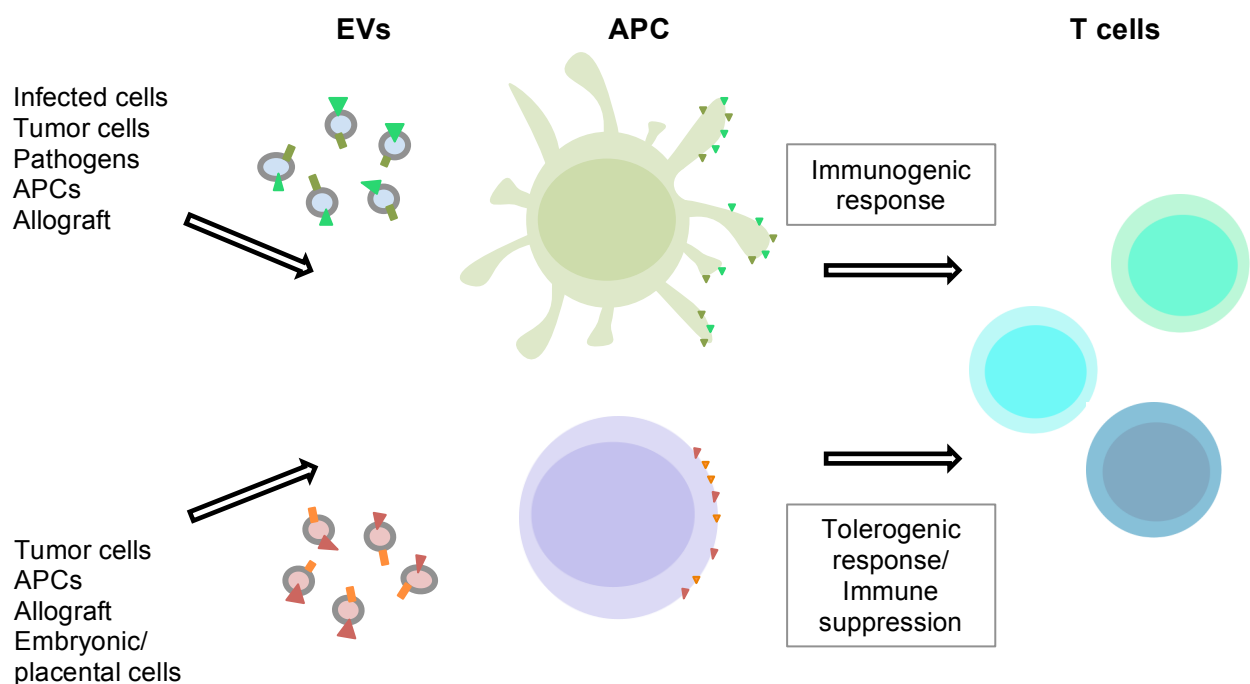


Fig. 2.2: Activating and inhibitory effects of EVs on immune responses

EVs secreted by different cell types, e.g. virus-infected cells, tumor cells, APCs or even parasites, can have opposite effects on immune responses. Once captured by APCs, e.g. DCs (green) or B cells (purple), EVs are degraded and serve as a source of antigens, resulting in activation of antigen-specific T-cell responses. On the other hand, EVs can also suppress immune responses, e.g. by promoting immune tolerance (*adapted from M. Yáñez-Mó et al., 2015 [4]*).

2.2.3 EVs and disease

EVs can also promote disease, as has been extensively studied in cancer. Generally speaking, the microenvironment of a tumor constitutes a complex system involving surrounding blood vessels, different types of immune and non-immune cells, soluble

factors, signaling molecules and the extracellular matrix [71,72]. Tumor cells constantly interact with their surrounding and release signals that promote their own survival, angiogenesis, metastasis, and at the same time blunt the immune system, resulting in tumor immune evasion. It is assumed that EVs contribute to many of these mechanisms and since they interact even with distant cells, EVs are able to mediate signaling in cancer metastasis, angiogenesis and support spread of the tumor [73-76]. Furthermore EVs transport molecules, which promote tumor survival, such as Fas ligand (FasL) or Survivin, and can even contribute to cancer drug- and radio-resistance [77–79].

EVs also play a part in virus infection. Virus-infected cells secrete EVs that contain viral proteins and fragments of viral genomes and that, upon interaction with APCs, facilitate induction of antiviral adaptive immune responses. On the other hand, it has been demonstrated that EVs are able to modulate the susceptibility of target cells to retrovirus infection or favor immune evasion [80,81]. EVs and enveloped viruses indeed share many physical and chemical characteristics as well as similar biogenesis pathways and can, therefore, only hardly be distinguished or separated [82].

Since EVs are present in biological fluids and their composition is directly linked to their parental cell, EVs are currently explored as circulating biomarkers of disease for clinical diagnostics [83,84]. Especially tumor-derived EVs are promising future targets for liquid biopsy [85].

2.3 EV-based therapeutics

Since EVs are involved in many physiological and pathophysiological conditions, an increasing interest in EV-based clinical applications has emerged. As important conveyors of cell-cell communication, EVs may be suitable tools for the development of novel therapeutics, such as anti-tumor therapy, vaccination or targeted drug delivery [86–88]. Various cell types secrete EVs with therapeutic potential. Mesenchymal stem cells release EVs, which have been beneficial for the treatment of neurological injuries in mouse models [89,90]. Also EV derived from cells infected with bacterial or parasitic pathogens are currently under investigation. For example, vaccination of mice with membrane vesicles derived from *Bordetella pertussis* generated long-lasting immunity and protection [91,92].

Furthermore, the controlled integration of immunogenic antigens into EVs ('EV engineering') holds promise for the development of new immunotherapeutic strategies against cancer and infectious diseases. DCs pulsed with tumor-specific peptides secrete highly immunogenic EVs that activate tumor-specific immune responses [44,93]. In a similar way DC-derived EVs loaded with *Toxoplasma gondii* antigens or diphtheria toxin have been demonstrated to stimulate protective immune responses in mice [94,95]. Since EV-based vaccines often induce T helper 1 (Th1)-type immune responses, they even appeared to be more effective in the induction of immune responses than vaccines based on soluble antigen [87]. EV engineering is also applicable to control the targeting of therapeutic EVs to specific recipient cell types and to facilitate their uptake [96–98]. For example incorporation of the EBV glycoprotein gp350 into EV membranes has been demonstrated to favor specific binding to the CD21 surface receptor on B lymphocytes [99].

Although the therapeutic effect of EV-based therapeutics in humans awaits full evaluation, previous phase I clinical trials revealed promising results and confirmed feasibility and safety of EV administration. Table 1 summarizes past and currently ongoing clinical studies involving EVs as therapeutic agents. The first two phase I clinical trials that analyzed the potential of EVs for therapy used autologous dendritic cell-derived EVs loaded with tumor antigens [100,101]. In melanoma and non-small cell lung (NSCL) cancer patients, the application of peptide-loaded vesicles was shown to be feasible, safe and nontoxic and resulted in disease stabilization and induction of specific immune responses in a few patients. Also EVs isolated from malignant ascites of colorectal cancer patients were demonstrated to be safe and well-tolerated vaccine candidates. In combination with GM-CSF (granulocyte-macrophage colony-stimulating factor), these EVs induced immune responses specific for the tumor antigen carcinoembryonic antigen (CEA) [88,102]. EVs are furthermore ideal delivery vehicles and, due to their lipid membrane, are stable and well protected from degrading enzymes in body fluids. Therefore delivery of therapeutic biomolecules like nucleic acids and drugs via EVs is currently under investigation. For example the immunosuppressive drug curcumin has been successfully packaged into EVs and will be tested in a clinical trial (NCT01294072, [103]).

Table 1: Previous and current NIH registered clinical trials investigating EV-based therapeutics (adapted from T. Lener et al., 2015 [86] & B. Györgi et al., 2015 [87])

Trial phase	Disease	No. of patients	EV source	Vesicle type	Results	Ref.
I	Melanoma (stage III/IV)	15	Autologous DCs pulsed with tumor antigens	Peptide loaded (MAGE3 antigen)	Treatment was safe and nontoxic, tumor shrinkage and immune response in one patient, disease stabilization in two patients	[101]
I	Non-small cell lung cancer (stage IIIb/IV)	13	Autologous DCs pulsed with tumor antigens	Peptide loaded (MAGE peptides)	Treatment was safe and nontoxic, specific T cell responses in one patient, increased NK lytic activity in 2 patients	[100]
I	Colorectal cancer (stage III/IV)	40	Autologous ascites	Unmodified or in combination with GM-CSF	Treatment was safe and well-tolerated, EVs + GM-CSF induced tumor-specific CTL response	[102]
II	Non-small cell lung cancer	22	Autologous DCs pulsed with tumor antigens	Peptide loaded	Disease stabilization in 7 patients, partial increase in NK cell functions	[104] NCT 01159288
I	Colon cancer	35 <i>(estimated)</i>	Plant <i>(not further described)</i>	Loaded with curcumin		NCT01294 072 (Start: 2011)
I	Head and neck cancer	60 <i>(estimated)</i>	Plant (grape)	Unmodified		NCT01668 849 (Start: 2012)
II	Malignant ascites/pleural effusion	30 <i>(estimated)</i>	Tumor cells	Loaded with chemotherapeutic drugs		NCT01854 866 (Start: 2013)
I	Type 1 Diabetes Mellitus	20 <i>(estimated)</i>	Cord blood	Unmodified		NCT02138 331 (Start: 2014)

All in all, EV-based therapeutics are promising and may be applicable for many different diseases. However, many further investigations are first necessary to fully understand the complex interactions between EVs and their environment.

In this context the present study aimed at the evaluation of an EV-based immunotherapeutic approach for treatment of a B-cell malignancy.

2.4 Chronic lymphocytic leukemia

2.4.1 Phenotype, origin and diagnosis

Chronic lymphocytic leukemia (CLL) is an incurable malignant disease and the most common leukemia among adults in Western countries [105]. CLL is mainly characterized by progressive accumulation of small, mature CD19+/CD5+/CD23+ B-lymphocytes in blood, bone marrow and secondary lymphoid organs [106,107]. *In vivo*, CLL cells are highly resistant to apoptosis, whereas *ex vivo* they undergo programmed cell death rapidly, indicating that CLL cells are strongly dependent on the cellular and cytokine components of their microenvironment [108,109].

The etiology of CLL is still a matter of debate, but recent studies indicate that CLL originates from CD5-expressing B cells, a subpopulation also present in the peripheral blood of healthy individuals [110]. Oncogenic mutations that promote CLL development probably occur at any stage of the B-cell development [106,111]. Two main subclasses of CLL exist: in approximately 60% of CLL cases the malignant cells express immunoglobulin (Ig) with somatic hypermutations in the variable regions and are defined as M-CLL. In contrast, around 40% carry Ig that is encoded by unmutated immunoglobulin heavy variable (IGHV) genes, known as U-CLL and associated with a more aggressive disease outcome [112]. Therefore, it is currently believed that CLL arises from either of two distinct CD5+ B-cell subsets. Furthermore, a variety of chromosomal aberrations in CLL have been described and often accumulate over time, such as del13q14, del11q22-q23, del17p13 or trisomy 12 [113,114]. They are directly linked to the clinical outcome and influence the response to treatment [115].

CLL is usually diagnosed by blood tests based on a complete blood count and blood smears. People with CLL have elevated numbers of lymphocytes (>5,000/ μ l of blood) and these cells display abnormal morphologic features [116,117]. Furthermore,

circulating CLL cells can easily be identified by flow cytometry by the characteristic co-expression of B-cell markers (e.g. CD19) and CD5 (Fig. 2.3). After diagnosis, additional bone marrow tests are usually performed to classify the CLL stage prior to treatment. Since CLL has a highly variable clinical course, cytogenetic tests are also recommended in order to adapt and optimize treatment options [117].

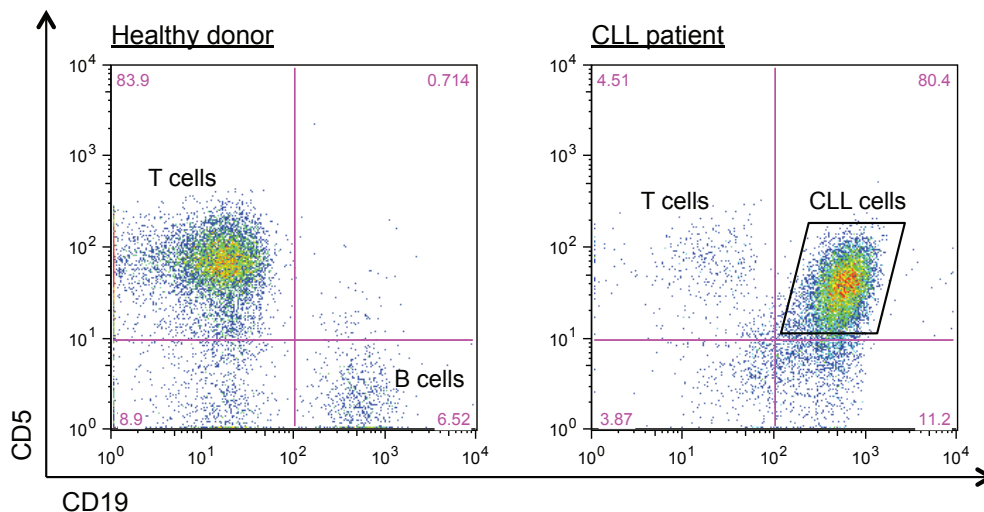


Fig. 2.3: CLL cells in the peripheral blood are characterized by the co-expression of CD19 and CD5

Peripheral blood mononuclear cells (PBMCs) were isolated from a healthy donor (left) and a CLL patient (right), stained for CD5 and CD19 and analyzed by flow cytometry.

2.5 Immunological situation in CLL

CLL patients exhibit progressive immunodeficiencies. Hypogammaglobulinaemia is common, also severe defects in cell-mediated immunity are usually present, as for instance abnormalities in T-cell numbers and function, low neutrophil counts (neutropenia) or reduced natural killer (NK) cell activity [118–120]. Also serum levels of complement proteins are reduced in the majority of CLL patients [121,122].

CLL cells express MHC class I and II molecules, surface Ig and differentiation antigens, yet are poor antigen-presenting cells. This is because CLL cells express immune-suppressing factors, such as TGF- β and IL-10, and lack important costimulatory molecules, such as CD54, CD80 and CD95, which are indispensable for efficient T-cell activation [123–125]. In order to become fully activated during immune responses, T cells interact with DCs and B cells. This interaction comprises a set of highly regulated

events: In addition to an antigen-dependent signal mediated by the T-cell receptor/CD3 complex and the peptide-loaded MHC molecules, subsequent engagement of costimulatory molecules is required (Fig. 2.4). This second signal induces expression of particular surface markers and cytokine secretion. Upregulated CD28 and CD40L (CD154) on T cells interact with the CD80/CD86 receptor and CD40 on the B-cell surface, respectively. As a result, IL-2 is produced and T-cell proliferation, clonal expansion and their differentiation into effector cells is induced [126]. In contrast antigen presentation to T cells in the absence of costimulatory signals results in immunological tolerance and T-cell anergy [127]. Interaction of CD40 with its ligand, CD40L, a type II membrane glycoprotein primarily expressed on activated T cells, is crucial for the activation of APC function, activates complex cellular signaling pathways and induces expression of immune accessory surface molecules [128,129]. Defects in CD40-CD40L interaction result in immunodeficiency, including absence of germinal centers and defective humoral immunity [130,131].

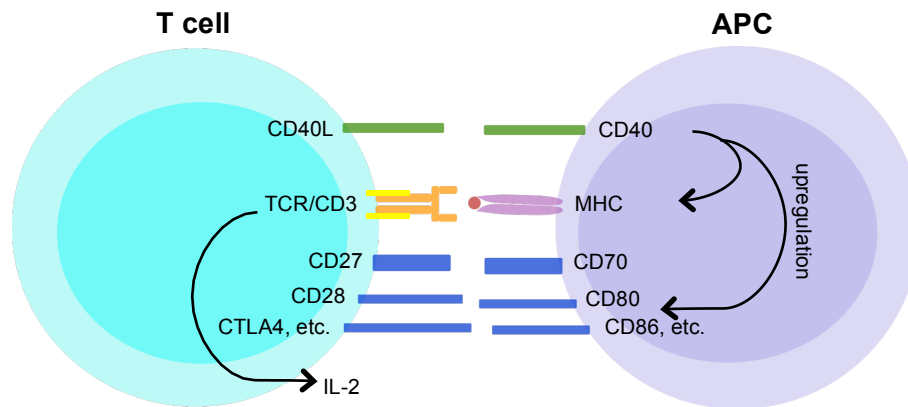


Fig. 2.4: B cell activation upon interaction with an antigen-specific T cell

The first cell-cell contact is mediated by the T-cell receptor (TCR) and the MHC/antigen complex presented by APCs. The costimulatory signal involves interaction of CD80/CD86 and CD28, leading to IL-2 production and upregulation of CD40L on the T-cell surface. Stimulation of CD40 on APCs by CD40L triggers important signaling pathways in B cells and promotes enhanced expression of costimulatory molecules (e.g. CD54, CD80, CD86) and MHC molecules. CTLA4: cytotoxic T lymphocyte-associated protein 4. (*adapted from J. Haanen et al., 2007 [132]*)

Several studies have shown that also CLL cells express CD40 and, as for normal B cells, engagement with CD40L induces upregulation of costimulatory molecules and thus significantly enhances the antigen-presenting capacity of CLL cells [133,134]. Once reactivated, CLL cells are susceptible to immune recognition and are effective stimulators of allogeneic and autologous T cell responses [125]. However, T cells in CLL patients express only low levels of CD40L and therefore efficient activation of CLL cells through CD40 and recognition by T cells are severely impaired [135].

2.5.1 CLL and infection

Infections have a major influence on the progression of CLL and are the most common cause of death [118]. CLL patients are particularly susceptible to infections due to both, the disease-related immunodeficiency and further immunosuppression related to therapy [119]. Bacterial infections of the respiratory tract, the urinary tract and the skin, e.g. by *Streptococcus pneumoniae*, *Staphylococcus aureus* or *Escherichia coli*, are the most common problems. Especially in advanced disease, pneumonia and viral infections with Herpes simplex and Herpes zoster occur. Also reactivation of other herpes viruses, such as Epstein-Barr virus (EBV) and cytomegalovirus (CMV) may occur in CLL patients treated with T cell-depleting agents [118,136]. Certain therapies have also been linked to an increase of fungal infections, e.g. with *Candida* or *Aspergillus* [119].

2.5.2 Cytomegalovirus infection influences the T-cell repertoire in CLL

One feature that is common to all herpes viruses is their life-long persistence within the infected host together with the possibility for frequent reactivations from latency to lytic virus replication. The worldwide seroprevalence of human cytomegalovirus is around 60% and persistent CMV infection promotes the accumulation of CMV-specific T cells, especially in older individuals [137,138]. Also the majority of CLL patients is CMV-seropositive and the accumulation of CMV-specific T cells is even more pronounced. In fact, elevated numbers of both CMV-specific CD4+ and CD8+ T cells have been detected in CLL patients, as compared to healthy age-matched CMV carriers [139,140]. These high T cell numbers may at least partially explain why clinically relevant reactivation of CMV infections in untreated CLL is relatively rare, although the overall T cell repertoire is functionally defective. Indeed, whereas CD8+ T cells in CLL patients in general exhibit an increased expression of inhibitory receptors, such as PD-1 and CD244, CMV-specific

CD8+ T cells do not display upregulated inhibitory molecules and remain functional in terms of cytokine production, cytotoxicity and immune synapse formation [141,142]. It is currently speculated that CLL-associated immunosuppression may trigger CMV reactivation and, as a result, activates and expands the CMV-specific T-cell repertoire, which in turn controls viral reactivation [140]. However, such expanded T-cell populations may also have negative consequences as they can impair the immune defense mediated by other T-cell populations [143]. For example, expanded CMV-specific T cells may suppress expansion of T cells specific for other latent viruses, such as EBV and Varicella zoster [144].

Although the mechanisms that drive the dominant role of CMV-specific T cells in CLL is not completely understood, evidence exists that it may be possible to take advantage of this strong CMV-specific T-cell immunity and redirect it towards CLL cells [145,146].

2.6 Treatment of CLL

The progression of CLL is very heterogeneous. In some patients the disease is stable for years, whereas in others it progresses rapidly and requires immediate treatment [147]. Survival after diagnosis therefore ranges from several months to decades. In approximately 5% of patients, CLL can furthermore transform into the Richter syndrome (RS), a fast-growing and aggressive large B-cell lymphoma, that is associated with a very poor prognosis [148,149].

Because of this heterogeneity, treatment of CLL comprises a variety of different options and needs to be adapted individually. The patient's age and fitness level, the manifestation of symptoms and the underlying genetic alterations need to be considered. Currently no curative treatment for CLL exists, but different drugs are available that can relieve symptoms and prolong survival. Especially in patients with poor physical fitness, cytostatic agents (e.g. chlorambucil) have been used successfully as initial front-line therapy [116]. However, since complete remission (CR) is rare, combination with monoclonal anti-CD20 antibodies (e.g. rituximab) is usually recommended and was shown to be effective [150]. Other monoclonal antibodies targeting CD23, CD40 or CD52 have also been proven to promote CR, depending on the patient's physical condition and existing genetic aberrations. Conventional

chemotherapy furthermore often includes administration of purine analogues, such as fludarabine or pentostatin [151]. Recently allogeneic stem cell transplantation (SCT) has been considered to be suitable for long-term disease control in CLL [152,153]. Nevertheless, given high rates of relapse and treatment-related mortality, the potential of SCT is limited and only beneficial for selected patients. For this reason, ongoing trials are focusing on anti-CD19 chimeric antigen receptor (CAR) T cells, which represent a safe and effective alternative to SCT [153,154]. Although clinical data on the application of CAR T-cell therapy are still limited, results published recently are encouraging, especially in patients with relapsed or high-risk CLL [155,156]. Also novel strategies that aim at overcoming the immunological defects in CLL cells, e.g. by targeting CD40, are currently under investigation.

2.6.1 CD40L-based therapy in CLL

As mentioned before, CLL cells express low levels of costimulatory molecules and, therefore, escape immune surveillance. However, several properties of CLL suggest that immune-based therapies may be promising. CLL cells are slowly dividing monoclonal B cells and express MHC class I and II molecules, as well as tumor antigens. Since transfer of functional CD40L to CLL cells restores their antigen-presenting capacity, CD40 is a potential target molecule for immunotherapy [157–159].

Indeed, a phase I study was published in 2000 that demonstrated successful *ex vivo* transduction of CLL cells with a replication-defective adenoviral vector expressing murine CD40L [160]. The transduced cells were reinfused into CLL patients and a specific immune response was observed, which resulted in decrease of circulating leukemic cells and lymph node size. Elevated cytokine levels and increased absolute T cells numbers were also detected. Subsequent investigations on the potential of CD40L-based CLL therapy based on adenoviral, herpesviral and lentiviral vectors confirmed the efficacy of CD40L transfer to enhance the immunogenicity of CLL cells [161–166]. In general, viral vectors represent an attractive tool for gene therapy due to their ability to provide high-efficiency gene transfer and high level of expression in a wide variety of cell types. However, there are also important safety concerns for the use of such vectors for therapy. One risk is that replication competent virus may potentially recover during infection. Furthermore, neutralizing antibodies against the viral and transgene products may be induced and can cause inflammation and serious adverse immune responses. In

contrast, EVs are safe and virus-free vectors and therefore a promising alternative for gene delivery and immunotherapeutic approaches. On that account, the current study aimed at evaluating the potential of engineered EVs to transfer functional CD40L and herpesviral proteins to CLL cells, thereby redirecting herpesvirus-specific T cells towards the tumor cells.

2.7 Aim of the current study

Chronic lymphocytic leukemia is considered a prototypic disease for immunotherapy. Since CLL cells divide slowly, express MHC class I and II molecules and tumor antigens and furthermore can be distinguished from normal B lymphocytes by expression of CD5, they are predisposed for immune recognition. Although the overall CLL T-cell repertoire is functionally defective, CMV-specific immunity is intact and may be advantageous for immunotherapy. However, the antigen-presenting capacity of CLL cells is poor, because they lack immune accessory molecules, which are required for efficient T-cell activation. Transfer of CD40L can overcome this obstacle and enhances the immunogenicity of CLL cells.

The aim of the current study was to generate engineered EVs carrying CD40L and the herpesviral proteins gp350 and pp65, and to analyze their features and immunotherapeutic potential by using primary CLL cells. For this purpose the following tasks were edited:

- I. Isolation of EVs from cell culture supernatants and evaluation of techniques for EV characterization
- II. Incorporation of CD40L and herpesviral proteins into EVs and confirmation of their functionality
- III. Examining the stimulatory effect of EV-associated CD40L on normal B-lymphocytes and CLL cells
- IV. Evaluation of herpesvirus-specific T-cell responses triggered by EV-loaded CLL cells *in vitro* and *in vivo*
- V. Evaluation of the potential of nanoparticle tracking for quantification and phenotyping of EVs

3 Material

3.1 Eukaryotic cells

Cell lines:

HEK293	Human embryonic kidney 293 cells, originally generated by transformation of human embryonic kidney cell cultures with sheared AV5 DNA [167]
HEK/2089	HEK293 cell clone stably transfected with a recombinant EBV-wt B95.8 genome, GFP-positive [168]
RAW264.7	Murine macrophage cell line, originally generated by transformation with Abelson murine leukemia virus
Raji	EBV-positive Burkitt lymphoma cell line
BJAB	EBV-negative Burkitt lymphoma cell line
LCL	Lymphoblastoid cell line established by <i>in vitro</i> transformation of human primary B cells by EBV (B95.8 strain)
Mini-LCL	Lymphoblastoid cell line established by <i>in vitro</i> transformation of human primary B cells by mini-EBV, a virus mutant incapable of lytic virus replication [169,170]
T cells	T cells clones specific for gp350 and pp65 were established from PBMCs isolated from voluntary blood donors and kindly provided by J. Mautner and A. Moosmann, Helmholtz Centre Munich: <ul style="list-style-type: none"> • gp350-specific HLA-DRB1*1301-restricted CD4+ T cells (epitope: FGQLTPHTKAVYQPR) • pp65-specific HLA-DQB1*0501-restricted CD4+ T cells (epitope: (GQNL)KYQEFFWDAND(IYRI) • pp65-specific HLA-A*0201-restricted CD8+ T cells (epitope: NLVPMVATV)
E μ -TCL-1	splenocytes obtained from E μ -TCL-1 transgenic mice

Primary cells:

B lymphocytes	B cells derived from human adenoids
CLL cells	PBMCs isolated from blood samples of CLL patients

3.2 Mice

All mice were maintained at the animal facility of the Institute for Pathology, University Hospital Cologne, according to the institutional guidelines.

C57BL/6	Wild-type C57BL/6 mice were purchased from Charles River Laboratories. For the immunization with recombinant EVs six weeks old female mice were used.
E μ -TCL-1	<i>TCL-1</i> gene transgenic B6C3 mice (E μ -TCL-1) were kindly provided by C. Reinhardt, University of Cologne, and used as a murine model for CLL. In these mice <i>TCL-1</i> expression is targeted to the B-cell compartment, as described in R. Bichi et al. [182].

3.3 Viruses

Lentivirus '241'	Lentiviral vector carrying a Cre/loxP reporter plasmid, generated and kindly provided by B. Vick, Helmholtz Centre Munich
2089	Recombinant wild-type EBV

3.4 Cell culture

3.4.1 Media and solutions

<u>Name</u>	<u>Source of supply</u>
Cytochalasin D	Sigma-Aldrich
DAPI	Sigma-Aldrich
Defibrinated sheep blood	Thermo Fisher Scientific
Fetal calf serum (FCS)	Bio & SELL
Ficoll	PAN Biotech
Geneticin (G418)	Milipore
Hygromycin B	Invitrogen
IL-2	Novartis
L243 antibody	E. Kremmer, Helmholtz Centre Munich
MTT	Invitrogen

Opti-MEM	Invitrogen
Optiprep	Sigma-Aldrich
PBS	PAN Biotech
Penicillin/streptomycin	Invitrogen
Polyethylenimine (PEI)	Sigma-Aldrich
Protease Inhibitor ULTRA tablets, EDTA-free	Roche
RPMI 1640	Invitrogen
Trypsin/0.05% EDTA	Invitrogen
Vectashield Mounting Medium	Vector Laboratories
W6/32 antibody	E. Kremmer, Helmholtz Centre Munich

3.4.2 Consumables

<u>Product</u>	<u>Source of supply</u>
96-well round bottom plates	Nunc
96-well V-bottom plates	Nunc
Cell scraper	TPP
Cell strainer	Corning
Cryo tubes	Thermo Fisher Scientific
Culture dishes & flasks	Nunc
Disposable scalpel	Aesculap; Swann-Morton
FACS tubes	Nunc
FACS tubes	BD Falcon
Filter units, 0.8 µm pore size	GE Healthcare
Flat-bottom plates (6-/12-/24-/96-well)	BD Falcon
LabTek II chamber slides	Nunc
Microscope glass slides	medco Diagnostika
Syringes	Ecoject

3.4.3 Equipment

<u>Product</u>	<u>Source of supply</u>
Electron microscope	EM 912, Carl Zeiss
Fluorescence microscope	Axiovert200M, Carl Zeiss

Incubator	UniEquip
Irradiation device Gammacell 40 (Cs-137)	Atomic Energy of Canada Ltd.
Laminar flow hood	Binder
Light microscope	Axiovert25, Carl Zeiss
Neubauer hemocytometer (disposable)	NanoEnTek

3.5 Antibodies

3.5.1 Antibodies & beads for flow cytometry, electron microscopy and NTA

<u>Specificity (clone)</u>	<u>Conjugate</u>	<u>Isotype</u>	<u>Source of supply</u>	<u>Dilution</u>
anti-CD4 (RPA-T4)	PE	mouse IgG1	BioLegend	1:50
anti-CD5	PE	mouse IgG1	BD Pharmingen	1:50
anti-CD8 (RPA-T8)	APC	mouse IgG1	BioLegend	1:50
anti-CD19 (HIB19)	PE, APC	mouse IgG1	BioLegend	1:50
anti-CD54 (HCD54)	PE	mouse IgG1	BioLegend	1:50
anti-CD63 (MEM-29)	-	mouse IgG1	Exbio	1:50
anti-CD80 (2D10)	PE	mouse IgG1	BioLegend	1:50
anti-CD86	PE	mouse IgG1	R&D Systems	1:50
anti-CD96	APC	mouse IgG1	BD Pharmingen	1:50
anti-CD40L	PE, APC	mouse IgG1	BD Pharmingen	1:50
anti-CD40L	Alexa488	mouse IgG1	BioLegend	1:50
anti-gp350 (72A1)	-	mouse IgG1	E. Kremmer	undil. (hybridoma SN)
anti-mouse-IgG	APC	rat IgG	eBioscience	1:50
anti-mouse CD3e (500A2)	Pac Blue	hamster IgG2	BD Biosciences	1:100
anti-mouse CD4 (H129.19)	FITC	rat IgG2a	BD Pharmingen	1:100
anti-mouse CD5 (REA421)	APC-Vio770	human IgG1	Miltenyi	1:20
anti-mouse CD8a (53-6.7)	Alexa700	rat IgG2a	BD Biosciences	1:100
anti-mouse CD19 (6D2)	PE/Cy7	rat IgG2a	BioLegend	1:100
anti-mouse CD45 (30-F11)	APC/Cy7	rat IgG2b	BD Biosciences	1:100
anti-mouse MHCII (M5/114.15.2)	Alexa700	rat IgG2b	BioLegend	1:100
anti-mouse NK1.1 (PK136)	PerCP Cy5.5	mouse C3H x BALB/c IgG2a	BD Pharmingen	1:100
anti-mouse F4/80 (BM8)	APC	rat IgG2a	BioLegend	1:100

anti-mouse CD11b (M1/70)	PE	rat IgG2b	BioLegend	1:100
anti-rabbit IgG	gold, 12 nm	goat	Dianova	1:20
anti-rat IgG	gold, 12 nm	goat	Dianova	1:20
Pro5 NLV pentamer	-	-	ProImmune	1:30
Pro5 PE Fluorotag	PE	-	ProImmune	1:10

3.5.2 Beads for flow cytometry and NTA

<u>Name</u>	<u>Source of supply</u>
APC counting beads	BD Biosciences
Aldehyde/Sulfate latex beads (4 µm)	Thermo Fisher Scientific
PS Beads (100 nm, 300 nm)	Polysciences Inc.
Fluoresbrite® fluorescent PS Beads	Polysciences Inc.

3.5.3 Antibodies for dot blot, Western blot and ELISA

<u>Name (clone)</u>	<u>Origin</u>	<u>Source of supply</u>	<u>Dilution</u>
anti-CD63 (24F9)	rat IgG2b	R. Zeidler, Helmholtz Centre Munich	1:2000
anti-Tsg101 (4A10)	mouse	GeneTex	1:1000
anti-Alix (3A9)	mouse	BioLegend	1:250
anti-Calnexin	mouse	BD Biosciences	1:1000
anti-gp350 (OT6)	mouse	J. M. Middeldorp, The Netherlands	1:2500
anti-CD40L (C-20)	rabbit	Santa Cruz	1:1000
anti-pp65	mouse	Abcam	1:1000
anti-Cre	rabbit	Cell Signalling	1:1000
anti-ERK1/2	rabbit	Cell Signalling	1:2000
phospho anti- ERK1/2 (Thr202/Tyr204)	rabbit	Cell Signalling	1:2000
anti-JNK1/3 (C-17)	rabbit	Santa Cruz	1:500
phospho anti-JNK 1/3 (Thr183/Thr221)	rabbit	Abcam	1:1000
anti-mouse IgG-HRP	horse	Cell Signalling	1:2000

anti-rabbit IgG-HRP	goat	Cell Signalling	1:2000
anti-rat IgG-HRP	goat	Cell Signalling	1:2000

3.6 Kits

<u>Name</u>	<u>Source of supply</u>
CMV IgG serum ELISA	Siemens Healthineers
Human Granzyme B ELISA Kit (ALP)	Mabtech
Human IFN γ ELISA Kit (ALP)	Mabtech
Human IFN γ ELISpot Kit (ALP)	Mabtech
Maxiprep DNA Kit	JetStar, Genomed
Murine IFN γ ELISA Kit (ALP)	Mabtech
MycoAlert mycoplasma detection kit	Lonza
PKH26 Red Fluorescent Cell Linker Kit	Sigma-Aldrich
QIAamp DNA Blood Mini Kit	Qiagen
QuantiTect Reverse Transcription Kit	Qiagen
RNeasy Mini Kit	Qiagen
Agilent RNA 6000 Pico Kit	Agilent
RNase-Free DNase Set	Qiagen
Alkaline Phosphatase (AP) Conjugate Substrate Kit	Bio-Rad

3.7 Enzymes

<u>Name</u>	<u>Source of supply</u>
RNase A	Promega
RNasin	Promega
Reverse transcriptase	Qiagen
DNase I	Qiagen
Taq DNA polymerase	New England Biolabs

3.8 Oligonucleotides

All oligonucleotides were synthesized by Metabion GmbH (Martinsried, Germany).

<u>Primer</u>	<u>Sequence</u>	<u>Product size</u>
BamHI W region forward	5'- TCGCGTTGCTAGGCCACCTT -3'	296 bp
BamHI W region reverse	5'- CTTGGATGGCGGAGTCAGCG -3'	
Cre forward	5'- AAATTTGCCTGCATTACCG -3'	797 bp
Cre reverse	5'- CGCCGTAAATCAATCGATGAGTTGC -3'	
GAPDH forward	5'- TTCTTTTTCGTCGCCAGC -3'	96 bp
GAPDH reverse	5'- GTGACCAGGCGCCCAATACGA -3'	
pp65 forward	5'- CTTGGTATCGCAGTACACGC -3'	179 bp
pp65 reverse	5'- GCGCGTACACATAGATCGAC -3'	

3.9 Plasmids

<u>Name</u>	<u>Description</u>	<u>Backbone</u>
p509	BZLF1 expression plasmid	pCMV
p1891	Cre expression plasmid	pCMV
p2385	gp350 expression plasmid	pcDNA 3.1 (+)
p2670	BALF4 expression plasmid	pRK5
p2713	murine CD40L expression plasmid	pRK5
p4102	hCD40L expression plasmid	pcDNA 3.1 (+)
p5528	pp65 expression plasmid	pRK5

3.10 Peptides, peptide mixes and recombinant proteins

<u>Name</u>	<u>Source of supply</u>
NLV peptide (pp65)	JPT Peptide Technologies
PepMix HCMVA pp65	JPT Peptide Technologies
PepMix EBV gp350/gp340	JPT Peptide Technologies
PepMix HAdV-3 (hexon protein)	JPT Peptide Technologies
EBV gp350 protein (His-tag)	Sino Biological Inc.
CMV pp65 protein (GST-tag)	BIOZOL

3.11 General equipment

<u>Name</u>	<u>Source of supply</u>
Agarose gel chamber	PeqLab
Blotting device (Trans-Blot semi-dry)	Bio-Rad
Centrifuges	5415R, Eppendorf; Rotana 460R, Hettich
Electroporation device	Neon Transfection System, Invitrogen
ELISA plate reader Infinite F200 Pro	Tecan
FACS machine/ cytometer	FACS Canto & FACS Fortessa, BD Biosciences
Film developing machine	Typon
Fluorescence plate reader CLARIOstar	BMG Labtech
NTA instrument ZetaView	Particle Metrix
PCR cyclers	Eppendorf
Pipetboy	Integra Biosciences
Pipets	Rainin
Refractometer	Reichert Technologies
Rotors for ultracentrifugation	SW60Ti, SW28, SW32, TL-100 Beckman Coulter
SDS PAGE device	Hoefer
Spectrophotometer NanoDrop 1000	PeqLab
Thermomixer	Eppendorf
Ultracentrifuges Optima L-60 & L-70	Optima L-60, L-70 Beckman Coulter
Agilent 2100 Bioanalyser	Agilent

3.12 General consumables

<u>Name</u>	<u>Source of supply</u>
ELISA plates	Nunc
Developing films	CEA
Tubes for ultracentrifugation	25 x 89 mm, Kisker Biotech 11 x 60 mm, Beckman Coulter 9.5 x 38 mm, Beckman Coulter
PCR tubes	Eppendorf

Pipet tips	Gilson; Rainin
Polystyrene tubes (15 ml, 50 ml)	Falcon
Reaction tubes (1.5 ml, 2 ml)	Eppendorf
ELISPOT plates (0.45 μ m, mixed cellulose)	Millipore
Amersham Protran nitrocellulose membrane (0.45 μ m)	GE Healthcare

3.13 Chemicals and reagents

<u>Name</u>	<u>Source of supply</u>
Agarose	Gibco
APS	Merck
Cytochalasin D	Sigma-Aldrich
Dimethyl sulfoxide (DMSO)	Carl Roth
DNA loading dye (6x)	Thermo Fisher Scientific
dNTP	Fermentas
ECL detection reagent	self-made
Ethidiumbromide	AppliChem
FACS Flow/Clean/Rinse	BD Biosciences
GeneRuler 100bp DNA ladder	Thermo Fisher Scientific
Standard Taq Buffer (10x)	NEB
NuPAGE MOPS SDS Running Buffer (20x)	Thermo Fisher Scientific
OptEIA substrate solutions	BD Biosciences
PageRuler Plus prestained protein ladder	Thermo Fisher Scientific
PEI transfection reagent	Sigma-Aldrich
Ponceau S solution	Sigma-Aldrich
Protease Inhibitor ULTRA tablets, EDTA-free	Roche
Protein Assay Dye Reagent	Bio-Rad
Rotiphorese Gel 30 (30% Acrylamide)	Carl Roth
TEMED	Carl Roth
Triton X-100	Carl Roth
Tween-20	Carl Roth

3.14 Buffers and solutions

<u>Name</u>	<u>Composition</u>
Bis-Tris/Acrylamide resolving gel (6%/10%)	8.57 ml 1.25M Bis-Tris (pH 6.8), 6 ml/10 ml 30% Acrylamide, ad 30 ml H ₂ O; add freshly: 10% APS (10 µl/ml), TEMED (1 µl/ml)
Bis-Tris/Acrylamide stacking gel	8.57 ml 1.25M Bis-Tris (pH 6.8), 4 ml 30% Acrylamide, 17.43 ml H ₂ O; add freshly: 10% APS (10 µl/ml), TEMED (1 µl/ml)
Coomassie destaining solution	30% Methanol, 10% acetic acid (v/v)
Coomassie staining solution	0.05% Coomassie Blue (w/v), 50% Methanol, 10% acetic acid (v/v)
ECL solution 1	0.1 M Tris/HCL (pH 8.8.), 200 mM p-Courmaric acid, 1.25 mM luminol
ECL solution 2	3% H ₂ O ₂
ELISA AP substrate	5 mg/ml p-Nitrophenylphosphate (p-NPP), 0.5 mM MgCl ₂ , 50% Diethanol-amine, pH 9.5 (store at -20°C)
ELISA wash buffer	0.05% Tween-20 in PBS
Protein sample buffer (Laemmli)	62.5 mM Tris/HCl (pH 7.4), 20% glycerol (v/v), 2% SDS (w/v), 5% β-mercapto-ethanol, 0.0625% bromphenol blue (w/v)
RIPA lysis buffer	50 mM TrisHCl, 0.1% SDS, 1% (v/v) NP40, 0.5% DOC, 150 mM NaCl, pH 8.0
SDS running buffer	NuPAGE MOPS SDS Running buffer (1x), 5 mM NaHSO ₃
WB blocking buffer	5% (w/w) milk powder in TBS-T
WB blotting buffer (10x)	30.3 g/l Tris, 144 g/l Glycine, 0.4% (v/v) SDS, add 20% Methanol to 1x buffer before use
WB wash buffer	0.05% Tween-20 in TBS

3.15 Software

<u>Name</u>	<u>Application</u>	<u>Source of supply</u>
Adobe® Illustrator CS5	Vector graphic editing	Adobe Systems Inc.
FlowJo 9.8.5	FACS analysis	Tree star
GraphPad Prism 6	Statistics software	GraphPad Software Inc.
MacVector	Analysis & alignment of nucleotide and protein sequences	MacVector, Inc.
Microsoft® Word 2011	Word processing	Microsoft
Microsoft® Excel 2011	Spreadsheet	Microsoft
Mendeley	Reference management	Mendeley Ltd.

4 Methods

4.1 Cell culture

All cells were incubated in an incubator at 37°C in a water-saturated atmosphere with 5% CO₂ in RPMI-1640 medium supplemented with 10% FCS and 1% Penicillin/Streptomycin.

4.1.1 Cultivation of stable cell lines

All adherent cell lines (HEK293, 2089, RAW264.7) were passaged when the cells had reached 70-90% confluency. HEK293 and 2089 cells were washed one time in 1 x PBS and treated with Trypsin-EDTA to detach the cells. Fresh medium was added to terminate trypsinization and the cells were centrifuged for 10 minutes at 300 x g to remove residual Trypsin-EDTA. Afterwards the cells were resuspended in fresh medium and split 1 in 10 into a sterile cell culture dish. For selection and maintenance of HEK293 cells stably transfected with the CD40L expression plasmid p4102, geneticin (G-418) was added to the cell medium at a final concentration of 1 mg/ml. RAW264.7 were washed one time in PBS and dislodged from the plate with a cell scraper. An appropriate aliquot of the suspension was transferred into a fresh plate. BJAB cells, LCLs and miniLCLs were cultivated in suspension. Depending on their proliferation rate they were expanded once or twice per week 10-fold each time. All cell lines were tested regularly for mycoplasma contamination by using a commercial detection kit.

4.1.2 Cultivation of T-cell clones

CD4⁺ and CD8⁺ T-cell clones specific for the gp350 and pp65 antigens were kindly provided by Andreas Moosmann and Josef Mautner (Helmholtz Centre, Munich) and had been generated as previously described [171]. The cells were cultivated in 96-well round bottom plates in RPMI-1640 supplemented with 10% FCS, 1% Pen/Strep and IL-2 (1,000 U/ml). T-cell stimulation was performed every two weeks. A mix of feeder cells consisting of irradiated PBMCs (40-50 Gy) isolated from three blood donors and irradiated autologous LCLs or mini-LCLs was used for T-cell stimulation. The LCLs and mini-LCLs stably expressed the pp65 or gp350 antigen (provided by A. Moosmann and J. Mautner). For the maintenance of the NLV-specific CD8⁺ T-cell clone HLA-matched LCLs

were loaded with NLV peptide for 30 minutes at 37°C. Cells were washed three times with PBS and resuspended in fresh medium.

The cells were mixed in the following concentrations and transferred to a 96-well plate (200 µl/well):

- T cells: 0.5 - 1 x 10⁶/ml
- LCLs/mLCLs: 1 x 10⁵/ml
- PBMCs: 1 x 10⁶/ml

Between restimulations, the cell culture medium was replaced as necessary or the cells were expanded in case of strong proliferation.

4.1.3 Freezing and thawing of cells

For long-term storage in liquid nitrogen approx. 10⁷ cells were harvested and pelleted by centrifugation. The cell pellet was resuspended in 1 ml FCS containing 10% DMSO (v/v) and transferred into cryovials, which were first placed in an -80°C freezer and a few days later transferred to the liquid nitrogen tank.

To thaw the cells, the cryovials were removed from the liquid nitrogen tank and immediately placed in a 37°C waterbath. The cells were transferred quickly into a sterile tube containing 20 ml pre-warmed cell medium. After centrifugation for 10 minutes the cell pellet was resuspended in an appropriate amount of medium and transferred to a cell culture dish or flask.

4.1.4 Transfection of HEK293 cells

Transient transfection

One day prior to transfection, HEK293 cells were plated into a fresh 15 cm cell culture dish at a 1:1 or 1:2 ratio in order to achieve 60-80% confluency at the time of transfection. For each plate 20 µg of total plasmid DNA were diluted in 2 ml of Opti-MEM medium. 6 µl PEI transfection reagent per µg DNA were diluted in 2 ml of Opti-MEM in a separate tube. After incubation at room temperature for 2 minutes, DNA and PEI were mixed together and incubated for further 20 minutes at room temperature. During incubation, the medium of the HEK293 cells was replaced by fresh Opti-MEM medium (10 ml/plate). Afterwards the PEI/DNA mixture was added dropwise to the cells. 4-6 hours later the medium was aspirated and replaced by 25 ml of fresh RPMI/10% FCS. For the production of EVs, RPMI supplemented with EV-depleted FCS was used. The transfected

cells were incubated for 72 hours. Afterwards the cell supernatant was collected for purification of extracellular vesicles and cell lysates were prepared, as described in 4.3.2 and 4.4.1.

Stable transfection

To generate HEK293 cells that stably express CD40L, the cells were transfected with the CD40L transfection plasmid p4102 as described above. After 24 hours fresh medium containing the selection antibiotic G-418 (1 mg/ml) was added. The cells were kept under antibiotic constantly and the medium was replaced every three days. After 2-3 weeks single colonies were picked with sterile whatman paper soaked in Trypsin-EDTA and transferred to 6-well plates. The cell growth was monitored and expanding cells were screened by Western blotting and flow cytometry for expression of CD40L. High expressing clones were expanded and aliquots from early passages were frozen down and stored in liquid nitrogen.

4.1.5 Lentivirus transduction of BJAB cells

The lentivirus '241' was generated in HEK293T cells and kindly provided by Binje Vick, Helmholtz Centre, Munich. Virus-containing cell culture supernatants were concentrated by filtration through an Amicon Ultra-15 centrifugal filter (2,000 x g, 30 min). For virus infection 1×10^6 BJAB cells were seeded in a 12-well plate in a total volume of 1 ml/well. 4 μ l of polybren and 25 μ l of purified virus were added to each well. After 24 hours, the cells were washed and resuspended in fresh medium. Expression of the transduced packaging plasmid was monitored after three days by flow cytometry.

4.1.6 Electroporation of BJAB cells

BJAB cells were transfected with the Cre expression plasmid p1819 by using the Neon Transfection System (Invitrogen). The electroporation was performed according to the manufacturer's protocol. Briefly, for ten transfections 2.5×10^6 cells were resuspended in 100 μ l of buffer R (provided by the kit) and 5 μ g of plasmid DNA were added. The electroporation was performed under different parameters to optimize the transfection efficiency. 10 μ l of the cell/DNA mix were therefore aspirated by using the Neon Tip and inserted into the Neon Tube electroporation device. For the electroporation of BJAB cells a voltage of 1350 V and two pulses at 20 ms was optimal. The transfected cells were

immediately transferred into a 24-well plate containing 500 µl of RPMI supplemented with 20% FCS per well. After 24 hours, the cells were expanded and cultured in normal culture medium containing 10% FCS.

4.1.7 Isolation of PBMCs from CLL blood samples by Ficoll gradient

Primary peripheral blood mononuclear cells (PBMCs) were isolated from voluntary blood donations of CLL patients. The samples were provided by the Oncology department of the Klinikum Schwabing, Munich, and the MLL München Leukämielabor. The blood was mixed 1:1 with sterile PBS and 25 ml were loaded carefully on top of a layer of 15 ml Ficoll/Hypaque in a Falcon tube. The tubes were centrifuged at 800 x g for 30 minutes. An aliquot of plasma was collected from the top of the gradient and stored at -20°C for later detection of CMV-specific antibodies by CMV IgG ELISA. PBMCs were carefully aspirated from the layer between the plasma and the Ficoll, and transferred into a fresh Falcon tube. The cells were washed three times in PBS and centrifuged at 650 x g (10 min), 500 x g (7 min) and 300 x g (7 min). Finally, they were resuspended in fresh medium and either used immediately or stored at -80°C for later experiments.

4.1.8 Isolation of primary B lymphocytes from human adenoids

Primary human mononuclear cells were isolated from adenoids obtained from young children undergoing routine adenoidectomy at the Klinikum Großhadern, Munich. The usage of the tissue samples has been granted by the ethic committee of the LMU. At first, the adenoids were cut into small pieces and passed through a cell strainer in PBS. The cell suspension was mixed with 500 µl of sheep blood and incubated for 15 minutes at room temperature to deplete T cells by rosetting. Afterwards the volume was adjusted to 25 ml with PBS and mononuclear cells were isolated by Ficoll gradient, as described previously (4.1.8). Flow cytometry analysis of purified cells confirmed that they consisted mainly of CD19+ B cells (> 85%).

4.1.9 Detection of EBV in primary B cells by PCR

To determine the transformation efficiency of 2089 by limiting dilution assay (5.2.1), only B cells from EBV-negative donors were used, in order to avoid spontaneous reactivation of endogenous virus. Therefore DNA was isolated from 200 µl of the adenoid cell suspension by using the QIAamp DNA Blood Mini kit (Qiagen), according to

the provided protocol. 200 ng of the extracted DNA were used in the standard PCR reaction mix according to the table below. Samples without DNA polymerase or template (NTC; no template control) were included as negative controls. The PCR reactions were mixed with 6x DNA loading dye and analyzed on a 1-2% agarose gel.

PCR protocol:

2.5 µl	Taq DNA Standard Buffer (10x)
0.5 µl	dNTPs (10 mM)
0.5 µl	region forward primer (5 pmol)
0.5 µl	reverse primer (5 pmol)
200 ng	DNA
<u>Ad 25 µl</u>	H ₂ O
0.2 µl	Taq DNA Polymerase

Standard PCR program:

95°C	30 sec	35 cycles
95°C	30 sec	
45-68°C	15-60 sec	
68°C	1 min/kb	
68°C	5 min	
10°C	hold	

4.1.10 Virus production and titration

Virus stock was recovered from EBV 2089 producer cells by transient transfection with BZLF1 (p509) and BALF4 (p2670) expression plasmids, as described in 4.1.4. After 72 hours the virus-containing supernatant was harvested, centrifuged at 300 x g for 10 minutes and filtered through a 0.22 µm membrane filter to remove cellular contaminants. The virus stocks were stored in sterile 50 ml Falcon tubes at 4°C. To determine the concentration of infectious virus, Raji cells were infected with different amounts of 2089 supernatant and the percentage of GFP+ cells was measured by flow

cytometry three days later. The virus titer was calculated by assessing the number of GFP-positive Raji cells per milliliters of virus stock, denoted as 'Green Raji Units' (GRU).

4.1.11 Limiting dilution assay and MTT assay

To evaluate the effect of CD40L+ EVs on the transformation of 2089, primary B cells isolated from adenoids were incubated overnight with EVs (1 µg EVs/1 x10⁶ cells) or left untreated. Next, virus stock was added in the indicated concentration and the cells were plated in 96-well plates (100 - 100,000/well) in a final volume of 200 µl per well. Every week half of the medium was replaced by fresh medium and after six weeks the cell viability was assessed by MTT proliferation assays. For this, the MTT stock solution (5 mg/ml) was mixed at a ratio of 1:5 with RPMI/10% FCS. 150 µl of the cell medium in each well were removed and 50 µl MTT mix were added and incubated in the incubator at 37°C for 4 hours. During this time viable cells with active metabolism convert MTT into a purple colored formazan product. Afterwards 100 µl of 10% SDS were added per well and mixed by repeatedly pipetting up and down. The plates were incubated overnight at room temperature to lyse the cells and solubilize the crystals. The absorbance was measured on the next day at 595 nm. Wells not containing any cells were included as negative controls.

4.2 Antibody staining and analysis of cells by flow cytometry

For the detection of particular surface molecules by flow cytometry, 1 - 5 x 10⁵ cells were washed in PBS and incubated with 50 µl of antibody diluted in FACS buffer (PBS/3% FCS) for 20 minutes at 4°C protected from light. Afterwards the cells were washed in 1 ml PBS and directly analyzed by FACS or counterstained with a secondary antibody (20 min, 4°C). For the detection of T cells specific for the pp65 epitope NLV, a pentamer staining was performed. Therefore 1 µl of the unlabeled Pro5 NLV pentamer was added to the cells. Incubation for 20 min was performed at room temperature. The cells were washed in PBS and resuspended in 30 µl of FACS buffer. Subsequently 4 µl of PE-conjugated Pro5 Fluorotag and 1 µl of a second antibody (e.g. CD8-APC) were added and incubated for 20 minutes at 4°C protected from light.

To quantify absolute cell numbers by flow cytometry a known concentration of APC counting beads (20,000/sample) was added to each sample. The acquisition of the cytometer was stopped when 5,000 beads had been recorded.

4.2.1 Staining of cells with CFSE

Primary B cells were stained with the cell permeate dye CFSE to track cell proliferation by flow cytometry. The CFSE stock solution (5 mM) was diluted in sterile PBS to a final concentration of 5 μ M. Cells were washed and resuspended in CFSE/PBS, followed by a incubation for 15 min at 37°C. Fresh cell culture medium was added to stop the staining reaction and the cells were washed thoroughly and seeded at appropriate density.

4.3 Purification and characterization of EVs

EVs were isolated from HEK293 cell culture supernatants. HEK293 cells stably expressing CD40L were used for the generation of CD40L+ EVs. Additional incorporation of gp350 and pp65 was achieved by transient transfection of the cells with expression plasmids, as described in 4.1.4.

4.3.1 Generation of EV-depleted medium

To avoid contamination of EV preparations with serum-derived EVs, RPMI-1640 containing 20% FCS was prepared and centrifuged overnight (> 16 h) at 100,000 x g, 4°C, in a swinging-bucket rotor (SW32 or SW28). On the next day the supernatant was filter sterilized by transferring the supernatant of each tube into a vacuum-connected 0.22 μ m filter fixed on top of a sterile bottle. The EV-depleted medium was diluted with FCS-free RPMI-1640 at a 1:1 ratio in order to reach the final FCS concentration of 10%. It was stored at 4°C up to four weeks.

4.3.2 Isolation of EVs by serial centrifugation and iodixanol density gradient

The HEK293 producer cells were grown for three days in EV-depleted medium until confluency. The cell supernatant was collected and cells and debris were removed by serial centrifugation (10 min at 300 x g, 20 min at 5,000 x g). The supernatant was filtrated (pore size 0.8 μ m) and EVs were pelleted by ultracentrifugation at 100,000 x g,

4°C for 2 hours in a swinging-bucket rotor (SW32 or SW28). Afterwards the supernatant was discarded and 500 µl sterile PBS containing protease inhibitors were added on top of the pellet. To resuspend the pelleted EVs the tubes were incubated on ice under gentle agitation for 30 minutes.

EVs were further separated from contaminating proteins by floatation into a discontinuous bottom-up iodixanol gradient. The EVs were mixed with the 60% (w/v) OptiPrep stock solution (Sigma-Aldrich), supplemented with protease inhibitor, at a 1:1.36 ratio to reach an OptiPrep concentration of 44%. This EV/OptiPrep mixture was transferred to the bottom of a SW60Ti centrifuge tube and carefully filled up to 3.4 ml with a layer of 30% OptiPrep/PBS. 600 µl of PBS supplemented with protease inhibitor were added on top and the tubes were balanced accurately with each other and centrifuged in a SW60Ti rotor overnight at 160,000 x g, 4°C. On the next day eight fractions à 500 µl were collected from the top to the bottom of each tube. A small volume of each fraction was analyzed by Western blot (15 µl/fraction) or dotplot (2 µl/fraction) to detect EV-associated proteins (4.4). EV-containing fractions were pooled and filled up with PBS to 30 ml and washed by ultracentrifugation (100,000 x g, 4°C, 2 h). The final EV pellet was resuspended in 500 µl PBS containing protease inhibitors. EVs were used immediately or stored at 4°C up to three months.

4.3.3 Determining the buoyant density of each fraction

The refractive index (hence the OptiPrep concentration and the density) of each gradient fraction was measured by using a refractometer. A table for converting the refractive index into the density can be downloaded from the Sigma-Aldrich website.

4.3.4 Electron microscopy analysis of EVs

The morphology of purified EVs was analyzed by electron microscopy. Preparation of the grids, the immunostaining of EVs and the capture of micrographs were performed by Manja Luckner, Department of Biology I, Ludwig-Maximilians University Munich.

Briefly, the samples were fixed with 1% glutaraldehyde in cacodylate buffer (pH 7.0) for negative staining. A drop of each sample was placed on a carbon-coated copper grid, freshly lypophilized by glow discharge. After incubation for 2 min, the drop was quickly removed with a Pasteur pipette. For immunostaining the grids were incubated with various antibodies for 1 h in a wet chamber. After washing, 12 nm gold particle-

conjugated secondary antibodies were applied for 1 h. Finally the grids were stained with 2% phosphotungstic acid and 0.05% glucose. Micrographs were taken with an EM 912 electron microscopy (Zeiss) equipped with an integrated Omega energy filter operated in the zero-loss mode.

4.3.5 Nanoparticle tracking analysis (NTA)

The NTA data presented in this study were generated by using the ZetaView PMX110 instrument (Particle Metrix) equipped with a 488 nm laser. Measurement settings were used as indicated in chapter 5.6.

4.3.6 Flow cytometry analysis of EVs bound to beads

EVs are too small to be directly analyzed by conventional flow cytometry. However when bound to Sulfate Aldehyde Latex beads EV surface molecules can be analyzed by antibody staining. 2-10 μg of purified EVs were mixed with 10 μl of beads (4% w/v, Thermo Fisher Scientific) and incubated overnight at 4°C under constant shaking. As negative control, beads were incubated with PBS containing 3% FCS. On the next day 500 μl of PBS were added to each tube and incubated for 2 h at room temperature on a tube rotator. The beads were pelleted (300 x g, 10 min) and incubated in 500 μl glycine (100 mM) for 30 min to saturate free binding sites. The beads were washed three times in FACS buffer (PBS/3% FCS) and incubated with fluorophore-conjugated antibodies as described in 4.2. The stained EV-bound beads were analyzed by flow cytometry. In forward and sideward scatter plots two populations are always visible that represent single beads and doublets. Therefore a gate was set to analyze fluorescence of single beads only.

4.4 Immunoblotting

To analyze the expression of certain proteins, dot blots and Western blots were performed with either cell lysates or purified EVs.

4.4.1 Preparation of cell lysates and EVs for Western blotting

Cell pellets of HEK293 cells were washed one time in PBS. The cells were resuspended in

1 x RIPA buffer mixed with protease inhibitor (100-500 μ l, depending on the size of the pellet). After incubation on ice for 15 minutes the lysed cells were pelleted in a tabletop centrifuge (10 min, full speed) and the supernatant containing the protein lysate was transferred into a fresh tube. A protein quantization assay based on the principle of Bradford's protein assay was performed to determine the protein concentration in the supernatants. For this purpose dye reagent concentrate (Bio-Rad) was diluted 1 in 5 in H₂O and 1 ml was transferred into a disposable 1.5 ml semi-micro cuvette. 1 μ l of protein lysate was added and mixed carefully. The zero value (blank) consisted of diluted dye reagent only. The cell lysates were either used directly for immunoblotting or stored at -20°C. For Western blot analysis 10-20 μ g of cell lysate were mixed with 6x Laemmli protein sample buffer and boiled for 10 minutes at 95°C. For the detection of CD63 by Western blot a loading buffer free of any reducing agents, e.g. β -mercapthoethanol, was required. Before loading, all samples were centrifuged briefly. EVs were isolated from cell culture supernatants as described in 4.3.2. To detect specific proteins in density gradient fractions 15 μ l of each fraction were mixed directly with 6x Laemmli protein sample buffer without further processing. The samples were boiled for 10 minutes at 95°C.

4.4.2 Bis-Tris PAGE and protein transfer

The samples were loaded onto Bis-Tris/Acrylamide gels (maximal loading volume 20 μ l). A low acrylamide concentration of 6% was used to separate high molecular weight proteins, such as gp350. For all other proteins a 10% resolving gel was used. The gels were run at a constant voltage of 80 V in the stacking phase and at 100 V during protein separation in commercial 1 x MOPS SDS running buffer (Thermo Fisher Scientific) supplemented with 5 mM sodium bisulfite. Afterwards the gel was either stained with coomassie blue (4.4.4) or the proteins were electroblotted on a nitrocellulose membrane using a semi-dry blotting system. The gel and the nitrocellulose membrane were set up sandwiched between two pieces of Whatman filter paper pre-soaked in 1 x blotting buffer. Blotting was carried out at 18 V for 45 minutes. The efficiency of the protein transfer was afterwards confirmed by staining the membrane with Ponceau Red solution (Sigma Aldrich) for 3-5 minutes. The stain was removed by rinsing the membrane thoroughly in H₂O. The membrane was then incubated for one hour in

blocking buffer (5% milk powder in 1 x TBS-T) at 4°C in order to block nonspecific binding sites.

4.4.3 Protein detection

For immunodetection of proteins the nitrocellulose membrane was incubated overnight with the first antibody (diluted in blocking buffer) at 4°C under gentle shaking. On the next day the membrane was washed three times for ten minutes in TBS-T. The HRP-coupled secondary antibody was diluted in TBS-T and added to the membrane for a minimum of one hour at room temperature. After washing 3 x 10 min with TBS-T, the blot was developed by chemiluminescence using premade ECL solutions. 1 ml ECL reagent 1 were mixed with 3 µl of reagent 2 and added on top of the membrane for no longer than five minutes. The membrane was then exposed to a CEA medical X-ray film in an autoradiograph cassette. Exposure times varied from 10 seconds to 20 minutes depending on the strength of the signal.

4.4.4 Staining of acrylamide gels with Coomassie protein dye

To visualize protein bands, the Bis-Tris gel was stained after gel electrophoresis with Coomassie staining solution for 30-60 min until desired band intensity was reached. The gel was destained in Coomassie destaining solution for at least 60 minutes until background was clear.

4.4.5 Dot blot

For the detection of proteins via dot blot 2 µl of each sample (cell lysates, density gradient fractions) were pipetted directly on a nitrocellulose membrane. After the liquid had completely dried, the membrane was incubated in blocking buffer for one hour and immunodetection of proteins was performed as described in 4.4.3.

4.5 Labeling of EVs with PKH26 membrane dye

For visualization of EV-cell interactions, EVs were stained with the PKH26 membrane dye by using the PKH26 Red Fluorescent Cell Linker Kit for General Cell Membrane Labeling (Sigma Aldrich). After ultracentrifugation at 100,000 x g, 100 µl of purified EVs

were mixed with 100 μ l Diluent C (provided by the kit). As control, 100 μ l PBS were mixed with 100 μ l Diluent C. 0.5 μ l of PKH26 dye were added and incubated for 5 minutes with periodic mixing. The staining reaction was stopped by adding 200 μ l of 1% BSA for another minute. Finally the PKH26-labeled vesicles were loaded on an OptiPrep density gradient to purify the EVs and to remove residual excess dye, as described in 4.3.2. EV-containing fractions were pooled, washed in PBS and pelleted by another round of ultracentrifugation. The stained EVs were added to BJAB cells or RAW264.7 macrophages and interaction was analyzed by flow cytometry and fluorescent microscopy (5.3.2). For immunofluorescence investigations the adherent RAW264.7 cells were plated on an 8-well LabTek II Chamber Slide ($1-3 \times 10^4$ cells/well). After incubation with stained EVs the cells were washed cautiously with PBS prior to fixation. BJAB cells were incubated with EVs in 24-well plates, afterwards washed and transferred in a small volume of PBS to a microscopy glass slide and dried at room temperature. The cells were fixed with 4% paraformaldehyde (PFA) for 20 minutes at room temperature and washed three times in PBS. Cell nuclei were counterstained with DAPI (1:10,000) for 1 min. After another three washing steps the cells were covered with Vectashield mounting medium and a coverslip. Microscopy images were recorded with an Axiovert200M fluorescence microscope (Zeiss).

4.6 Isolation and analysis of vesicular and cellular RNA

EVs were isolated by serial centrifugation and ultracentrifugation as previously described (4.3.2). The HEK293 producer cells were harvested, washed and stored at -80°C for subsequent RNA extraction. The pelleted EVs were washed in 30 ml PBS ($100,000 \times g$, 2 h) and concentrated by ultracentrifugation in 1.5 ml tubes ($100,000 \times g$, 90 min, TL-100 rotor). The pellet was resuspended in 100 μ l PBS and 1 μ g of RNase A was added in order to digest free RNA (37°C , 30 min). The reaction was stopped by adding 10U of RNasin (37°C , 30 min). Afterwards the RNA was isolated by using the RNeasy Mini Kit (Qiagen) according to the manufacturer's protocol. At the same time RNA was extracted from HEK293 cells. Additional DNase digestion was performed during RNA purification by using the RNase-Free DNase Kit (Qiagen). Finally the RNA was eluted in 50 μ l of RNase-free water and either stored at -80°C or used

directly for reverse transcription. The concentration of each RNA sample was measured by using the Nanodrop instrument.

4.6.1 RNA quality assessment

RNA isolated from EV samples or HEK293 cells was analyzed in the Agilent 2100 bioanalyzer instrument. For this purpose the Agilent RNA 6000 Pico kit was used according to the manufacturer's instructions. The RNA samples were diluted to a concentration of 2 ng/ μ l and 1 μ l was used for the bioanalyzer analysis.

4.6.2 Reverse Transcription

The QuantiTect Reverse Transcription Kit was used for the synthesis of cDNA from cellular and vesicular RNA samples. For cellular RNA, 1 μ g of RNA was applied for reverse transcription. Since the amount of RNA present in EVs was always much lower, the maximum possible amount of RNA (12 μ l) was used as template. For each RNA sample a reaction mix without reverse transcriptase was included as negative control. Particular cDNA sequences were afterwards detected by standard PCR using gene-specific primers, as described in 4.1.9.

4.7 T-cell assays

To determine the immunogenicity of EVs, APCs (e.g. LCLs, primary CLL cells) were incubated with EVs overnight in a 96-well round bottom plate (10,000 cells/well), as indicated in Fig. 5.15. The cells were then mixed with T cells at a 1:1 ratio in a 96-well V-bottom plate and the supernatants were collected after 16-20 hours, stored at -20°C or used immediately for the detection of IFN γ or granzyme B via ELISA.

4.7.1 ELISA

For measuring IFN γ and granzyme B concentration in cell culture supernatants Mabtech ELISA kits were used according to the manufacturer's protocol. All samples were run in duplicates. A standard curve was created for each ELISA plate by applying standard concentrations of IFN γ or granzyme B. P-Nitrophenylphosphate (p-NPP) was added as a colorimetric soluble substrate of alkaline phosphatase (ALP). The staining reaction was

stopped by adding 1 M NaOH and photometrically assessed at 405 nm by using the Tecan ELISA plate reader. By using the standard curve the cytokine concentration in each sample was calculated.

For the detection of specific antibodies in mouse serum ELISA plates were coated with the recombinant protein of interest diluted to 1 µg/ml in PBS. On the next day, the plates were washed 4x with PBS/0.05% Tween and incubated with blocking buffer (5% milk powder in 1x TBS-T) for 1 hour. Mouse serum samples were diluted in blocking buffer and 50 µl/well were added in duplicates for 2 hours. Detection was performed by using an HRP-coupled anti-mouse IgG antibody diluted 1:1000 in PBS. The plates were developed with OptEIA substrate solutions (BD Biosciences), stopped with 1 M H₂SO₄ and read immediately on a plate reader at 450 nm.

4.7.2 ELISPOT

To quantify IFN γ - or granzyme B-secreting T cells the Human ELISPOT Kits (ALP) from Mabtech were used according to the manufacturer's protocol. Briefly, 96-well ELISPOT plates were coated overnight with the capture antibody. On the next day the plates were washed 6x with RPMI-1640 medium supplemented with 10% FCS. 200 µl/well of the same medium were added and incubated for 1 hour to block unspecific binding sites. The medium was removed and cell suspensions were added in duplicates. Depending on the experiments between 1 x 10⁵ and 5 x 10⁵ cells per well were seeded. They were incubated in the presence of different antigenic stimuli. As positive control the cells were stimulated with a combination of TPA (50 ng/ml) and the Ca²⁺ ionophore ionomycin (0.5 µM). Antigenic peptides were diluted in cell culture medium and added to the cells in a final concentration of 2 µg/ml. EVs were added in different amounts, as indicated. Negative controls consisted of cells in the absence of any stimuli.

The cells were incubated in a 37°C incubator for approximately 16 hours. Detection of T cells secreting the cytokine of interest was performed according to the manufacturer's instructions. The Alkaline Phosphatase (AP) Conjugate Substrate Kit (Bio-Rad) was used for spot development. Per well 50 µl of the substrate solution were added and the plates were developed in the dark for 30 min – 1 h until spots were clearly visible. The reaction was stopped by rinsing the plates thoroughly with tap water. The membranes were air-dried and spots per well were enumerated visually.

4.8 CLL *in vivo* model

Mouse experiments were performed in collaboration with Lukas Frenzel, University of Cologne, according to the protocol described in 5.5. The mice were maintained and immunized in Cologne by Dunja Baatout, who also performed the preparation of murine splenocytes and the measurement of immune cell subsets in splenocytes by multicolor flow cytometry (5.5.3). Preparation of recombinant EVs, the analysis of serum antibody levels and the evaluation of the flow cytometry data were carried out in Munich.

Briefly, six weeks old female C57BL/6 mice were simultaneously immunized with 10 µg of recombinant EVs (per mouse per immunization) mixed with Freund's incomplete adjuvant (250 µl, Sigma F5506), CpG oligonucleotides (5 nmol, ODN 1668, Invivogen) and PBS (total volume 500 µl). All mice received a boost injection without adjuvant six weeks later. To monitor the growth of murine CLL cells in these immunized mice, splenic mononuclear cells were isolated from a highly leukemic Eµ-TCL-1 mouse and loaded with gp350 and pp65 peptide pools (0.5 µg/ml) at 37°C for one hour. Afterwards the cells were washed three times in PBS and subsequently injected into the immunized C57BL/6 mice (5×10^6 cells/mouse). Three weeks later blood samples were collected from the tail vein to monitor serum antibody levels by ELISA, as described in 4.7.1. Furthermore the frequency of CD19+/CD5+ leukemia cells in the blood was measured by flow cytometry. Ten weeks after the injection of TCL-1 cells, mice showing high leukemic blood cells counts were euthanized, splenocytes were isolated and immune cell subsets were analyzed by flow cytometry.

5 Results

5.1 Generation of extracellular vesicles (EVs) in HEK293 cells

According to current knowledge probably all kind of cells are able to secrete EVs, which can be isolated from body fluids. Also permanent cell lines constantly release EVs into the cell culture supernatant from where they can be easily isolated and purified. For this study the HEK293 cell line, a widely used cell line easy to grow and transfect, has been chosen as the principal source for EVs. HEK293 cells were incubated in medium supplemented with EV-depleted fetal calf serum (FCS) to minimize contamination with bovine EVs. The cell culture supernatant was harvested three days later and EVs were purified by serial centrifugation, filtration and ultracentrifugation at 100,000 x g. The pelleted vesicles were then loaded on a bottom-up self-forming iodixanol density gradient to eliminate protein aggregates (Fig. 5.1A). Eight fractions were collected and analyzed by SDS-PAGE. Coomassie staining of the gel showed that most of the soluble proteins were located in fractions 5-8 (Fig. 5.1B). The most prominent band was visible at around 60-70 kDa and represented bovine serum albumin, a major component of FCS present in the cell culture medium. In contrast, Western blotting showed that the tetraspanin CD63, known to be highly abundant in human EVs, TSG101, a cellular protein involved in biogenesis of multivesicular bodies, and ALIX, an accessory protein of the ESCRT complex, were present in fractions 2 and 3, corresponding to a buoyant density of 1.06 to 1.13 g/ml (Fig. 5.1C). Calnexin, a protein of the endoplasmatic reticulum, was used as a negative EV marker and was not detected in any fraction of the gradient. For further purification and concentration the indicated vesicle-containing fractions were diluted with a large volume of PBS, finally the vesicles were pelleted by ultracentrifugation at 100,000 x g and resuspended in a small volume of PBS (around 500 – 800 μ l).

The analysis of EV preparations by electron microscopy demonstrated that the isolated material contained round cup-shaped membrane vesicles with a mean diameter of 100 to 120 nm (Fig. 5.1D). Beyond that, immunogold labeling using an anti-CD63 antibody confirmed the successful enrichment of CD63-positive EVs.

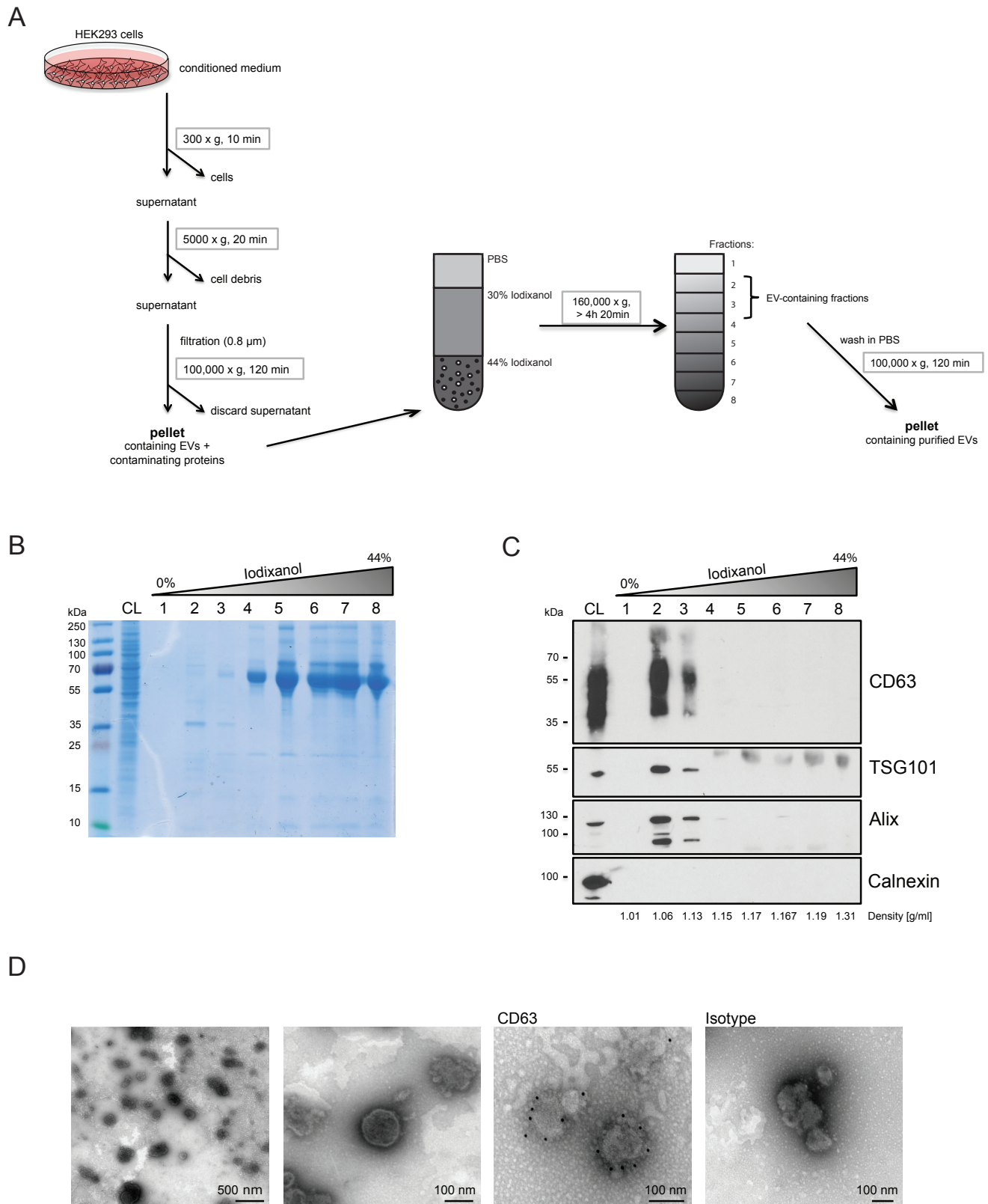


Fig 5.1: Isolation and characterization of HEK293-derived extracellular vesicles

A: Extracellular vesicles (EVs) were isolated by differential centrifugation from conditioned cell culture supernatants containing EV-depleted FCS. The EVs in the 100,000 x g pellet were further purified by floating into a bottom-up iodixanol gradient. Eight fractions were collected from top to bottom and the fractions containing the EVs were washed in PBS and finally pelleted at 100,000 x g. **B:** Coomassie staining of a 10%

acrylamide gel showing eight iodixanol gradient fractions and the corresponding cell lysate (CL). C: Western blot showing the EV-enriched proteins CD63, TSG101 and Alix in cell lysate and the fractions 2 and 3. Calnexin was used as a negative EV marker to exclude contamination with cellular proteins. The density of each fraction was measured with the help of a refractometer. D: Electron microscopy analysis of EV preparations. For immune electron microscopy an antibody against CD63 was added and detected by a gold-conjugated secondary antibody.

5.2 Stimulatory effect of EV-associated CD40L on B lymphocytes

Human naïve and memory B lymphocytes can be activated by targeting their constitutively expressed surface receptor CD40. The interaction of CD40 with its ligand CD154 (CD40L) promotes B-cell proliferation and survival, induces immunoglobulin class switching and plays an essential role in the induction of adaptive and innate immune responses [129,172,173]. CD40-activated B cells are highly efficient antigen-presenting cells (APCs) and represent a readily available and cost-effective source for *ex vivo* T cell stimulation and expansion. In contrast to dendritic cells (DCs), which are the most potent APCs, B lymphocytes can be easily obtained in large numbers from peripheral blood or adenoid tissue and do not lose their antigen-presenting capacity during long-term cultivation or cryopreservation.

Several models have been established in order to deliver CD40L in either soluble or cell-associated form and they opened the doors for many *in vitro* investigations on human B-cell activation [129]. The origin of CD40L in these model systems is diverse and ranges from monoclonal anti-CD40 antibodies, recombinant CD40L proteins and CD40L-positive membrane fractions to CD40L-expressing cells. Especially CD40L-positive feeder cells are still in use today and greatly contributed to extend our knowledge about human immune responses in both health and disease [174].

Potential applications for CD40-activated B cells include the development of novel immunotherapies, e.g. for treatment of graft-versus-host disease, autoimmune diseases or cancer. Also malignant B lymphocytes derived from patients suffering from chronic lymphocytic leukemia (CLL) have been shown to be sensitive to CD40 stimulation.

To investigate the stimulatory potential of CD40L transferred via extracellular vesicles, the following section focused on the generation of CD40L+ EVs and their impact on B-lymphocytes and CLL cells. For this purpose a HEK293 cell line stably expressing full-length human CD40L was generated (Fig. 5.2A). EVs were isolated from conditioned cell culture supernatant as described previously (5.1) and CD40L was detected by Western blotting mainly in fractions 2-4 after density gradient centrifugation (Fig. 5.2B). Immunogold labeling of purified EVs with an anti-CD40L antibody and subsequent electron microscopy confirmed the incorporation of CD40L into the EV membrane (Fig. 5.2C).

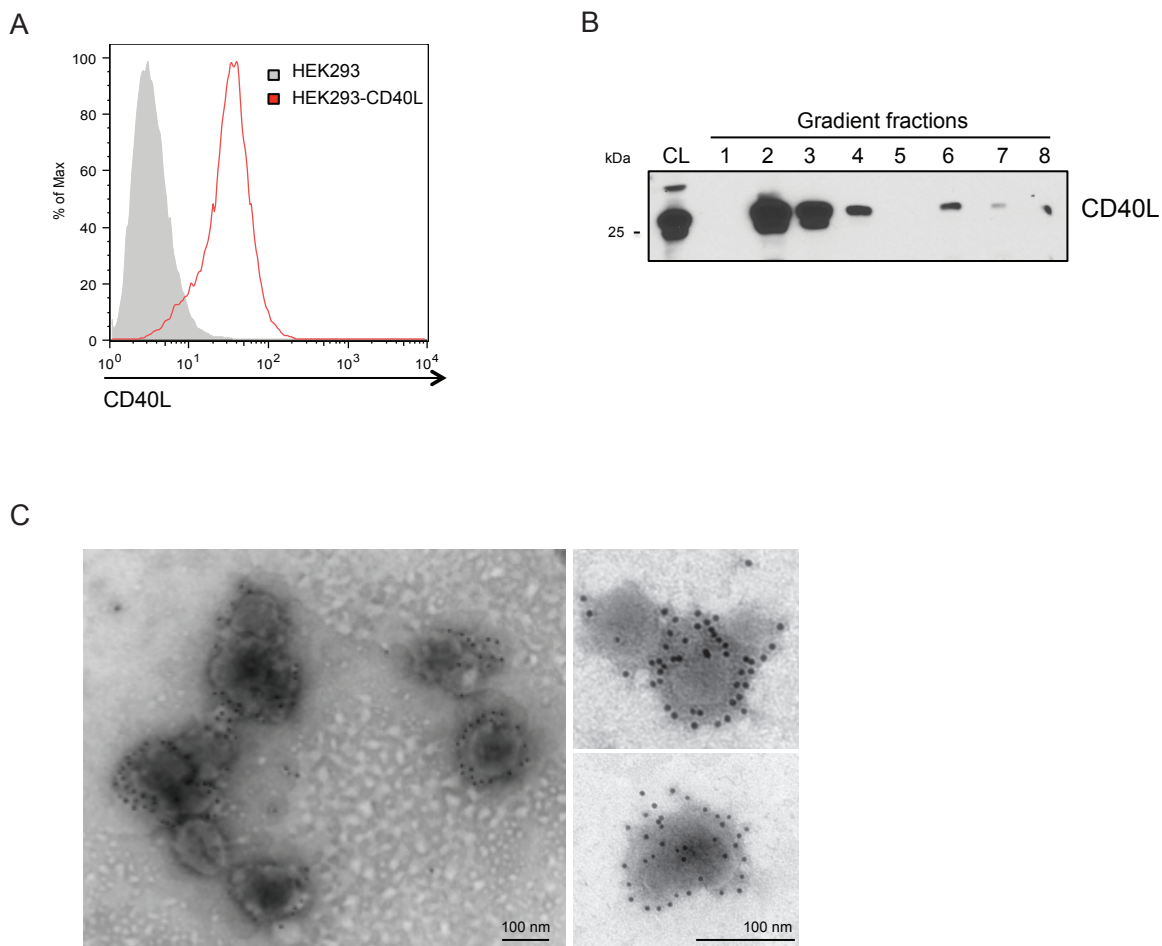


Fig. 5.2: CD40L is incorporated into HEK293-derived extracellular vesicles

HEK293 cells were transfected with a CD40L expression plasmid and selected with G418 (1 mg/ml) to generate a stable cell line. A: CD40L expression on HEK293-CD40L cells was verified by flow cytometry using a CD40L-specific antibody. B: EVs were isolated from HEK293-CD40L cell supernatants by serial centrifugation and subsequent iodixanol gradient. Eight fractions were collected and analyzed by Western blot. CL: cell lysate. C: Immunoelectron microscopy of EVs derived from HEK293-CD40L cells stained with a CD40L-specific antibody and a gold-labeled secondary antibody.

5.2.1 CD40L-positive EVs enhance EBV-mediated transformation of human B-lymphocytes

A well-established method to immortalize primary human B-lymphocytes is based on infection with Epstein-Barr virus (EBV). *In vitro* infection with EBV results in progressive proliferation of B cells and growth transformation of some cells into lymphoblastoid cell lines (LCLs), which provide a widely used model system to investigate EBV latency and tumorigenesis. Additionally, LCLs are long-living functional antigen-presenting cells, are able to generate virus-specific T-cell responses and furthermore provide a reliable source for human monoclonal antibodies.

Since B cells can be activated via CD40, we hypothesized that stimulation of primary B cells with CD40L+ EVs could enhance the infection efficiency of EBV. To confirm this hypothesis primary B-lymphocytes were isolated from routinely ectomized adenoids. For virus production, the GFP+ EBV producer cell line HEK293/2089 was transfected with expression plasmids encoding the viral transactivator BZLF1 and the glycoprotein BALF4 [168]. Three days later the cell culture supernatant containing the virions was collected and filtrated. Raji cells were infected and GFP+ cells were measured by flow cytometry to calculate the virus titer in “Green Raji Units” (GRU). Prior to infection primary human B lymphocytes were treated overnight with CD40L+ EVs, HEK293 control EVs or left untreated. The cells were washed to remove excess EVs and infected with 2089 virus at an multiplicity of infection (MOI) of 0.1 GRU and early infection was monitored by flow cytometry (Fig. 5.3). After eight days infected B cells displayed the typical morphology of lymphoblastic cells in the forward and sideward scatters and were located in the so-called ‘LCL gate’, as indicated in Figure 5.3A. By contrast, uninfected cells showed the phenotype of small and resting cells. Cells treated with CD40L+ EVs also exhibited the characteristics of activated cells, regardless of whether they were infected with EBV or not. The outgrowing LCLs grew as GFP+ clusters and displayed a typical morphology of rosette-forming cells (Fig. 5.3B, upper panel). This cell clumping was enhanced when the cells were treated with CD40L+ EVs prior to infection (Fig. 5.3B, lower panel).

The absolute numbers of CD19+/GFP+ cells present in the LCL gate were counted at days 2, 5 and 8 after infection (Fig. 5.3C). Treatment with CD40L+ EVs clearly increased the number of infected cells at all time points in comparison to untreated cells or cells incubated with CD40L-negative control EVs.

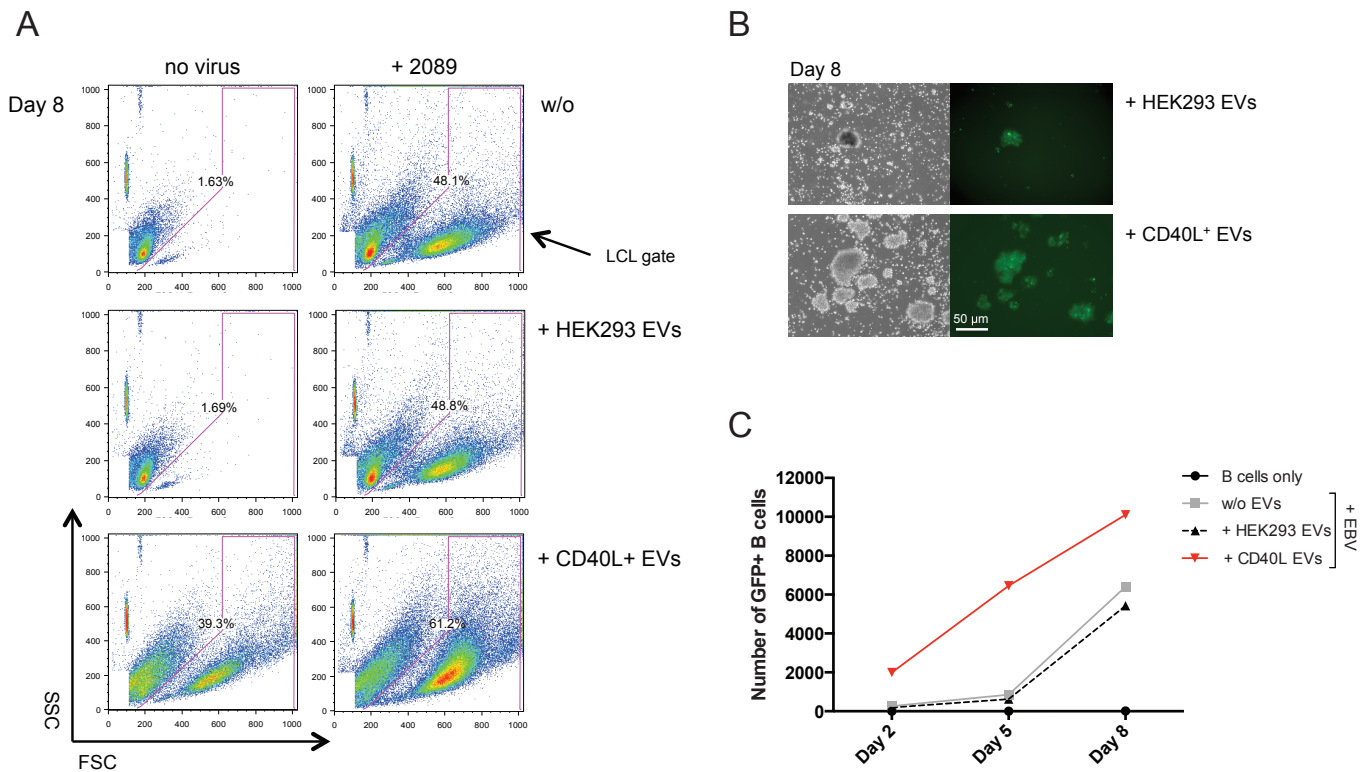


Fig. 5.3: Pretreatment with CD40L+ EVs enhances EBV infection of B cells

A: Forward (FSC) and sideward (SSC) scatter of uninfected and EBV-infected B cells at day 8. Prior to infection, the cells were treated with HEK293 control EVs, CD40L+ EVs or were left untreated (w/o). The outgrowing lymphoblasts were gated as indicated. **B:** Morphological analysis of B cells infected with GFP+ 2089 EBV. On day 8, infected cells displayed typical rosette morphology. Triggering of CD40 in these cells via EV-associated CD40L enhanced clustering (10x magnification). **C:** Absolute numbers of CD19+/GFP+ cells were enumerated by flow cytometry on day 2, 5 and 8 post infection by adding APC-coupled calibration beads before measurement. One representative experiment out of three is shown.

These observations confirmed that the stimulatory effect of EV-associated CD40L enhances EBV infection within the first eight days. Next, limiting dilution assays were performed to investigate whether this improved early infection resulted in increased viral transformation efficiency. Primary B cells were prepared from fresh adenoid samples and in order to avoid reactivation of endogenous virus, the EBV status of each donor was analyzed by PCR using primers specific for the BamHI-W region of the EBV genome (Fig. 5.4A). Only B cells from EBV-negative donors were used. After overnight incubation with CD40L+ EVs or HEK293 control EVs, the cells were washed, infected with 2089 EBV at an MOI of 0.1 GRU and plated in 96-well plates at different cell densities ranging from 100 to 10,000 cells per well. The cell outgrowth was determined

after six weeks by colometric MTT assays (Fig. 5.4B). Treatment of the cells with CD40L+ EVs prior to infection resulted in the highest frequency of transformation compared to cells infected with EBV alone, especially at low cell numbers, i.e. between 1,000 and 5,000 cells per well. CD40L-negative control EVs did not significantly influence cell outgrowth.

In the same line, the transformation efficiency of EBV was also increased by CD40L+ EVs when the cells (100,000/well) were infected with serial dilutions of virus supernatant (Fig. 5.4C). Infection at an MOI of 0.1 GRU resulted in outgrowth in all wells, in the absence or presence of CD40L. However, a 10-fold reduction of the virus amount reduced the transformation frequency by 75% in the absence of CD40L, whereas CD40L+ EVs still triggered outgrowth of LCLs in all of the wells. Further dilution of the virus supernatant to an MOI of 0.001 GRU completely prohibited LCL growth in the absence of EVs. By contrast, when pretreated with CD40L+ EVs, viable LCLs were still detected in 5 out of 8 wells.

Taken together, these data showed that stimulation of primary B cells with EVs carrying CD40L increased the frequency of EBV-mediated transformation. Particularly when the titer of infectious virus was low or when less than 10,000 cells were seeded per well, CD40 triggering was advantageous for the infection efficiency.

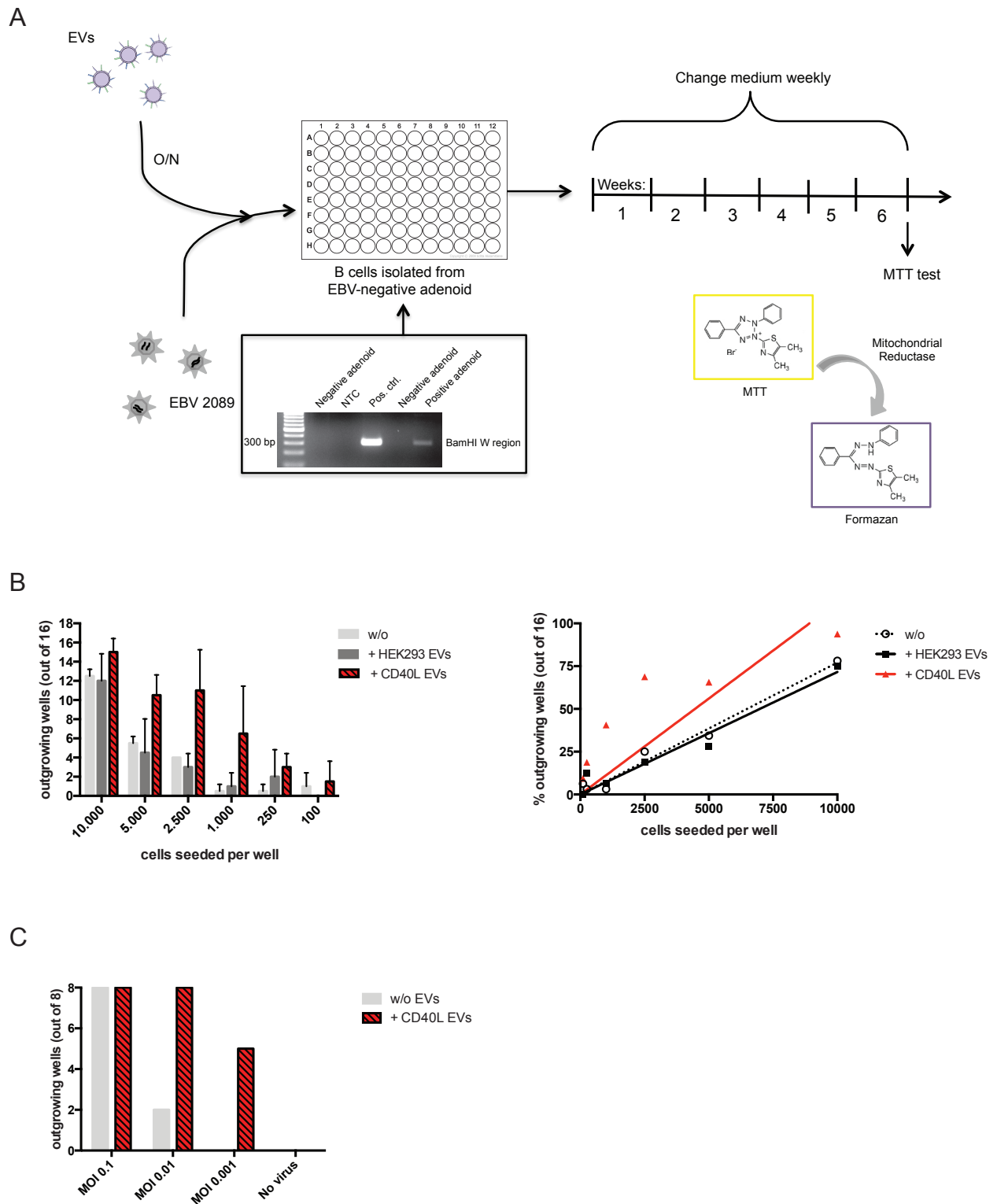


Fig. 5.4: CD40L+ EVs improve the transformation efficiency of EBV

A: Schematic representation of a limiting dilution assay for measuring the frequency of LCL outgrowth after EBV infection. DNA was isolated from a small amount of adenoidal cells to determine the EBV status of each donor by PCR. NTC: no template control. B cells from negative donors were isolated by Ficoll gradient centrifugation and incubated overnight with EVs. On the next day, the cells were seeded in 96-well plates and infected with 2089 EBV. Half of the cell culture medium was replaced weekly and after six weeks the wells containing viable cells were enumerated by MTT proliferation assays. This

colometric test is based on the reduction of MTT to formazan by mitochondrial reductase in viable cells. B: B cells from two EBV-negative donors were seeded at different cell numbers and infected with EBV at an MOI of 0.1 GRU. The left diagram shows the numbers of wells containing outgrowing cells after six weeks. Right panel: the correlation between the number of seeded cells and wells containing LCLs after six weeks is shown as linear regression curves. C: B cells (100,000/well) were incubated with CD40L+ EVs or left untreated and infected with different amounts of virus supernatants. The transformation efficiency after six weeks is shown.

5.3 Engineered EVs for immunotherapy of chronic lymphocytic leukemia (CLL)

As shown above, CD40L was successfully targeted to the surface of HEK293-derived EVs and transferred to B-lymphocytes *in vitro*. Next, the impact of these CD40L+ vesicles on primary CLL cells was investigated. These malignant cells are made up of slowly dividing, monoclonal B cells, which express MHC class I and II molecules, as well as tumor antigens. However CLL cells are poor antigen-presenting cells, which is at least partially attributable to the fact that they lack expression of important costimulatory molecules, which are necessary for effective activation of T cells. CD40L+ EVs may represent an efficient system for stimulation of CD40 on CLL cells, resulting in restored antigen-presenting capacity.

In order to specifically direct HEK293-derived EVs towards CLL cells, the B cell-tropic EBV envelope protein gp350 was additionally incorporated into the vesicular membrane. Furthermore, the interaction between EVs and CLL cells was investigated in detail and the immunostimulatory effect of CD40L+/gp350+ EVs was analyzed.

5.3.1 EV-associated gp350 confers tropism for B lymphocytes

Gp350 is the most abundant glycoprotein in the envelope of the Epstein-Barr virus and mediates attachment of the virus to B lymphocytes via interaction with the complement receptor 2 (CR2, CD21). Additionally, gp350 represents a highly immunogenic antigen and, due to its exposure at the outside of the virion, is the principal target of naturally occurring neutralizing antibodies and is a prime vaccine candidate [175,176].

Since EBV's tropism for B cells is mainly attributable to gp350, we decided to incorporate this viral antigen into the membrane of HEK293-derived EVs to trigger specific cell targeting. For this purpose, HEK293 cells were transiently transfected with a gp350 expression plasmid. Conditioned cell supernatant was collected three days post transfection and EVs were isolated as described in 5.1. Gp350 was detected by Western blotting in fractions 2 and 3 of an iodixanol density gradient (Fig. 5.5A). Moreover flow cytometry of EVs bound to aldehyde/sulfate latex beads confirmed that gp350 was present on the surface of intact CD63+ vesicles (Fig. 5.5B). In the same line gp350+ EVs were detected by immunoelectron microscopy (Fig. 5.5C). Incubation of PBMCs derived from CLL patients with gp350-containing vesicles clearly showed that these vesicles bound specifically to CD19+ B cells but not to CD19-negative cells (Fig. 5.5D).

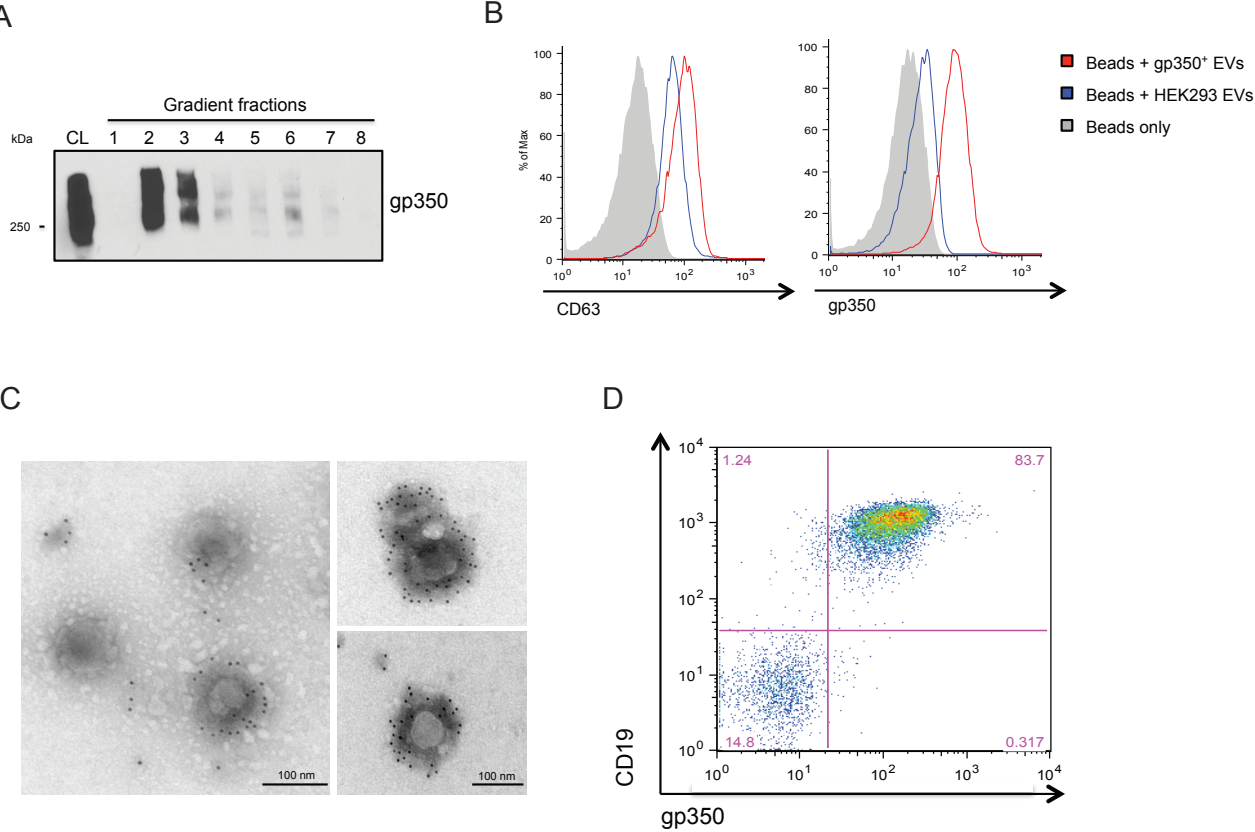


Fig. 5.5: Gp350+ EVs bind specifically to B lymphocytes

A: HEK293 cells were transfected with a gp350 expression plasmid and EVs were purified from conditioned cell culture medium after three days by differential centrifugation and density gradient fractionation. Eight fractions were collected and gp350 was detected in fractions 2-3 and in the cell lysate (CL) by Western blotting. B: Gp350+ EVs were bound overnight to sulfate aldehyde latex beads and stained with antibodies specific for gp350 and CD63 for flow cytometry. C: Immunoelectron microscopy images showing gp350 on the surface of vesicles. D: Flow cytometry analysis showing that gp350+ EVs bind specifically to CD19+ B cells.

microscopy of gp350+ EVs using a gp350-specific antibody followed by a gold-conjugated secondary antibody. D: Gp350+ EVs were incubated with primary CLL cells for two days. The cells were stained for CD19 and gp350 and analyzed by flow cytometry.

5.3.2 Interaction of engineered EVs with CLL cells

Upon release, EVs actively transfer information to recipient cells. However, how EVs interact with target cells and what defines their fate and distribution is still not completely understood. There is a high probability that the mechanism for vesicle uptake strongly depends on the recipient cell. In fact, it has been reported that phagocytic cells, such as macrophages and dendritic cells, internalize EVs efficiently via phagocytosis, whereas in non-phagocytic cells EVs remain mostly attached to the cell surface [57].

EVs derived from HEK293 cells expressing CD40L and gp350 interact with B-lymphocytes and malignant CLL cells. In the following experiments the mechanism and kinetics of this interaction were investigated in greater detail by using isolated EVs labeled with the fluorescent membrane dye PKH26. To get rid of free excess dye the stained vesicles present in the pellet after ultracentrifugation at 100,000 x g were immediately loaded on a bottom-up iodixanol density gradient. As a control, staining buffer and PKH26 dye were mixed in the absence of EVs and also loaded on a density gradient. After gradient centrifugation 16 fractions were collected from top to bottom. The fluorescence signal in each fraction was measured and showed that vesicle-bound PKH26 accumulated in fractions 3 to 6, whereas free dye was found mainly in fractions 12-15 (Fig. 5.6A). Dot blot analysis confirmed the enrichment of CD63+ EVs in fractions 3-6 (Fig. 5.6B).

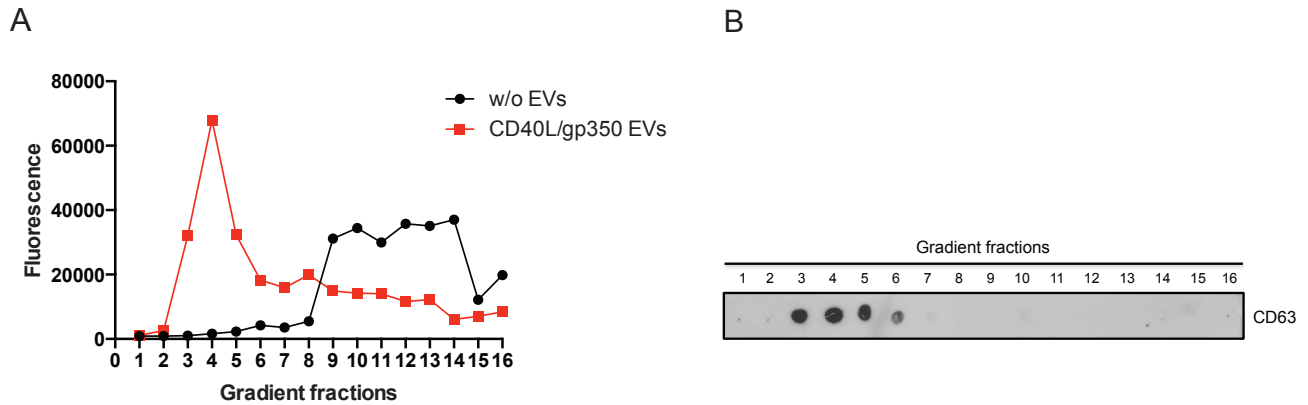


Fig. 5.6: Labeling of EVs with PKH26 membrane dye

Vesicles stained with PKH26 were separated from free excess dye by iodixanol density gradient centrifugation. 16 fractions were collected from top to bottom. A: Measuring the fluorescence in each fraction confirmed enrichment of PKH26-positive vesicles in fractions 3-6 and accumulation of free dye in lower fractions. B: 2 μ l of each fraction were spotted on a nitrocellulose membrane and detected by a specific anti-CD63 primary antibody.

First, the dynamics of EV-cell interaction was studied by flow cytometry. PKH26+ EVs were mixed with primary CLL cells derived from two donors and PKH26 fluorescence of CD19+ B cells was recorded at three different time points. RAW264.7 macrophages were used as a control, since they are known to be professional phagocytes. Comparing the kinetics of labeled CD40L+ and CD40L+/gp350+ EVs showed that both types of vesicles were taken up by RAW264.7 macrophages to a similar extent. In sharp contrast, CLL cells interacted with CD40L+/gp350+ EVs much more efficiently than with CD40L+ EVs, indicating the crucial role of gp350 for a stronger affinity to B lymphocytes (Fig. 5.7A).

In a second experiment different amounts of PKH26-labeled EVs were added to primary CLL cells or RAW264.7 macrophages and analyzed by flow cytometry after 24 hours, clearly showing a direct correlation between the amount of EVs and the PKH26 fluorescence (Fig. 5.7B). Confocal microscopy confirmed these observations and PKH26+ EVs were detected in both primary CLL cells and RAW267.4 macrophages (Fig. 5.7C).

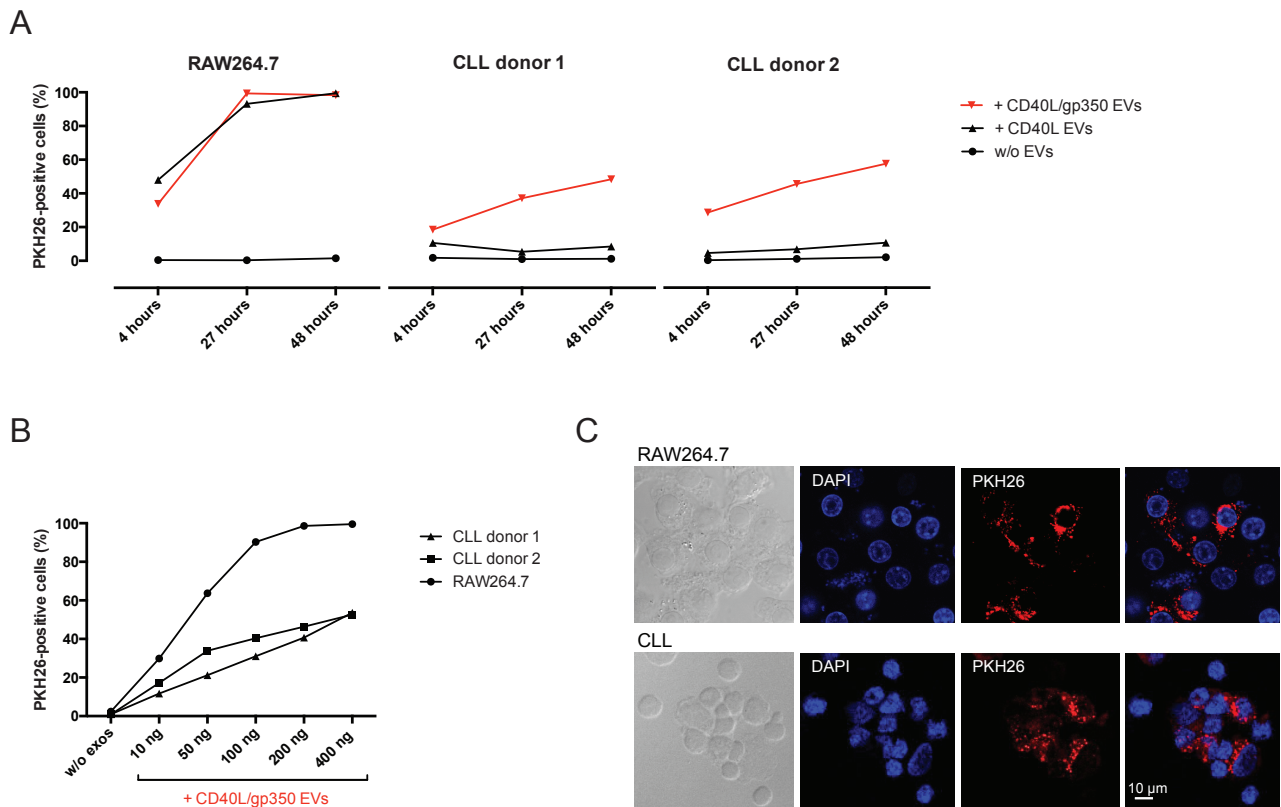


Fig. 5.7: Interaction of PKH26-labelled EVs and primary CLL cells

A: 1×10^6 RAW264.7 cells or primary CLL cells from two patients were incubated with 200 ng PKH26-labelled CD40L+ EVs, CD40L+/gp350+ EVs or left untreated. PKH26 fluorescence was measured by flow cytometry after 4, 27 and 48 hours. B: Correlation between amount of CD40L+/gp350+ EVs and PKH26 fluorescence measured by flow cytometry after 24 hours of incubation. C: Confocal microscopy of CLL cells and RAW267.4 macrophages incubated with PKH26+ EVs (200 ng) for 24 hours. Cell nuclei were counterstained with DAPI (40x magnification).

Next, RAW264.7 macrophages and CLL cells were incubated with PKH26-labelled EVs for 20 hours at either 37°C or 4°C (Fig. 5.8A). Interaction of EVs with RAW264.7 cells was decreased by $86.5 \pm 2.5\%$ at 4°C, indicating that the EV uptake involves an active process. In contrast, interaction of CLL cells and EVs was only slightly reduced when incubated at 4°C. PKH26 fluorescence was reduced by $11 \pm 0.9\%$ and $22 \pm 14.5\%$, respectively. These results suggest that HEK293-derived gp350+ EVs primarily stick to the surface of CLL cells.

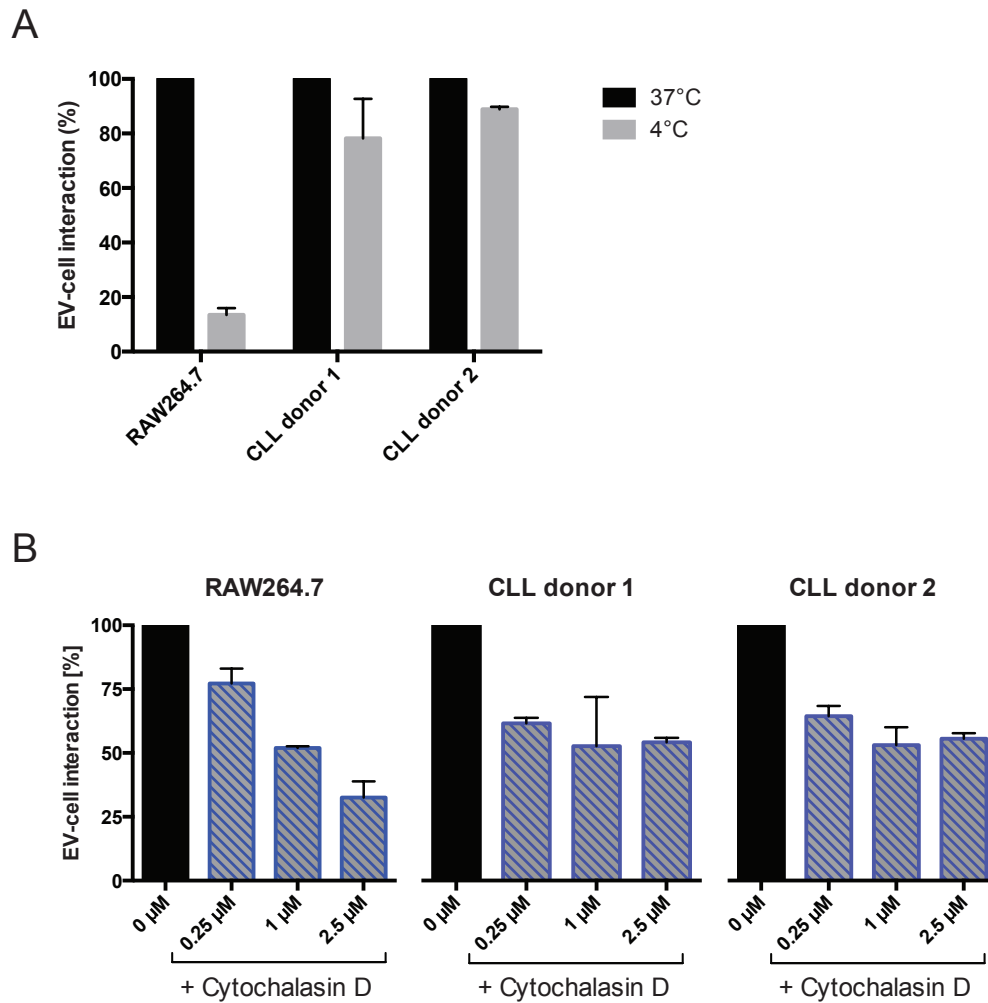


Fig. 5.8: CLL cells interact with HEK293-derived EVs in a different way than macrophages

A: RAW264.7 macrophages and primary B-CLL cells were incubated with PKH26-labelled CD40L+/gp350+ EVs (200 ng/1 x 10⁶ cells) for 20 hours at 37°C or 4°C, as control for active uptake. PKH26 fluorescence was measured by flow cytometry. B: Cells were left untreated or preincubated with the indicated concentrations of cytochalasin D for 30 minutes (blue bars). 200 ng of PKH26-stained CD40L+/gp350+ EVs were added for 4 hours. Cells were washed and PKH26 fluorescence was analyzed by flow cytometry.

Prior to cocultivation with labeled EVs, the cells were treated with cytochalasin D, an inhibitor of actin polymerization (Fig. 5.8B). Control cells were treated with 0.1% DMSO only (not shown). In RAW264.7 macrophages internalization of EVs was inhibited in a dose-dependent manner. In the presence of 1 μM and 2.5 μM of cytochalasin D EV uptake was decreased by 48 ± 0.65% and 67.5 ± 6.4%, respectively. CLL cells were also affected by cytochalasin D treatment, however interaction with EVs was less restricted

in comparison to RAW264.6 cells. Application of 2.5 μ M cytochalasin D reduced EV uptake by $45 \pm 2\%$ on average.

Taken together, these experiments showed that labeling of EVs with the membrane dye PKH26 is a suitable technique to assess the interaction between cells and EVs *in vitro*. It became apparent that HEK293-derived EVs are taken up by primary CLL cells in a dose-dependent manner, although much lower than by professional phagocytes. As expected, CD21+ CLL cells only interacted efficiently with gp350+ EVs, whereas the EBV glycoprotein was completely dispensable for interaction with CD21-negative RAW264.7 cells. Disruption of the actin cytoskeleton by cytochalasin D treatment restricted uptake in both RAW264.7 macrophages and CLL cells, indicating that the actin cytoskeleton is required for efficient uptake of EVs. All in all, the interaction of CLL cells and gp350+ HEK293-derived EVs seemed to be mainly comprised of passive vesicle binding to the cellular surface and partial actin-dependent uptake.

5.3.3 EV-mediated delivery of functional *Cre* mRNA to B lymphocytes

Tracking EVs *in vivo* and analyzing their fate in a recipient cell remains a great challenge for the EV field. Especially demonstrating EV-mediated transfer of functional mRNA or miRNA is crucial to understand the impact of EVs on cellular signaling pathways and cell-cell communication.

An elegant method to visualize EV-mediated RNA delivery is based on the expression of Cre recombinase in EV-secreting cells. Since this enzyme is located in the cell nucleus, secreted EVs contain *Cre* mRNA, but are devoid of Cre protein. Transfer of functional mRNA can be monitored by using target cells, which express a fluorescence or enzymatic reporter gene. Recently this technique has been used successfully to demonstrate tumor-derived EV transfer to cancer cells or immune cells [177-179]. To show that functional mRNA can also be transferred to human B lymphocytes via HEK293-derived vesicles, a Cre/LoxP reporter system was established (Fig. 5.9). For this, EVs were purified from HEK293 cells that overexpressed Cre and gp350. Due to the nuclear localization of the Cre enzyme, Cre protein was only detected in the cell lysate, but not in vesicles (Fig. 5.9B).

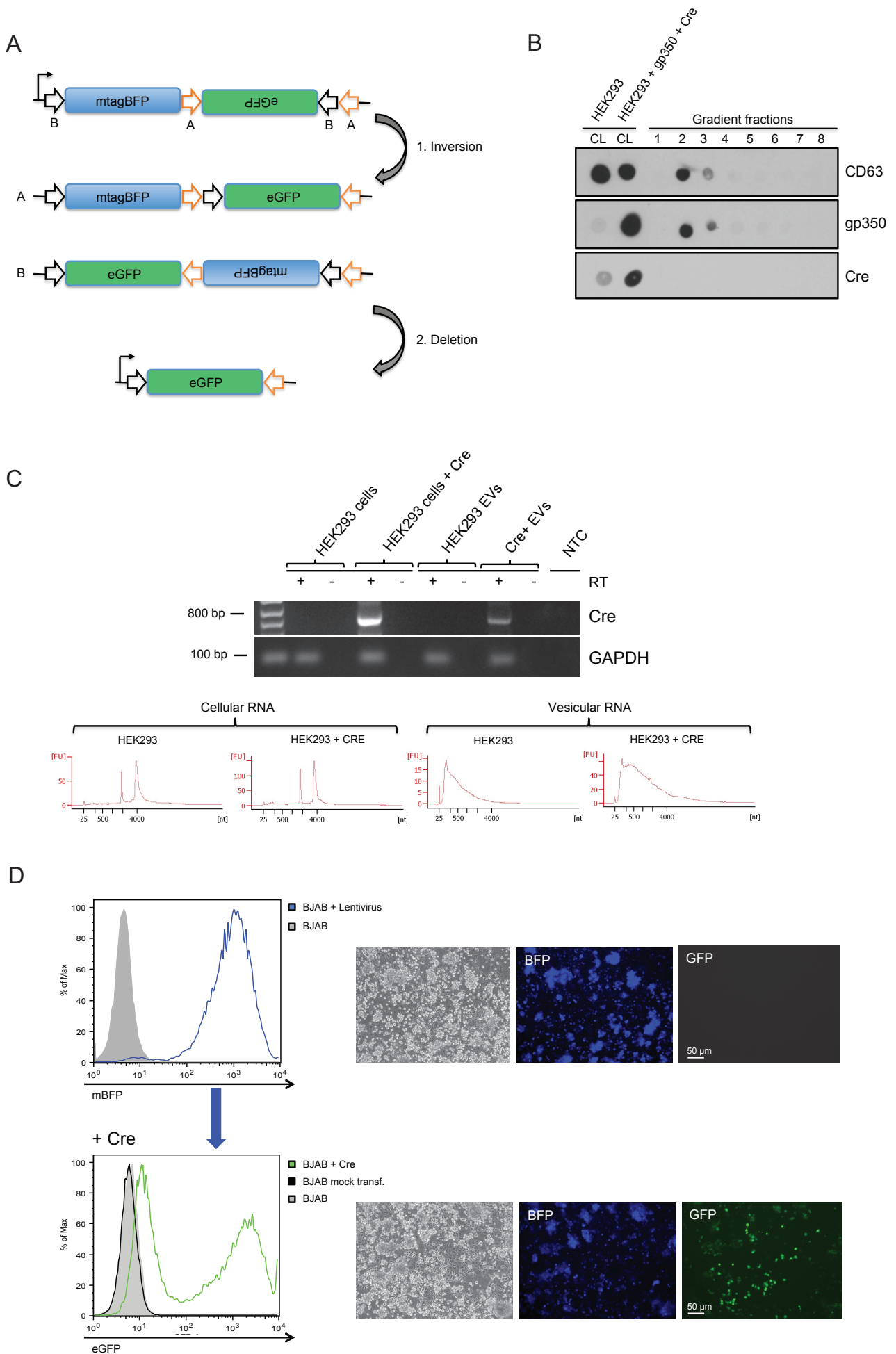


Figure 5.9: A reporter system for tracing EV-mediated Cre transfer was established in BJAB cells

A: Schematic presentation of the experimental strategy. The diagram shows the recombination of the FLIP cassette. In the presence of Cre the mtagBFP-containing cassette is deleted and GFP is expressed. Black and orange arrows mark the LoxP sites. B: EVs were purified from cell culture supernatants from HEK293 cells overexpressing Cre recombinase and gp350 by serial centrifugation and density gradient fractionation. Eight fractions were collected and analyzed by dot blot. CL: cell lysate. C: RNA was extracted from cells and the corresponding EVs and analyzed using the Agilent Bioanalyzer picoRNA chip (lower panel). Using reverse transcriptase (RT-) PCR, *Cre* mRNA was detected in EVs derived from CRE-expressing HEK293 cells (upper panel). As a control, RNA was isolated from vesicles released from untransfected HEK293 cells. In both samples also *GAPDH* mRNA was detected, but only when reverse transcriptase was present, which confirmed the absence of DNA contamination. D: BJAB cells were stably transduced with a lentivirus in the presence of polybrene to constitutively express the Cre/LoxP reporter plasmid containing the mBFP gene. mBFP expression was monitored by fluorescence microscopy (magnification 10x) and flow cytometry (upper panel). Transfection of a Cre expression plasmid into the cells by electroporation induced a switch from BFP to GFP expression, which was visualized after three days (lower panel). As negative control cells were mock-transfected with an empty vector control plasmid (black histogram).

Total RNA was extracted from both HEK293 producer cells and purified EVs (Fig. 5.9C). Bioanalyzer data showed that EVs contain a broad range of small RNAs and lack ribosomal 18S and 28S RNA, confirming that the isolated RNA was not contaminated with cellular RNA. *Cre* mRNA was successfully detected by PCR in Cre-expressing HEK293 cells and corresponding EVs (Fig. 5.9C).

Primary B-lymphocytes and CLL cells are notoriously resistant to most conventional transfection methods. For this reason BJAB cells, an EBV-negative Burkitt lymphoma cell line, were used as EV target cells. The cells were stably transduced with a lentivirus carrying a Cre/LoxP FLIP cassette. When Cre recombinase is present the marker construct flanked by tandem LoxP sites gets inverted, resulting in GFP expression (Fig. 5.9A). At the same time the original mBFP marker gene is deleted. The lentivirus transduction of BJAB cells was monitored by visualization of mBFP-expressing cells by flow cytometry and fluorescent microscopy after 7 days (Fig. 5.9D, upper panel). The prevalence of successfully transduced cells reached almost 100% and was stable even upon cryopreservation. To prove the functionality of the system a Cre expression plasmid was introduced into transduced BJAB cells by electroporation and induced the switch to GFP expression (Fig. 5.9D, lower panel).

EVs released by gp350/Cre-expressing HEK293 cells were added to lentivirus-transduced BJAB cells and interaction was visualized after two days by flow cytometry using an antibody against gp350 (Fig. 5.10A). Furthermore GFP-expressing cells were monitored after one week by fluorescence microscopy (Fig. 5.10B). Although gp350+ EVs clearly bound to the cells, most of the cells remained mBFP-positive and only a few (< 0.01%) displayed detectable GFP expression. This low frequency could be explained at least partially by the fact that switch from mBFP to GFP expression requires more than one Cre molecule. Furthermore, as already shown in 5.3.2, interaction between HEK293-derived gp350+ EVs and B cells mainly comprises vesicle binding to the cell surface. Therefore uptake of an adequate number of *Cre*+ EVs, translation of mRNA into Cre protein and thus Cre-loxP recombination appeared to be a rather rare event in this reporter system.

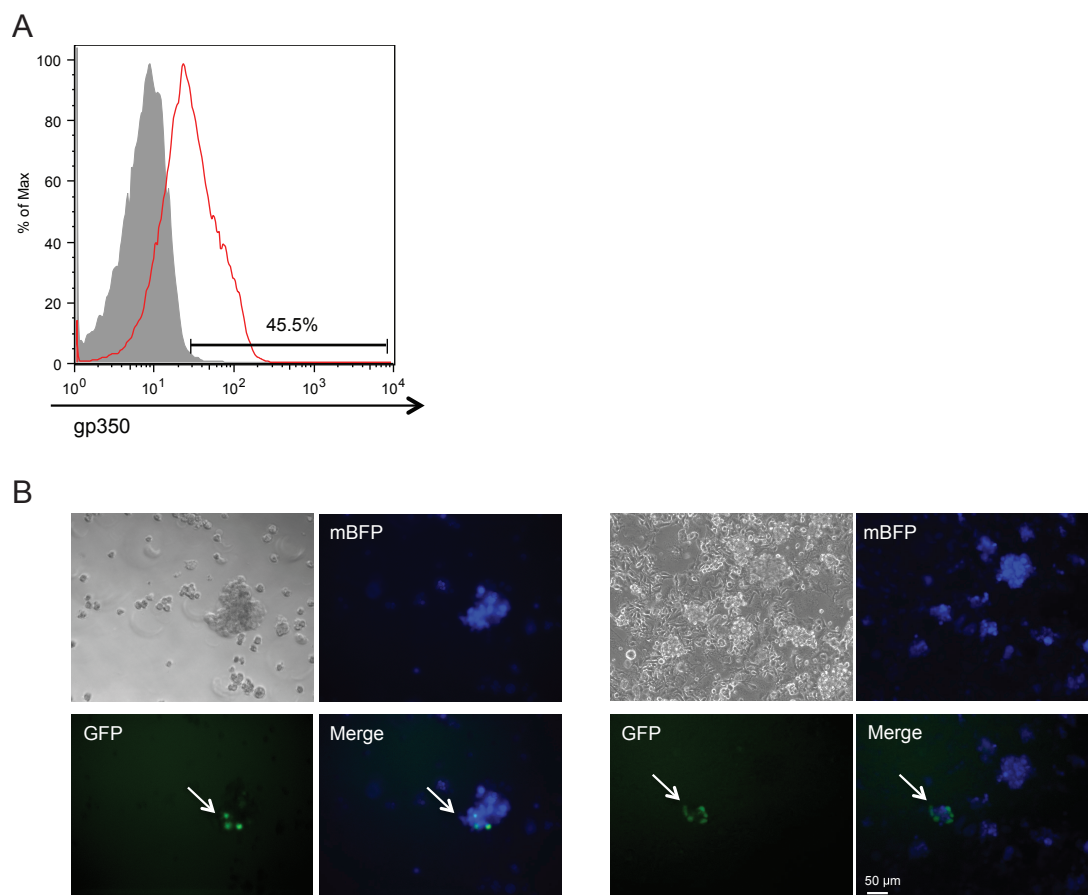


Fig. 5.10: Transfer of functional *Cre* mRNA via EVs to BJAB cells

BJAB cells expressing a Cre/LoxP reporter plasmid were incubated with EVs derived from gp350 and Cre expressing HEK293 cells. A: After two days the BJAB cells were stained with a gp350-specific antibody and analyzed by flow cytometry. B: Expression of mBFP and GFP in EV-treated BJAB cells was visualized by fluorescence microscopy after one week of coinubation (10x magnification). White arrows point towards GFP+ cells.

As shown in the chapter above (5.3.2), RAW264.7 macrophages are able to take up HEK293-derived EVs very efficiently and where therefore used again as positive control. The RAW264.7 cells were transduced with the Cre/LoxP reporter system and mBFP expression was monitored after 7 days by flow cytometry. In contrast to BJAB cells, only about 35% of RAW264.7 cells were successfully transduced and expressed mBFP stably (Fig. 5.11A). Addition of gp350/*Cre*-positive EVs induced GFP expression in some cells already after two days of incubation. GFP+ cells were enumerated visually by fluorescence microscopy (Fig. 5.11B). In comparison to BJAB cells, the prevalence of GFP-expressing RAW264.7 cells was higher, but did not reach more than 1.8% of the transduced cell population, even when EVs were added to the cells repeatedly. Interestingly, as already seen for BJAB cells, GFP+ cells were not distributed randomly, but occurred in clusters in close proximity to each other.

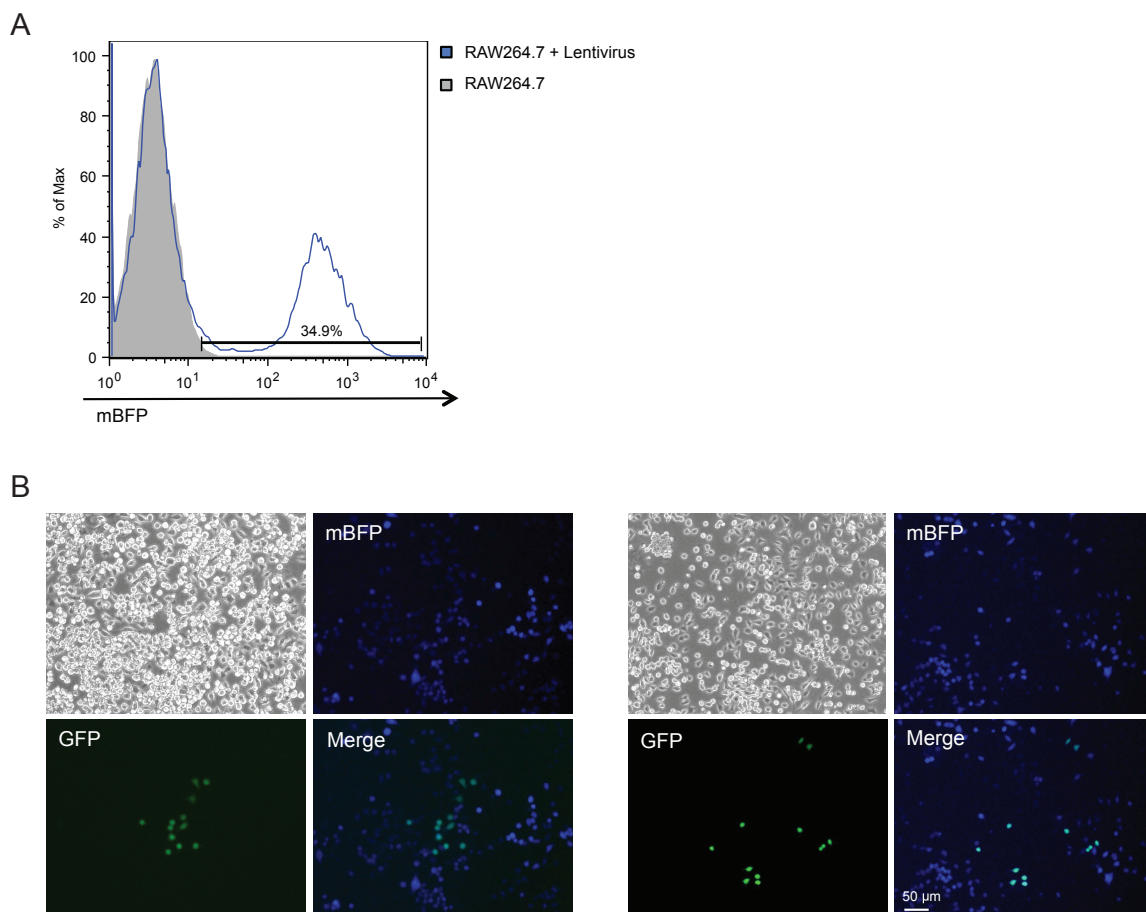


Fig. 5.11: Evidence of EV-mediated delivery of *Cre* mRNA to RAW264.7 cells

A: Cre/LoxP reporter plasmid was introduced into RAW264.7 macrophages by lentiviral transduction. Expression of mBFP in stably transduced cells was analyzed by flow cytometry. **B:** EVs derived from Cre/gp350-expressing HEK293 cells were added to transduced RAW264.6 cells. Expression of GFP was visualized after five days (10x magnification).

In summary, these proof-of-concept experiments confirmed that gp350+ HEK293-derived EVs not only bind to the surface of macrophages and B lymphocytes, but are furthermore able to deliver their RNA content. EV-derived *Cre* mRNA became translated into functional protein within the recipient cells. As shown in chapter 5.3.2, interaction of HEK293-derived EVs with RAW264.7 macrophages was more efficient than with B cells, most likely due to the phagocytic activity of the macrophages.

Establishment of such reporter systems in order to visualize EV trafficking is of particular importance to further investigate the biodistribution of EVs *in vivo* and to understand how they influence biological processes in both health and disease. The Cre/LoxP system is a suitable technique to follow the fate of EVs and to identify potential EV target cells.

5.3.4 CD40L+ EVs protect CLL cells transiently from undergoing spontaneous apoptosis *in vitro*

CLL cells were treated with CD40L+/gp350+ EVs and the influence on the cells' activation status was evaluated. CLL cells were isolated from voluntary CLL blood donors and the percentage of malignant CD19+/CD5+ blasts was determined (average $74.1 \pm 24.7\%$, n=8). The cells were incubated with different types of HEK293-derived EVs and cell growth was monitored (Fig. 5.12). CLL cells incubated for two days in media resembled normal B-lymphocytes under the microscope. However, when treated with CD40L+/gp350+ EVs, the cells formed aggregates and displayed cellular enlargement (Fig. 5.12A). Furthermore, as shown in Figure 5.12B, CD40L+ EVs were able to stimulate proliferation of CFSE-labeled CLL cells, whereas CD40L-negative control EVs did not. Enumeration of CD19+ B lymphocytes isolated from two CLL patients clearly showed that EV-associated CD40L supported cell survival within the first 10 days, whereas cells left untreated or incubated with HEK293 control EVs underwent cell death rapidly (Fig. 5.12C). Moreover the stimulatory effect of CD40L+/gp350+ EVs was stronger in comparison to CD40L+ EVs, pointing out the enhanced EV-cell interaction mediated by gp350. However, after 14-20 days the viability of the CD40-stimulated cells was not significantly higher compared to the control groups.

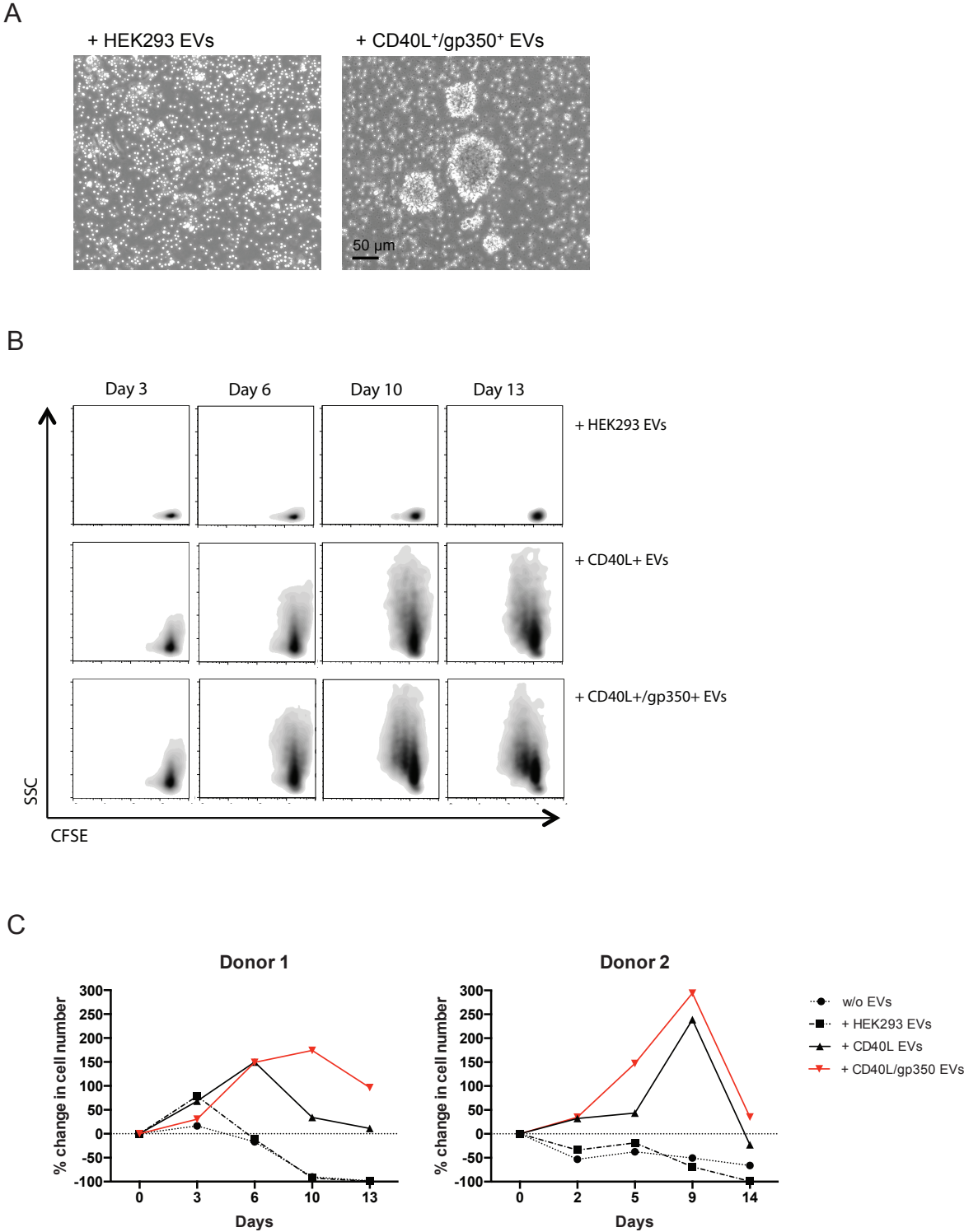


Fig. 5.12: Impact of CD40L+ EVs on CLL cell proliferation and survival
A: Morphologies of CLL cells cocultured for the three days with CD40L-negative or -positive EVs were examined by light microscopy (10x magnification). B: Primary CLL cells were labeled with CFSE and incubated with different EVs as indicated. Cell proliferation was analyzed by flow cytometry. One donor out of two is shown. C: CLL cells isolated from two fresh blood samples were cultured for two weeks with or without addition of different EVs. Counting of CD19+ cells was performed by flow cytometry at the indicated time points by adding APC-coupled counting beads before measurement.

In patients CLL cells show a prolonged survival, which is mainly driven by their interaction with the local microenvironment. However *ex vivo*, CLL cells undergo spontaneous apoptosis rapidly, thus complicating *in vitro* studies on CLL cells. My experiments showed that a single treatment of CLL cells with CD40L+ EVs induced cell proliferation and prolonged survival and therefore represent a useful method for studying the mechanisms that lead to long-term survival of CLL cells *in vivo*.

5.3.5 CD40L+ EVs induce upregulation of immune accessory molecules

In general, CLL cells display a reduced expression of several cell surface molecules, which is why efficient interaction with T cells is severely impaired. CD40 engagement can overcome this dysfunction and the following experiments addressed the question whether EV-associated CD40L is able to improve the functionality of CLL cells.

CLL cells isolated from eight CLL patients were incubated for 72 hours in the presence or absence of EVs and expression of surface molecules was evaluated by flow cytometry. Treatment with CD40L+/gp350+ EVs induced upregulation of the cell adhesion molecule CD54 ($p=0.03^*$), the costimulatory molecules CD80 ($p=0.0077^{**}$) and CD86 ($p=0.0143^*$) and the death receptor CD95 ($p=0.1465$, not significant), in comparison to untreated cells or cells treated with CD40L-negative EVs (Fig 5.13A,B).

To examine whether CD40-stimulated cells could transfer this activating effect to neighboring cells, CLL cells were labeled with CFMDA cell tracker dye and incubated overnight with CD40L+/gp350+ EVs. Afterwards the cells were washed and mixed with untreated, unlabeled cells at a 1:1 ratio. Flow cytometry analysis after 24 hours showed that CD54 expression was upregulated in both cell populations, indicating that EV-loaded cells were able to stimulate neighboring bystander cells that had not been in direct contact with CD40L+ EVs (Fig. 15.13C). Microscopy furthermore demonstrated EV-induced clustering and direct cell contact between CFMDA+ cells and unstained cells.

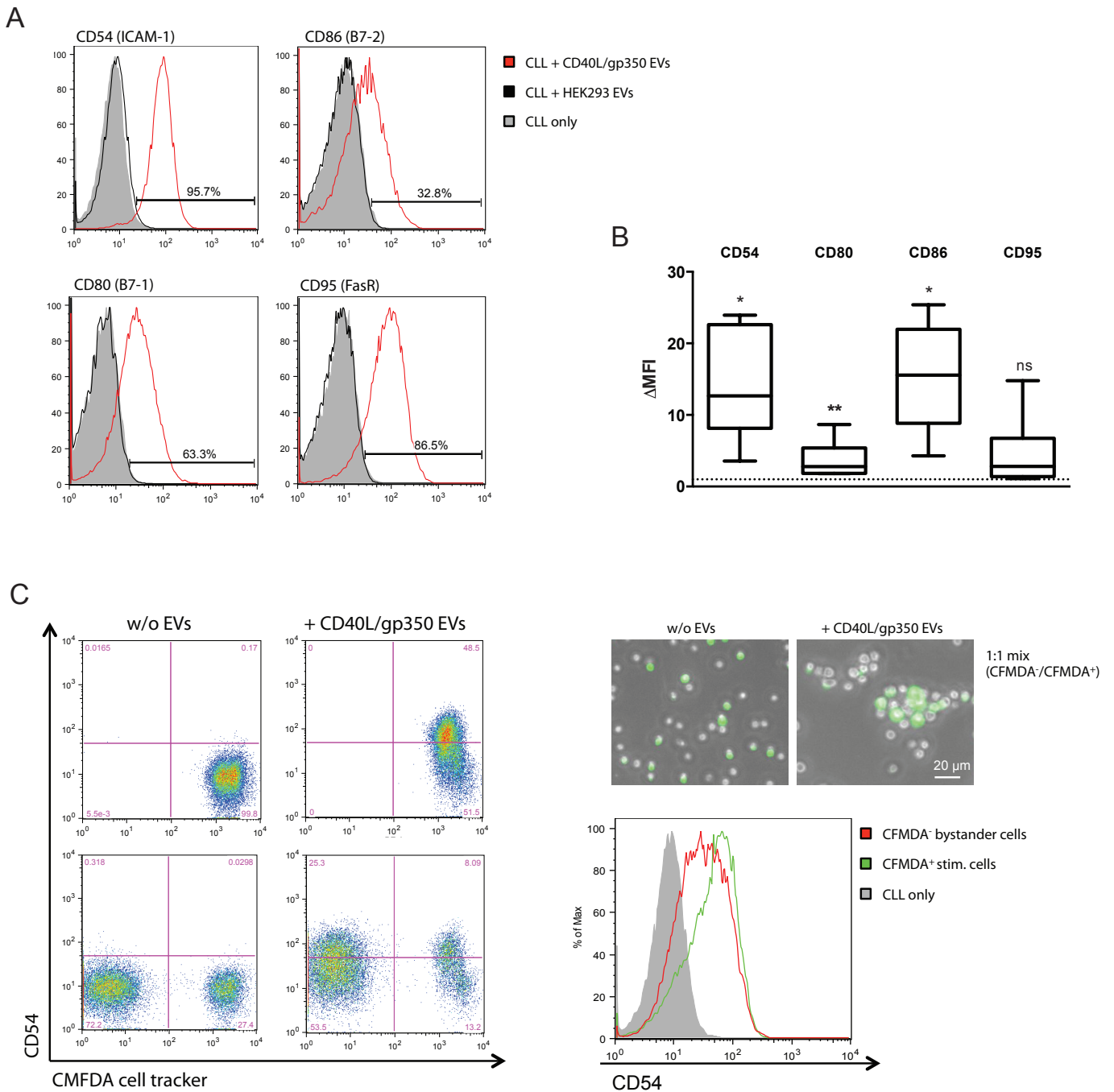


Fig. 5.13: CD40L+ EVs induce expression of cell surface markers in CLL cells

A: Primary CLL cells were incubated with CD40L+/gp350+ EVs, HEK293 control EVs or left untreated. Three days later, changes in expression of the surface molecules CD54, CD86, CD80 and CD95 were analyzed by flow cytometry. Shaded histograms represent untreated cells; black and red open histograms represent cells treated with HEK293 EVs or CD40L+/gp350+ EVs, respectively. One representative donor out of 8 is shown. **B:** Box plot diagrams show the mean fluorescence intensity (MFI) ratio, which represents the up-regulated expression of each indicated surface molecule in CLL cells when incubated with CD40L+/gp350+ EVs for three days versus control HEK293 EVs. The horizontal line in each box represents the median. The boundary of the boxes shows the 25th-75th percentiles, and the whiskers show the highest and lowest Δ MFI value. Each box represents eight CLL donors. Differences with *p<0.05 and **p<0.005, were

considered statistically significant by paired Student's t-test. Ns: not significant. C: CLL cells were labeled with CFMDA cell tracker dye and incubated overnight with CD40L+/gp350+ EVs. The cells were mixed with untreated CFMDA-negative cells and verified by fluorescence microscopy after 24 hours (10x magnification). Furthermore CD54 expression in stained and unstained cells was analyzed by flow cytometry. The green histogram represents EV-stimulated CFMDA-positive cells; the red histogram shows unstained bystander cells.

Engagement of CD40 on B cells regulates a wide spectrum of molecular and cellular processes including the induction of adaptive immune responses. The downstream signaling pathways initiated by binding of CD40L to CD40 include activation of the noncanonical and canonical NF- κ B pathways and the mitogen-activated protein (MAP) kinases ERK and JNK [173,180].

Western blot analysis of CLL cell lysates showed that treatment with CD40L+/gp350+ EVs did not alter the level of ERK1/2 or JNK protein, but induced ERK and JNK phosphorylation already within 20 minutes (Fig 5.14). This indicates that CD40L transferred by EVs efficiently triggers CD40 downstream signaling pathways.

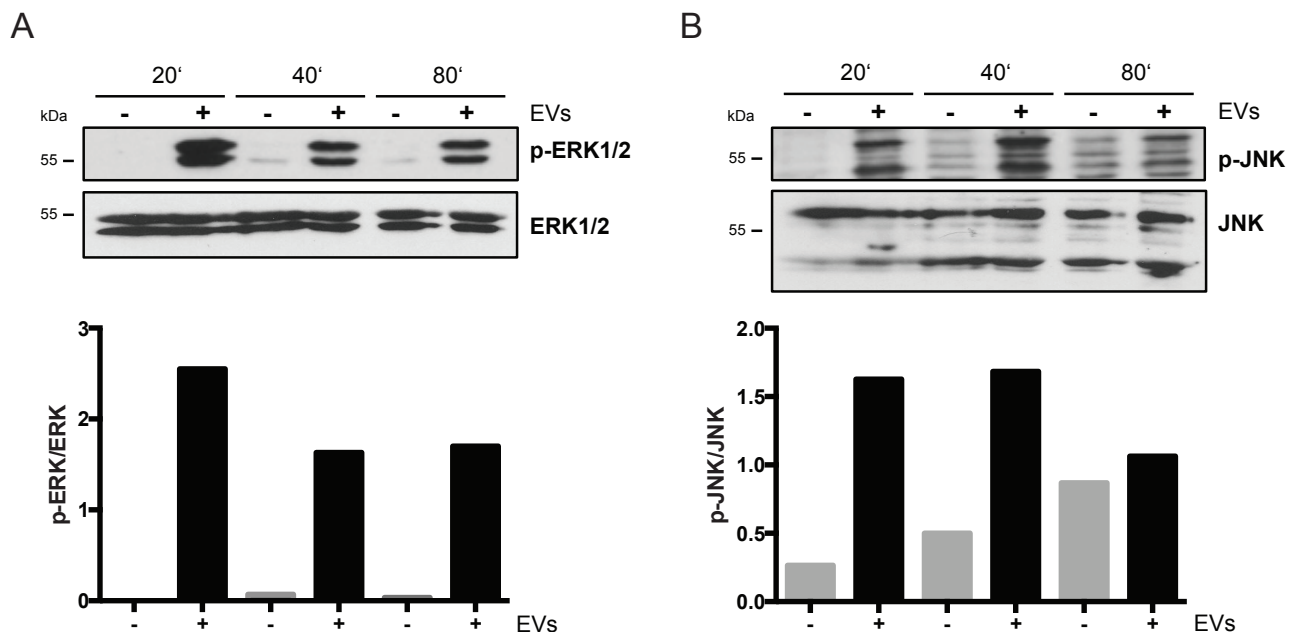


Fig. 5.14: CD40L+ EVs trigger the ERK/JNK pathway in primary CLL cells

Western Blot and densitometric analysis of ERK1/2 (A) and JNK (B) phosphorylation in untreated CLL cells or cells treated with CD40L+/gp350+ EVs. Cell lysates were prepared after 20, 40 and 80 minutes of incubation. The levels of phosphorylation were calculated by densitometry as the band intensity ratio of p-ERK/ERK and p-JNK/JNK, respectively (lower panels).

5.3.6 CLL cells stimulated with CD40L+ EVs become efficient APCs

In the next step, it was investigated whether CLL cells reactivated by CD40L+ EVs are functional antigen-presenting cells (APCs) and consequently are able to interact efficiently with T cells. To address this question, a T-cell assay with a gp350-specific HLA DR13-restricted CD4+ T cell clone was performed, according to the scheme in Fig. 5.15A. HLA-matched primary CLL cells as well as mini-LCLs, a B-cell line generated by immortalization with an EBV-derived vector, were used as APCs [169]. The cells were incubated overnight with different EVs (Fig. 5.15B). Additionally, HLA mismatched LCLs and CLL cells were used as negative controls. The EV-loaded cells were incubated with T cells at a 1:1 ratio for 24 hours and IFN γ in the cell culture supernatants was measured by ELISA. As expected, HLA-matched mini-LCLs loaded with gp350+ EVs induced IFN γ secretion. HLA-matched primary CLL cells were not able to induce T cell activation when gp350+ EVs were used. However, EVs positive for both gp350 and CD40L significantly increased IFN γ secretion, pointing out the crucial role of CD40L for the antigen-presenting capacity of CLL cells.

Taken together, these findings clearly showed that engineered extracellular vesicles are effective tools to specifically target cells, induce cellular signaling pathways and transfer antigens. CD40L+/gp350+ EVs successfully restored the antigen-presenting function of CLL cells directly as well as indirectly in bystander cells.

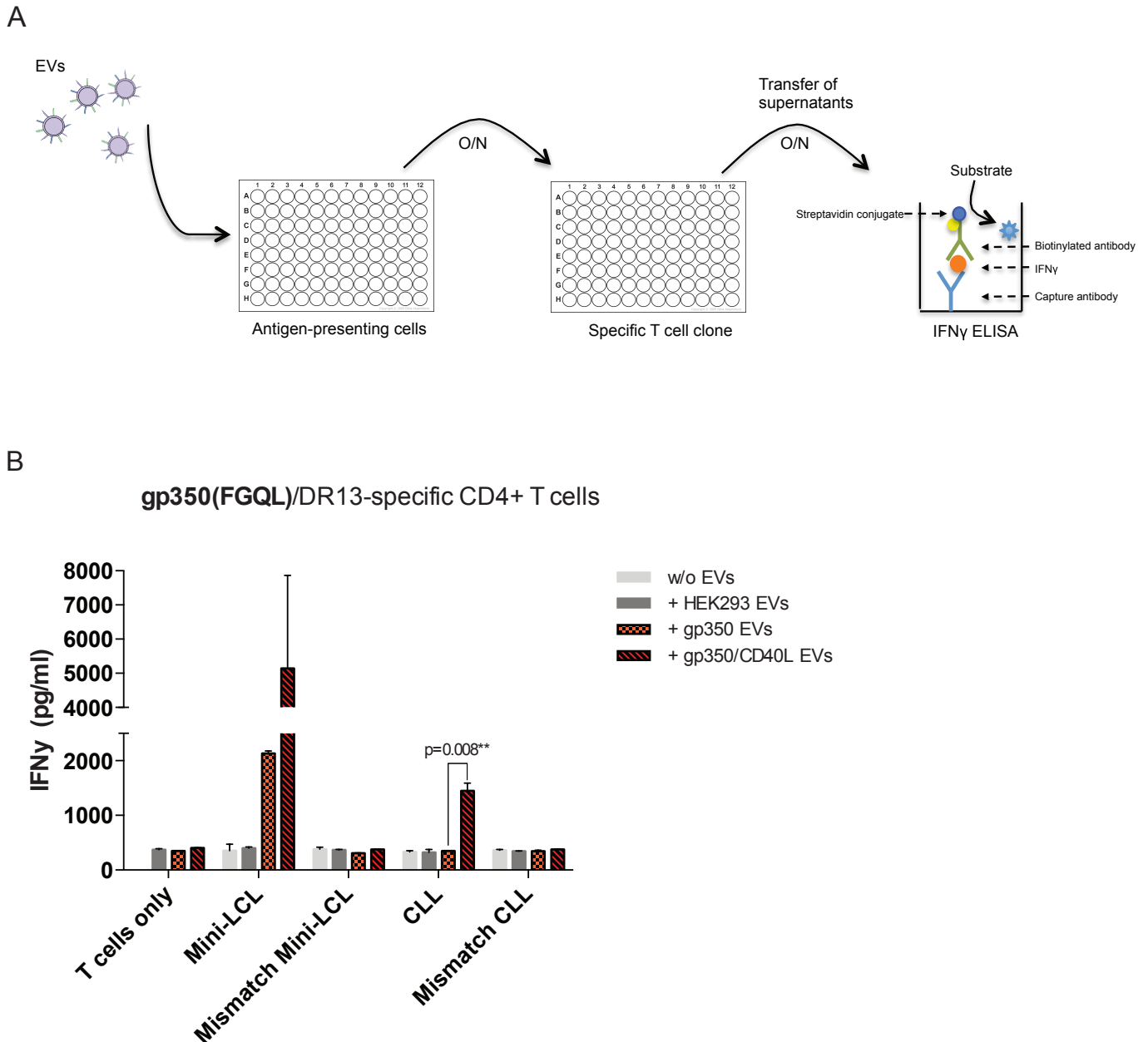


Fig. 5.15: CD40-stimulated CLL become immunogenic for CD4+ T cells

A: Schematic representation of an EV/T-cell assay. Antigen-presenting cells were incubated overnight with EVs and on the next day mixed with an HLA-matched T-cell clone. After 24 hours the supernatants were collected and T-cell activation was measured by enzyme-linked immunosorbent assay (ELISA). B: HLA-DR13+ Mini-LCLs and primary CLL cells, as well as mismatched control cells, were used as APCs and incubated with different EVs, as indicated. After coincubation with HLA-DR13-restricted gp350-specific CD4+ T cells, IFN γ secretion was measured by ELISA. P value was calculated by the two-tailed Student's *t* test.

5.4 Redirection of CMV-specific immunity towards CLL cells

In CLL patients the overall T-cell repertoire is functionally impaired and displays increased expression of inhibitory molecules and defects in cytokine production, immune synapse formation and cytotoxicity. Nevertheless clinically relevant reactivations of latent CMV infections in untreated CLL are rare, most likely because T-cell numbers of functionally intact CD4⁺ and CD8⁺ CMV-specific T cells are significantly increased in CLL, thus maintaining the anti-viral immunity efficiently [141,142].

The previous chapters confirmed that CD40L⁺/gp350⁺ EVs are effective tools for enhancing the poor antigen-presenting capacity of CLL cells. It was therefore investigated next whether EV-stimulated CLL cells can activate allogeneic and autologous CD4⁺ and CD8⁺ T cells. Particularly, CMV-specific T cells in CLL samples were targeted by EVs carrying the highly immunogenic CMV protein pp65.

5.4.1 EV-associated pp65 stimulates CMV-specific T cells

The CMV tegument protein pp65 was integrated into EVs by overexpressing the protein in HEK293 cells. As previously described, EVs were isolated from conditioned cell cultured media by differential centrifugation and subsequent density gradient fractionation (5.1). Pp65 was detected by Western blotting mainly in the gradient fractions 2, 3 and 4, thus co-migrating with the EV marker CD63 (Fig. 5.16A). In addition pp65 mRNA was detected in pp65 expressing HEK293 cells and EVs secreted by these cells (Fig. 5.16B).

To analyze the reactivation of pp65-specific immunity, different engineered EVs positive or negative for pp65, CD40L and gp350, were used to stimulate pp65-specific CD4⁺ and CD8⁺ T-cell clones (Fig. 5.16C,D). The EVs were incubated with HLA-matched LCLs or mini-LCLs overnight, as described in 5.3.6. As expected, only CD40L⁺/gp350⁺/pp65⁺ EVs were able to efficiently induce IFN γ release in the T cells in a dose-dependent manner. EVs negative for gp350 were less effective, most likely due to reduced binding affinity to the LCLs. Furthermore, EVs per se did not induce T-cell stimulation. Once activated, CD8⁺ T cells secrete cytotoxic granules containing granzyme and perforin molecules to kill target cells, e.g. virus-infected cells or tumor cells. Especially granzyme B has a strong proapoptotic function and mediates rapid cell death of target cells [181]. Secretion of granzyme B by the CD8⁺ T-cell clone was induced by stimulation with LCLs

loaded with CD40L+/gp350+/pp65+ EVs, indicating that these EVs were efficiently activating cytotoxic CD8+ T cells (Fig. 5.16D).

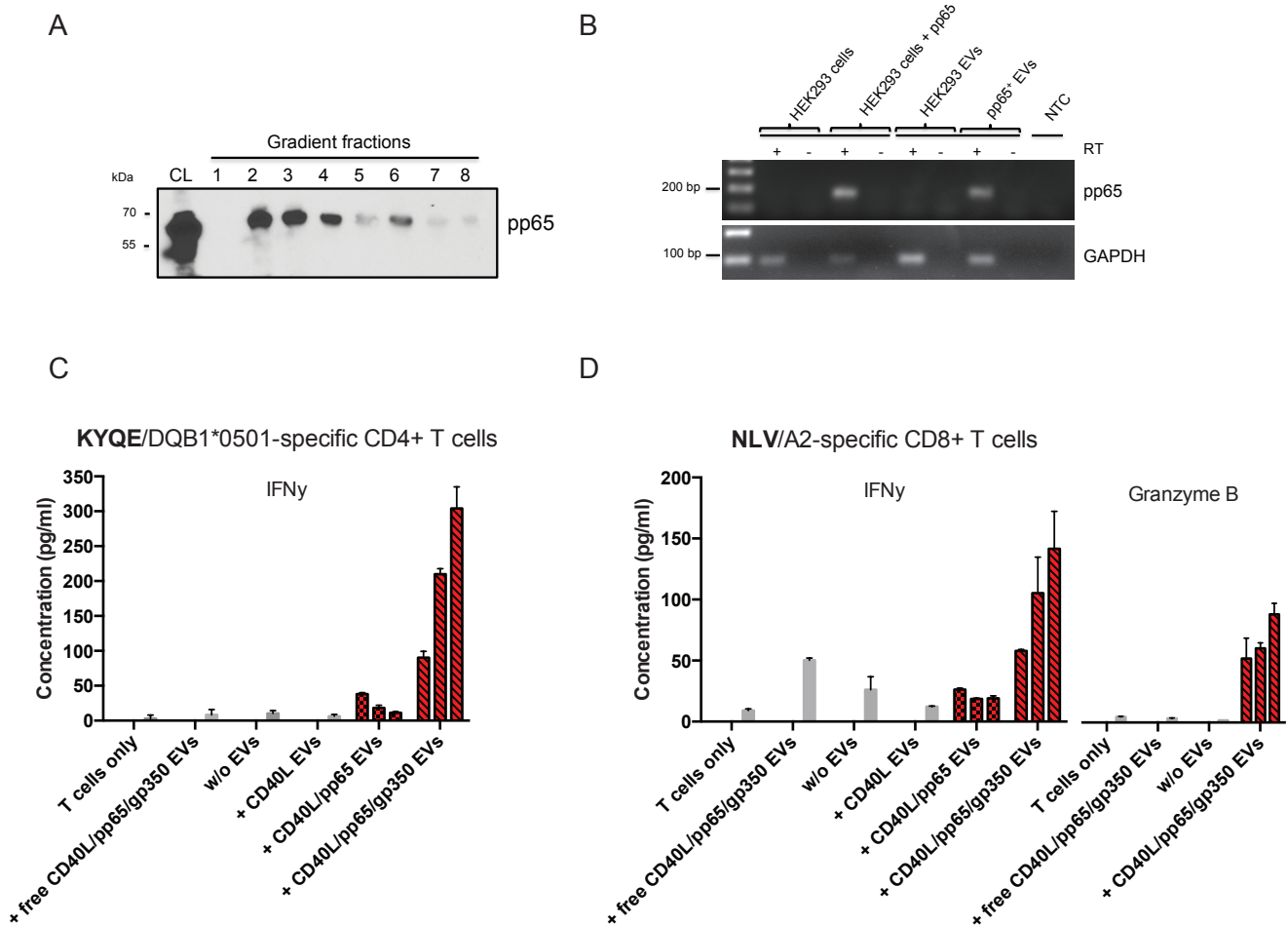


Fig. 5.16: CMV antigen pp65 is incorporated into HEK293-derived EVs and induces specific CD4+ and CD8+ T cells responses

A: HEK293 cells were transiently transfected with a pp65 expression plasmid and EVs were isolated three days later by serial centrifugation and density gradient fractionation as described in 5.1. Eight fractions were collected and analyzed for pp65 by Western blotting. CL: cell lysate. B: EVs derived from HEK293 cells overexpressing pp65 contain pp65 mRNA, as confirmed by RT-PCR using pp65-specific primers and cDNA isolated from HEK293 and the corresponding EVs. GAPDH mRNA was detected in both EVs from untransfected and transfected HEK293 cells. C: HLA-DQB1+ mini-LCLs were incubated overnight with 1000 ng of different types of EVs, as indicated. CD40L+/pp65+ and CD40L+/gp350+/pp65+ EVs (red bars) were applied in three different concentrations (250 ng, 500 ng, 1000 ng). EV-loaded mini-LCLs were cocultured with an HLA-DQB1-restricted pp65-specific CD4+ T-cell clone at a 1:1 ratio. As control, T cells were incubated alone or with 1000 ng of CD40L+/gp350+/pp65+ EVs in the absence of LCLs ('free' EVs). After 16 hours IFN γ secretion was measured by ELISA. D: HLA-A2+ LCLs were used for stimulation of an HLA-A2-restricted pp65-specific CD8+ T-cell clone. The same settings as in (C) were used. The concentrations of IFN γ and granzyme B in the supernatants were measured by ELISA.

When EVs are internalized by phagocytic cells, they are delivered to phagolysosome compartments, whereby the presentation of EV-associated antigens on MHC class II molecules is favored [57]. However, as demonstrated in figure 5.16D, engineered pp65+ EVs also induce pp65-specific CD8+ T-cell responses. This can be explained by the fact that these EVs not only contain pp65 protein but also pp65 mRNA (Fig. 5.16B). When delivered to target cells these mRNA molecules are presumably translated into functional proteins and, consequently, presented on MHC class I molecules. Moreover, it is also possible that antigens delivered by EVs are cross-presented by APCs, a mechanism that allows exogenous antigens to enter the MHC class I pathway. Cross-presentation is of particular importance for therapeutic vaccines that need to stimulate humoral and cellular immune responses, especially MHC class I-restricted CD8+ T cells. Since it was demonstrated in chapter 5.3.3 that delivery of functional mRNA by HEK-derived EVs to B cells is possible, but a rather rare event, it can be assumed that both pp65 mRNA and pp65 protein enter the target cell, are processed and contribute to the induction of specific CD8+ T-cell responses.

Next it was investigated whether primary CLL cells can equally function as APCs for the stimulation of CMV-specific T cells. CLL cells were isolated from peripheral blood samples from previously untreated CLL patients. Plasma was used for the detection of the patients' CMV status by a commercial CMV IgG ELISA kit. 15 out of 24 CLL patients (62.5%) were found to be CMV-seropositive. CLL cells of CMV-negative donors were pretreated with NLV peptide or increasing amounts of CD40L+/gp350+/pp65+ EVs, washed and incubated with allogeneic pp65-specific CD8+ T cells in an IFN γ ELISPOT setting (Fig. 5.17). Generally speaking ELISPOT is a highly sensitive method that, in contrast to ELISA, detects cytokine-producing cells at the single cell level. Furthermore this technology permits direct enumeration of even low frequencies of antigen-specific T cells and for this reason was used in the following experiments. LCLs matching the HLA type of the T cells, as well as mismatched CLL cells, were used as positive and negative control, respectively. Unspecific activation of the T cells by TPA/ionomycin treatment confirmed their functionality. The spot-forming units (SFU) of duplicates were enumerated (Fig. 5.17B).

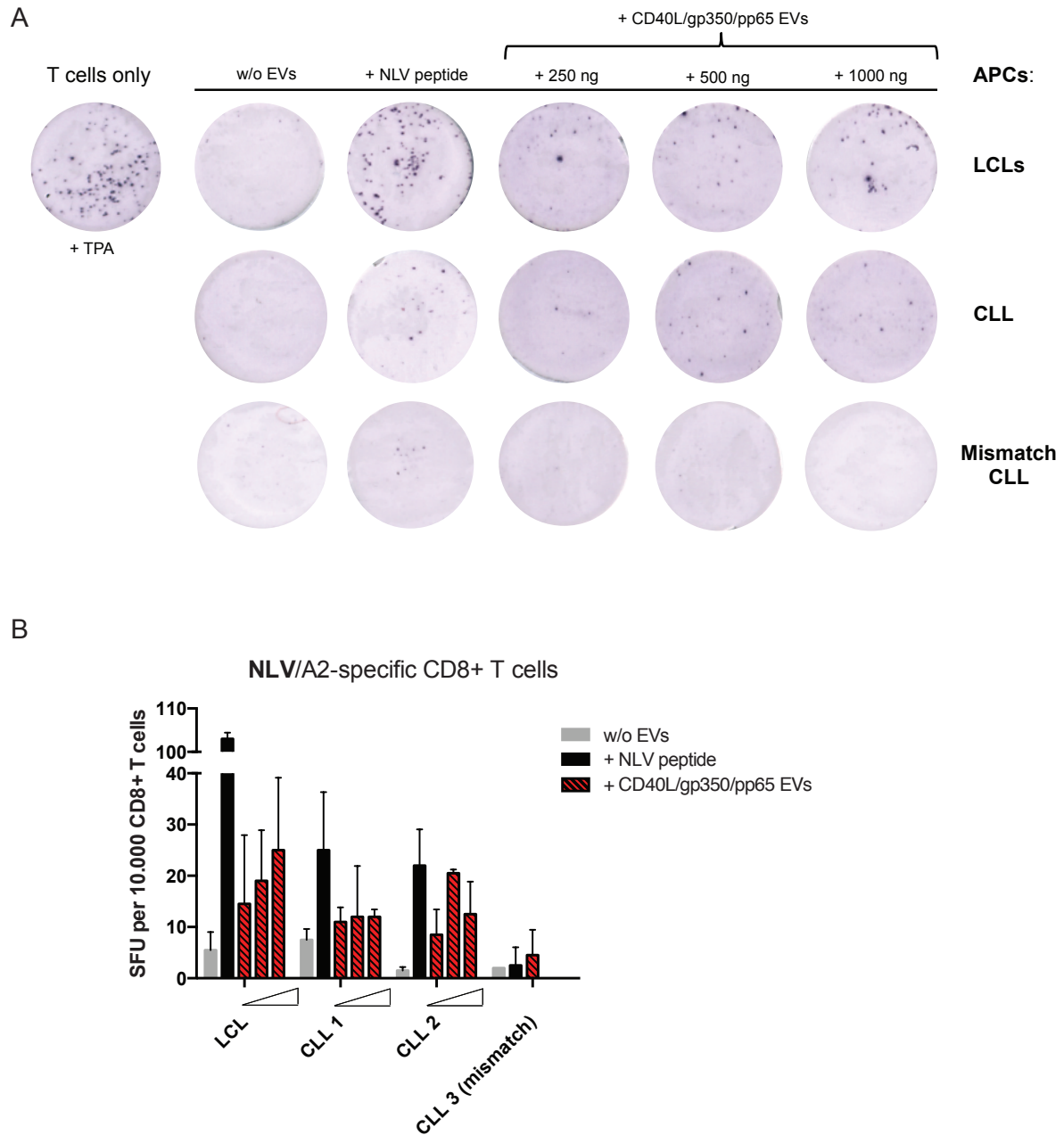


Fig. 5.17: EV-loaded CLL cells stimulate allogeneic pp65-specific CD8+ T cells

A: Representative wells of an IFN γ ELISPOT assay. LCLs or primary CLL cells were loaded with increasing amounts of CD40L+/gp350+/pp65+ EVs and co-cultured with a HLA-A2-restricted pp65-specific CD8+ T-cell clone (10,000/well) at a 1:1 ratio for 16 hours. Wells containing T cells stimulated with TPA/ionomycin and T cells co-cultured with unloaded APCs served as controls. Furthermore HLA-mismatched CLL cells were used to confirm the specificity of the assay. One representative well for each condition is shown. B: CLL cells from two HLA-A2+ patients were used, whereas CLL 3 was from an A2-negative donor. Mean \pm SD of IFN γ spot forming units (SFU)/10,000 T cells was enumerated in duplicates.

The ELISPOT assay showed that both LCLs and primary CLL cells preincubated with NLV peptide or CD40L+/gp350+/pp65+ EVs served as APCs for the stimulation of pp65-specific CD8+ T cells. However, the efficiency of CLL cells to induce IFN γ spot-forming units was lower in comparison to LCLs. As expected, HLA-mismatched CLL cells did not induce IFN γ secretion by T cells.

5.4.2 EV-associated pp65 stimulates autologous pp65-specific T cells in CLL

Next, the question was addressed, whether also EV-loaded CLL cells are able to stimulate autologous T cells. First, the presence of pp65-specific T cells in the blood of CMV-seropositive CLL patients was analyzed by staining CLL cells with a pp65-derived NLV/HLA-A2 pentamer (Fig. 5.18A). Three patient samples were selected that contained 1.8%, 5.4% and 9.5% NLV-specific T cells in the CD8+ T-cell pool, as indicated in Table 4.

Table 4: Frequency of CD4+, CD8+ and pp65/NLV-specific T cells in three CLL patients

Sample	CD4+ (%)	CD8+ (%)	% NLV-specific CD8+ (within CD8+ pool)
CLL 4	3.0	2.0	0.186 (9.5)
CLL 5	1.7	2.2	0.040 (1.8)
CLL 6	4.7	4.2	0.21 (5.0)

The CLL cells were incubated with CD40L+/gp350+/pp65+ EVs overnight in IFN γ ELISPOT microwells. As a positive control, the cells were challenged with TPA or NLV peptide. The results of the ELISPOT assay showed that functional pp65-specific T cells were present in the blood of CLL patients and that these cells became activated by CLL cells loaded with CD40L+/gp350+/pp65+ EVs or NLV peptide (Fig. 5.18B). Incubation with HEK293 control EVs did not result in spot formation and thus in T-cell activation.

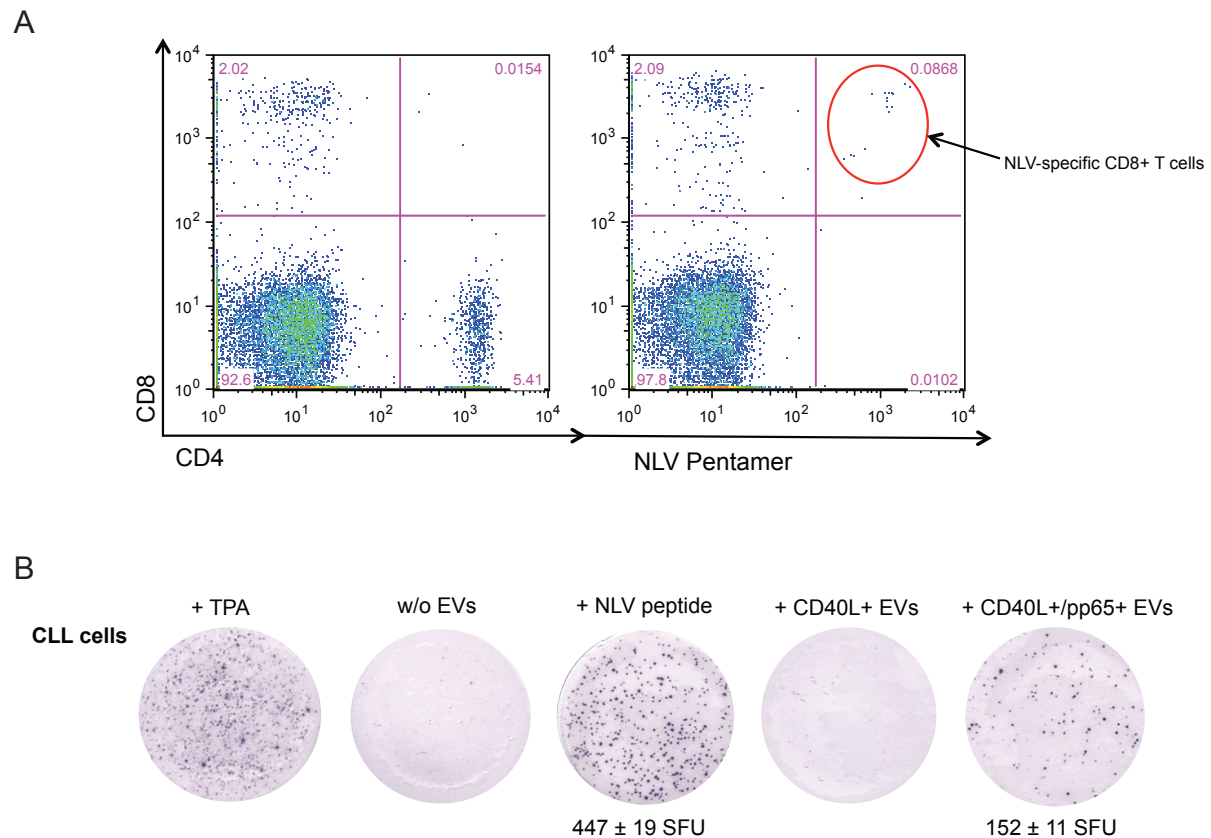


Fig. 5.18: Pp65-specific T cells in CLL are stimulated by pp65+ EVs

A: PBMCs from HLA-A2+ CLL patients were stained with antibodies against CD4 and CD8 or the HLA-A2.1/NLV pentamer and analyzed by flow cytometry. Results from one representative donor are shown. B: CLL cells from CMV-positive patients were seeded in IFN γ ELISPOT microwells (500,000 cells/well) and challenged with TPA/ionomycin, NLV peptide or different EVs, as indicated. SFU: spot-forming unit.

5.4.3 Enrichment of CLL-derived T-cell populations by EV stimulation

PBMCs isolated from three HLA-A2+, CMV+ CLL patients were treated with different EVs in the presence of IL-2. After seven and 14 days the cells were restimulated with EVs, and fresh medium supplemented with IL-2 was added.

The PBMC samples contained $4.91\% \pm 2.94\%$ T cells on day 0. After 20-30 days the cells were harvested and analyzed by flow cytometry. As indicated in Fig. 5.19 no viable cells could be detected after 30 days in the absence of EV stimulation or when stimulated with HEK293 control EVs. In contrast, stimulation with CD40L+/gp350+/pp65+ EVs promoted survival of the cells. The living cells almost exclusively contained CD4+ and CD8+ T cells (range 64 – 94%, Fig 5.19B). Furthermore numbers of CD8+ T cells specific for the pp65-derived peptide NLV were enriched, thus identifying EVs as HLA-

independent powerful tools for stimulation and enrichment of specific T-cell subpopulations (Fig. 5.19A, lower panel).

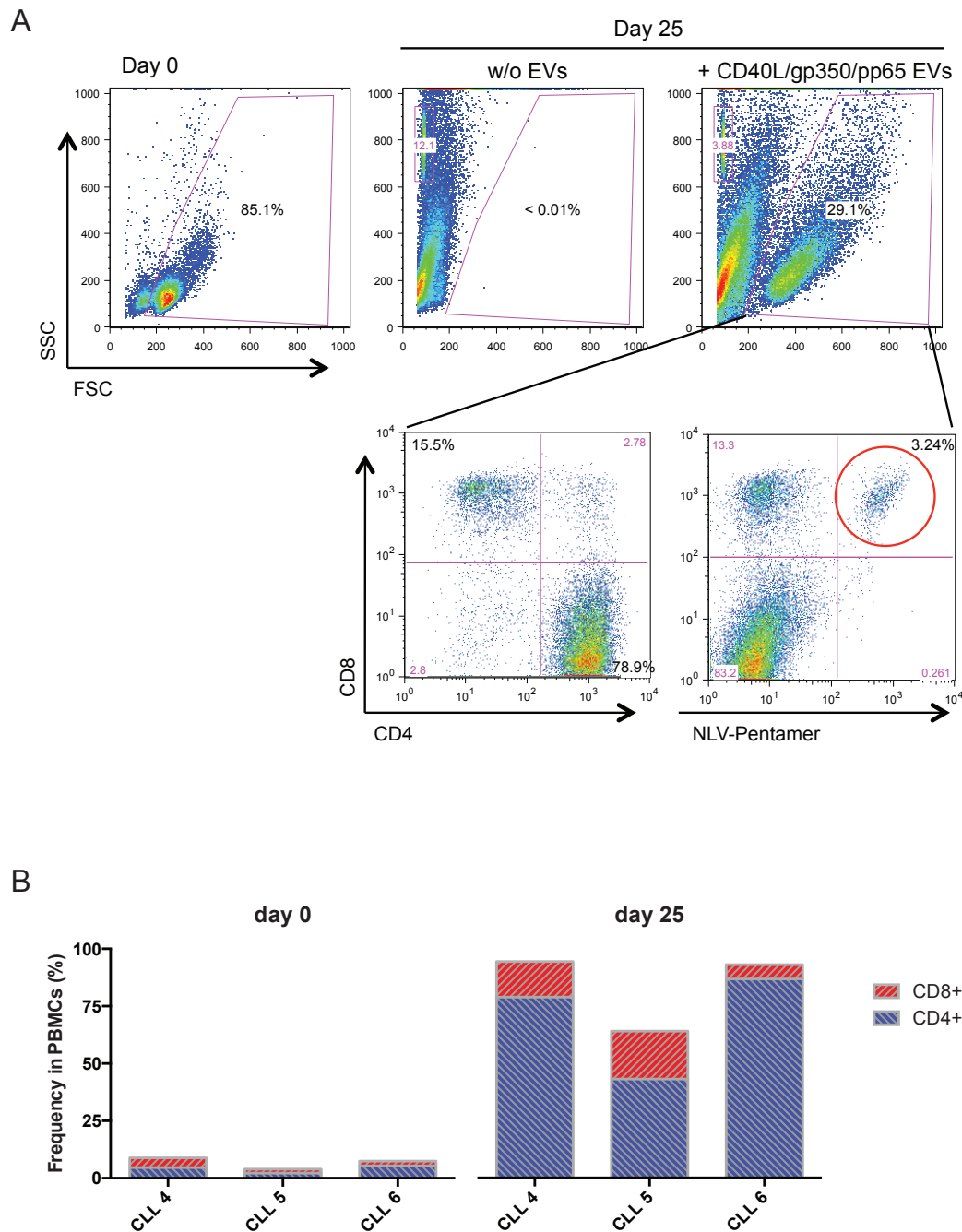


Fig. 5.19: EV-mediated expansion of CD4+ and CD8+ T cells in CLL

PBMCs were isolated from peripheral blood samples of three CLL donors. At day 0, the samples contained 8.9, 3.9 and 7.4% CD4+/CD8+ T cells. A: Forward scatter and sideward scatter plot of CLL cells from one patients recorded at day 0 and at day 25. Without EV treatment no viable cells were detectable after 25 days. Repetitive stimulation with CD40L+/gp350+/pp65+ EVs promoted cell survival. These enriched cells were staining with CD4- and CD8-specific antibodies and the NLV pentamer B: Frequency of CD4+ and CD8+ T cells in three CLL donors measured at day 0 and at day 25 by flow cytometry. The frequency of T cells within the total cell population is shown.

To further investigate the specificity of EV-enriched effector cells, they were mixed on day 20 with freshly thawed autologous CLL target cells loaded with EVs, a pp65 peptide pool or an Adenovirus-derived control peptide pool (Adv3). Target and effector cells were incubated at two different ratios and secretion of IFN γ and granzyme B was analyzed in an ELISPOT (Fig. 5.20). Enumeration of spot-forming units showed that CLL cells loaded with a pp65 peptide mix induced a higher IFN γ secretion than CLL cells loaded with the control peptide pool Adv3. Also treatment with CD40L+/gp350+/pp65+ EVs resulted in a higher number of SFUs compared to incubation with pp65-negative EVs, indicating that pp65-specific T cells are present in the effector cell population (Fig. 5.20A). Effector cells or target cells alone did not result in SPUs (not shown). Treatment of target cells with the MHC class II blocking antibody L243 prior to loading with pp65 peptides reduced the number of IFN γ -secreting effector cells (Fig. 5.20B). In contrast, an effect of the MHC class I blocking antibody W6/32 on IFN γ -secreting cells was not observed, thus identifying CD4+ T cells as major effector T cells. However, measurement of granzyme B secretion showed clearly that target cells loaded with either pp65 peptides or CD40L+/gp350+/pp65+ EVs amplify granzyme B secretion of effector cells and therefore indicated that functional pp65-specific cytotoxic T cells are present (Fig. 5.20C).

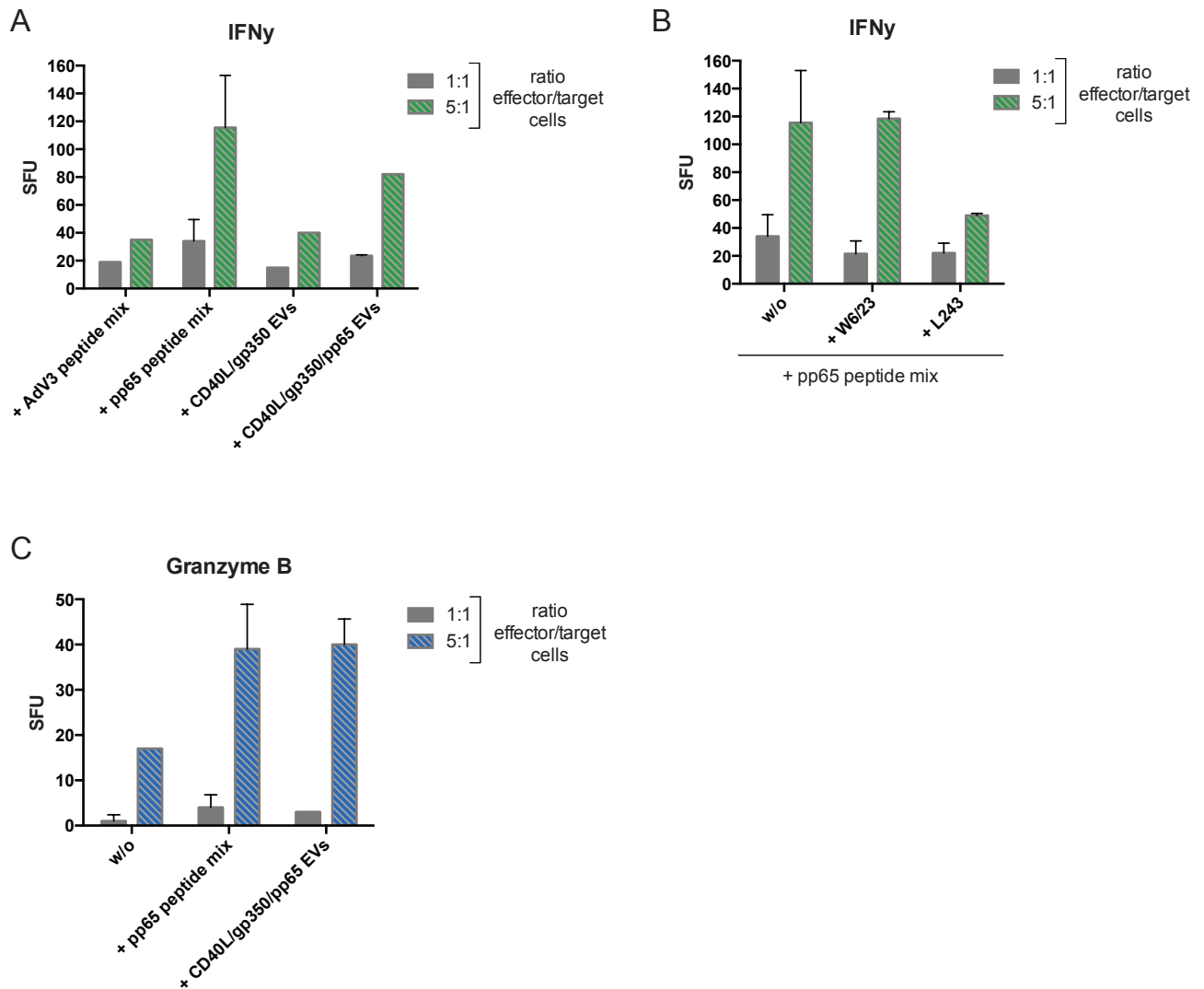


Fig. 5.20: T cells enriched by stimulation with CD40L+/gp350+/pp65+ EVs are functional effector cells

PBMCs isolated from a CMV-positive CLL patient were treated with CD40L+/gp350+/pp65+ EVs and IL-2 (20 U/ml) in order to enrich specific effector cells. Addition of EVs was repeated after 7 days and half of the medium was replaced by fresh medium containing IL-2. After 20 days of incubation autologous CLL cells were thawed and loaded overnight with EVs or the indicated peptide pools (0.5 $\mu\text{g}/\mu\text{l}$ final conc. of each peptide). These target cells were mixed with the effector cells at 1:1 and 1:5 ratios. IFN γ (A,B) and granzyme B (C) secretion was measured by ELISPOT. Mean \pm SD of IFN γ spot forming units (SFU)/10,000 target cells was enumerated in duplicates. B: The CLL target cells were incubated with the MHC class I blocking antibody W6/32 or the MHC class II blocking antibody L243 for 30 minutes prior to pp65 peptide loading.

5.5 Development of a novel *in vivo* model to evaluate an EV-based immunotherapy for CLL

The previous *in vitro* experiments revealed that CD40L+/gp350+/pp65+ EVs are effective tools to target and activate CMV-specific immunity in CLL patients. Next, the potential of these engineered EVs as immunotherapeutic agents was evaluated in a novel *in vivo* model. Because CLL is a very heterogeneous disease, comprising different genetic aberrations and variably regulated leukemia-associated genes, *in vivo* studies remain challenging. Several transgenic mouse models for CLL have been described; the best-studied one is known as E μ -TCL-1 and mimics an aggressive form of CLL. In those mice, the T-cell leukemia-1 (*TCL-1*) oncogene, a critical molecule in the pathogenesis of CLL, is highly expressed in the B-cell compartment of spleen and bone marrow [182]. As a consequence, E μ -TCL-1 mice develop a lymphoproliferative disease that is similar to human CLL and therefore represent an adequate animal model system [182-184].

However, mice are in general not susceptible to infection with human herpesviruses and therefore lack T cells specific for these viruses (which are a prerequisite for our immunotherapeutic strategy). Therefore, to translate our EV-based immunotherapeutic strategy into an *in vivo* system at the best possible rate, wild-type female C57BL/6 mice first were immunized with EVs carrying murine CD40L (mCD40L) and gp350 (mCD40L+/gp350+) or pp65 (mCD40L+/pp65+), in order to induce immune responses specific for these viral antigens (Fig. 5.21). The control groups were treated with mCD40L+ EVs or PBS. All mice were boosted six weeks later. After one more week, a murine CD19+/CD5+ CLL cell clone derived from the spleen of a leukemic E μ -TCL-1 mouse was loaded *ex vivo* with gp350- and pp65-derived peptide pools and injected intraperitoneally (IP) into all C57BL/6 mice. Humoral and cellular immune responses against EV-associated antigens were analyzed and the engraftment of CLL cells was monitored over time, in order to investigate whether a pre-existing immunity against gp350 or pp65 hampers the cell growth.

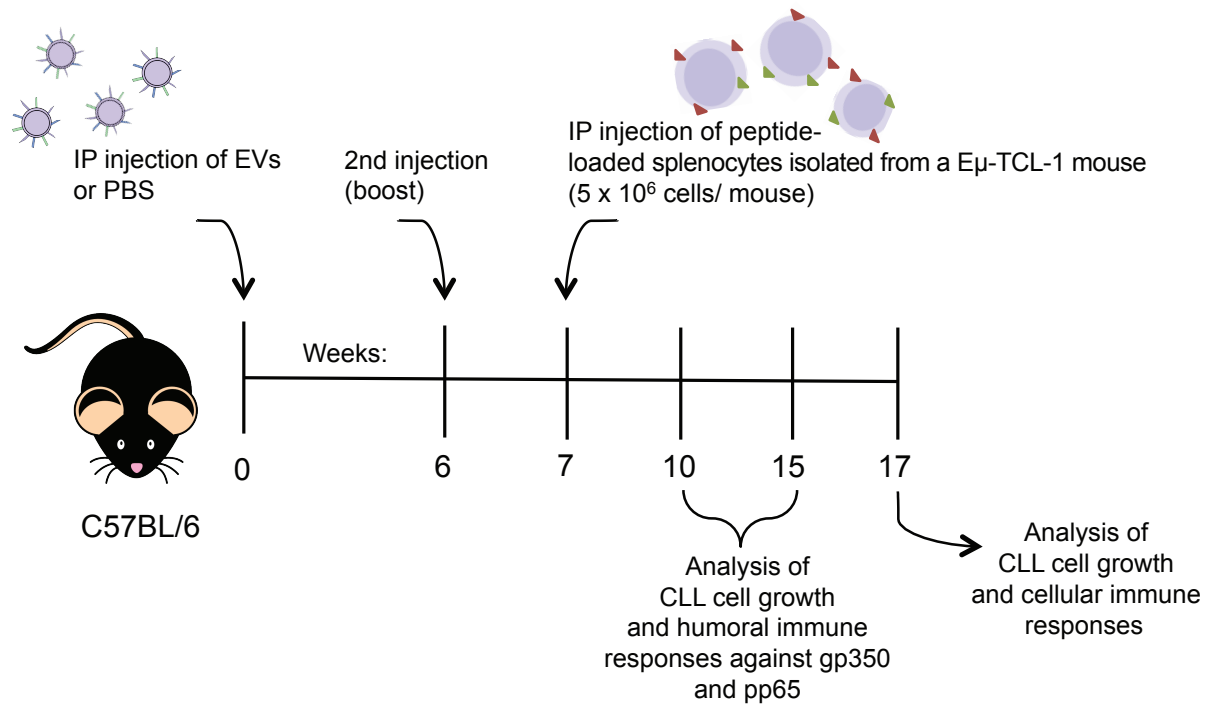


Fig. 5.21: Experimental strategy for evaluation of immunotherapeutic EVs *in vivo*

The experiments were performed in collaboration with the University Hospital of Cologne, where the mice were maintained and immunized. Preparation of recombinant EVs, the analysis of serum antibody levels and data analysis were carried out in Munich, recording of flow cytometry data was performed in Cologne. IP: intraperitoneal.

5.5.1 Humoral immune responses against mCD40L+/gp350+ and mCD40L+/pp65+ EVs

Sera from immunized C57BL/6 mice were collected 15 weeks after the first EV injection and antibodies against gp350 and pp65 were measured by ELISA (Fig. 5.22). For this purpose the ELISA plates were coated with purified recombinant gp350 or pp65 protein and serum samples in three different dilutions were added. High concentrations of gp350-specific antibodies were present in all mice immunized with mCD40L+/gp350+ EVs, but not in control mice (Fig. 5.22A). In contrast, antibodies against pp65 were only detectable in the serum of one (#11) out of three mice that had been immunized with mCD40L+/pp65+ EVs (Fig. 5.22B). These results can presumably be ascribed to the fact that gp350 is a highly immunogenic glycoprotein present on the surface of gp350+ EVs (5.3.1), whereas pp65 is a viral tegument protein. Although this protein was detected in pp65+ EVs by Western blotting (5.4.1), it is likely that pp65 is located within EVs, as it is in CMV virions. Therefore pp65 may not be accessible to B-cell recognition.

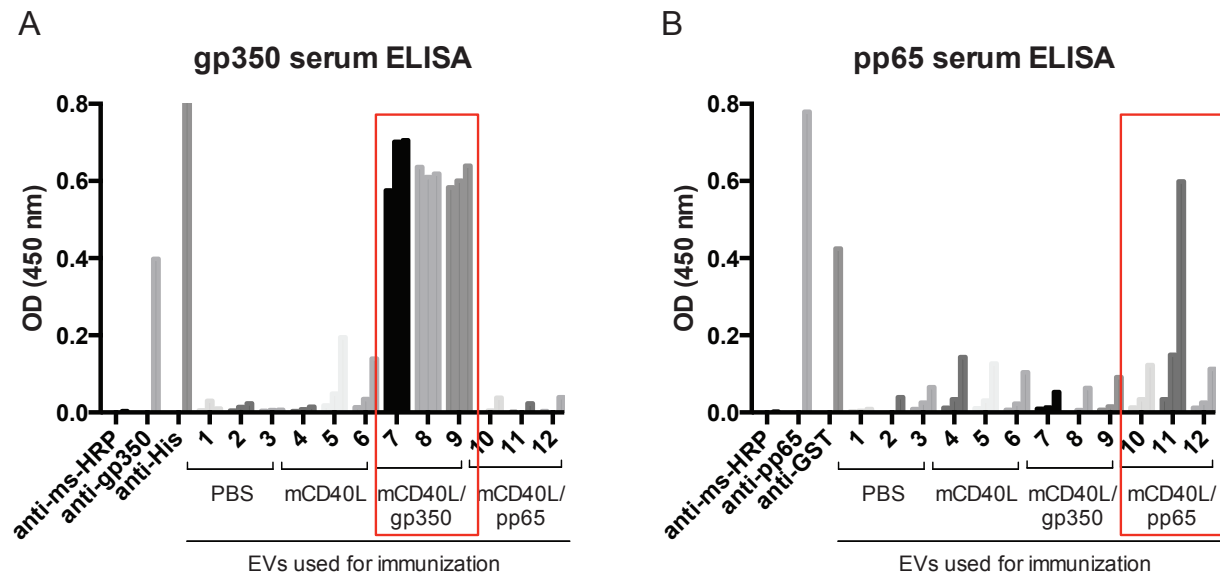


Fig. 5.22: Detection of specific antibodies against EV-associated gp350 and pp65 in the sera of immunized C57BL/6 mice

ELISA plates were coated with recombinant His-tagged gp350 or GST-tagged pp65 protein. Sera of 12 C57BL/6 mice were added at three different dilutions (1:1000, 1:250, 1:50) and gp350 (A) or pp65 (B) antibodies were detected by sandwich ELISA, using an HRP-coupled anti-murine IgG antibody. As positive controls, gp350-, pp65-, His- and GST-specific antibodies were applied.

5.5.2 Engraftment and proliferation of murine CLL cells

After immunization with EVs, a murine TCL-1 cell clone isolated from the spleen of a leukemic E μ -TCL-1 mouse was loaded *ex vivo* with gp350 and pp65 peptide pools and injected into all C57BL/6 mice at week 7. The numbers of CD5+/CD19+ TCL-1 cells present in the bloodstream were measured 3 and 8 weeks later, in order to analyze engraftment of the malignant cells. As indicated in Figure 5.23, at week 3 the percentage of TCL-1 cells in the blood was ranging from 1.1 – 5%. A lower frequency of TCL-1 cells in mice immunized with mCD40L+/gp350+ and mCD40L+/pp65+ EVs was evident, although this trend did not reach statistical significance due to the small sample size of only three animals per group. After 8 weeks the frequency of TCL-1 cells was very heterogeneous ranging from 1.4 – 66%. In two PBS control mice around 60% of TCL-1 cells were found in the blood, whereas in the third PBS mouse the malignant cells did not proliferate. The average percentage of TCL-1 cells in mice immunized with mCD40L+/gp350+ or mCD40L+/pp65+ EVs was tendentially lower, but also heterogeneous, ranging from two mice in each group showing less than 4% of TCL-1 cells and one mouse with 48 or 37%, respectively. Because the TCL-1 cells were only

loaded with gp350 and pp65 peptides prior to injection, thus presenting the peptides transiently instead of expressing them constitutively, recognition of these cells by gp350-or pp65-specific T cells is only possible for a short period of time. Nevertheless, these preliminary experiments indicate that initial recognition of peptide-loaded murine CLL cells results in delayed growth in mice immunized with mCD40L+/gp350+ and mCD40L+/pp65+ EVs.

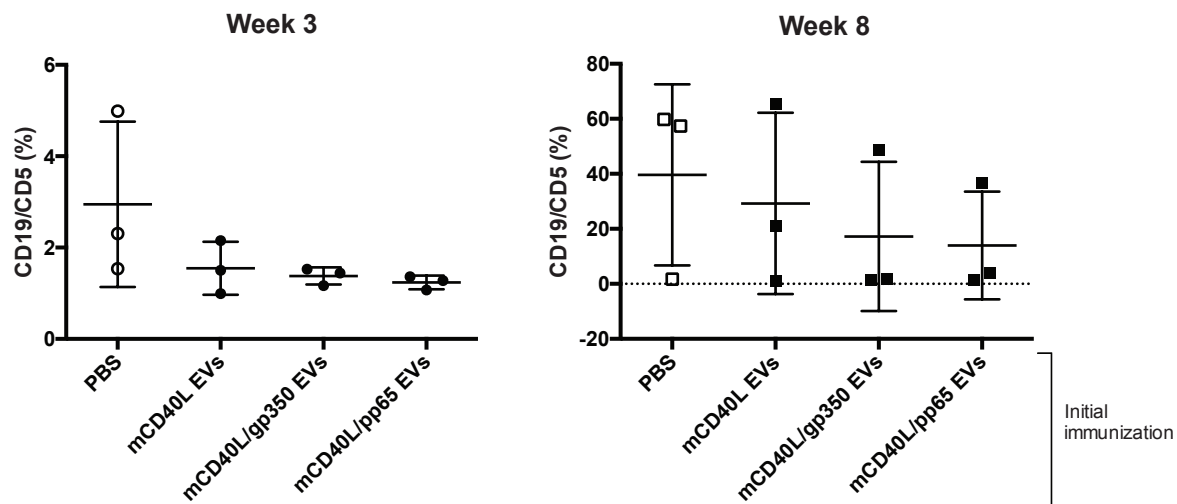


Fig. 5.23: Delayed growth of murine CLL cells in immunized C57BL/6 mice

Blood samples from the tail vein of immunized C57BL/6 mice were collected at weeks 3 and 8 after injection of TCL-1 cells (i.e. 10 and 15 weeks after the first immunization, respectively). The percentage of CD19⁺/CD5⁺ cells was measured by flow cytometry.

5.5.3 Analysis of immune cell subsets in murine splenocytes

10 weeks after injection of TCL-1 cells four C57BL/6 mice that were showing high leukemic blood cell counts were euthanized and the splenocytes were collected and analyzed by multicolor flow cytometry (Fig. 5.24). The numbers of CD19⁺/CD5⁺ TCL-1 cells were similar in all mice, ranging from 87 to 91% (Fig. 5.24B). Interestingly, the numbers of normal CD19⁺ cells, CD3⁺ T cells, NK1.1⁺ natural killer (NK) cells and macrophages (F4/80^{high}/CD11b^{low}) were increased in those mice that had been initially immunized with mCD40L+/gp350+ and mCD40L+/pp65+ EVs compared to the mice treated with PBS or mCD40L+ EVs (Fig. 5.24C). Moreover, immunization with EVs carrying gp350 induced a shift in the CD4/CD8 T-cell ratio. This observation fits to the fact that gp350 mainly elicits humoral and CD4⁺ T-cell responses.

All in all, these *in vivo* experiments indicate that immunization of mice with EVs carrying viral antigens led to an induction of specific humoral and, presumably, also cellular immune responses. As expected, immunization with mCD40L+/gp350+ or mCD40L+/pp65+ EVs prior to injection of peptide-loaded murine CLL cells delayed the proliferation within the first weeks after engraftment, but was not able to inhibit CLL formation completely. This can be most likely be ascribed to the only transient presentation of peptides on the CLL cell surface. Although many open question remain and further investigations that include a larger cohort of mice are surely necessary, these preliminary experiments represent a first proof-of-concept for the evaluation of an EV-based CLL immunotherapy *in vivo*.

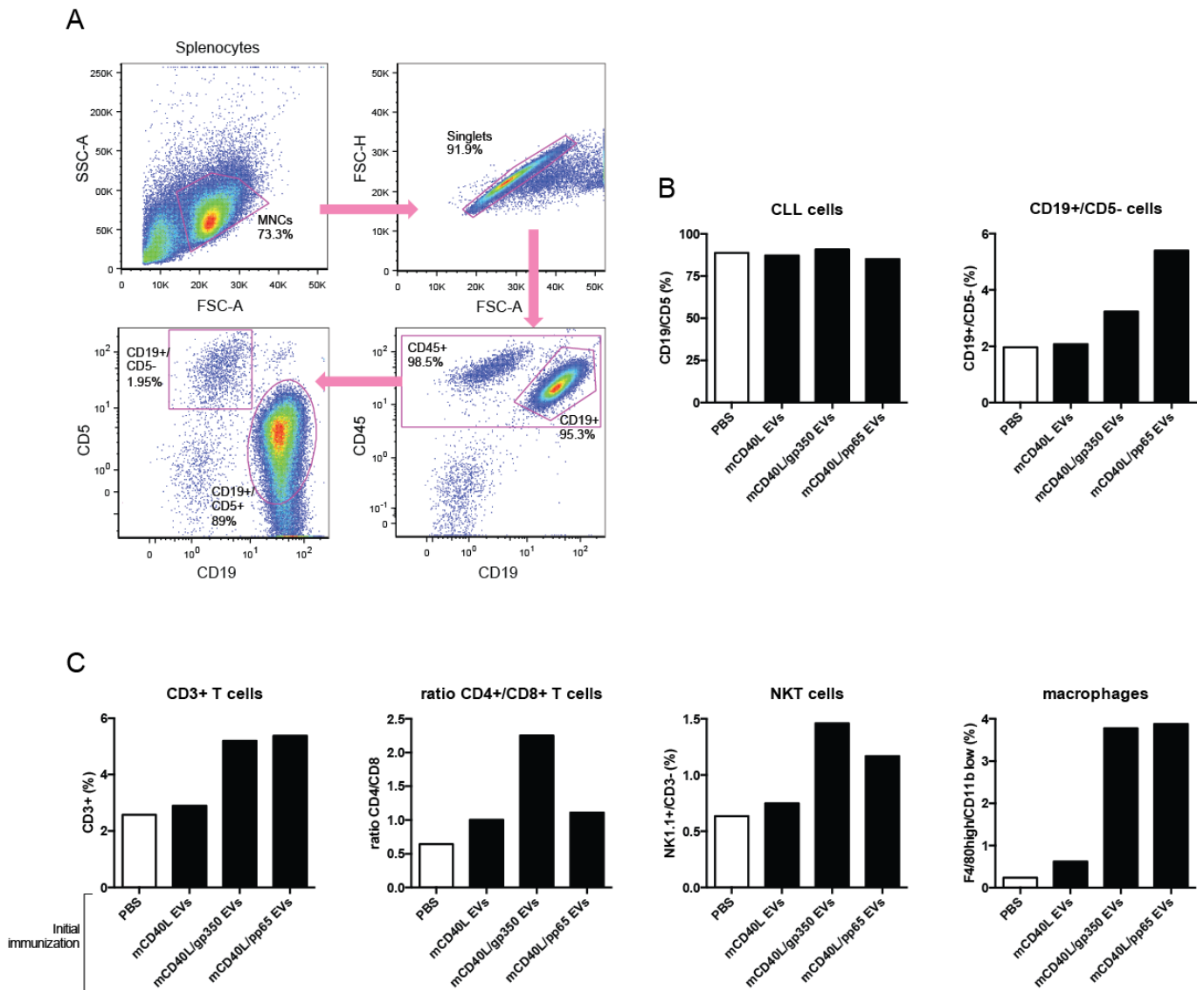


Fig. 5.24: FACS analysis of B- and T-cell subsets in leukemic mice

10 weeks after injection of CLL cells, splenocytes were isolated from four mice and analyzed by antibody staining and multicolor flow cytometry. A: Gating strategy for the detection of CD19+/CD5+ CLL cells. First the splenocytes were gated for mononuclear cells (MNCs) and singlet cells. Next, CD45+ cells were identified and then plotted on a dot-plot of CD19 vs. CD5. B: Comparison of the percentage of CD19+/CD5+ CLL cells and CD19+/CD5- cells in the PBS control mouse and immunized mice. C: The splenocytes were further stained for CD3, CD4 and CD8, or the murine NK cell marker NK1.1 (CD161). Red pulp macrophages were measured based on their expression of MHC II and F4/80, and the absence of CD11b.

5.6 Characterization of EVs by Nanoparticle Tracking Analysis (NTA)

Due to their small size and polydispersity, accurate characterization of EV populations requires a combination of different methods, such as electron microscopy, Western blotting or high-sensitive flow cytometry. However all these techniques display several limitations and do not allow precise EV quantification. For this reason the characterization of nanoparticles in solution by Nanoparticle Tracking Analysis (NTA), which was first commercialized in 2006, has gained increasing attention over the last decade. However, reliability and reproducibility of this novel technique still has to be clarified. NTA is based on a combination of laser light scattering microscopy and a charge-coupled device (CCD) camera. Figure 5.25A shows the setup of the ZetaView NTA instrument, fabricated by Particle Metrix. The hardware consists of a laser illuminated sample chamber and an optical microscope. Both, the laser beam and the microscope move on a motorized carriage along the sample chamber and scan eleven positions, while an auto-focus feature automatically aligns their focal points. The NTA software tracks individual particles that move under Brownian motion and calculates their hydrodynamic radius through the Stokes-Einstein equation (Fig. 5.25B). This formula relates the diffusion constant D of a nanoparticle with radius r undergoing Brownian motion to the viscosity of the fluid in which it is immersed. For accurate particle measurement temperature and viscosity need to be constant.

The following section aimed at evaluating the suitability of NTA for measuring size and concentration of nanoparticles by using (i) polystyrene (PS) standard particles and (ii) HEK293-derived EVs. For all measurement the ZetaView PMX110 instrument was used, which enables detection of nanoparticles with a size ranging from 50 to 1000 nm.

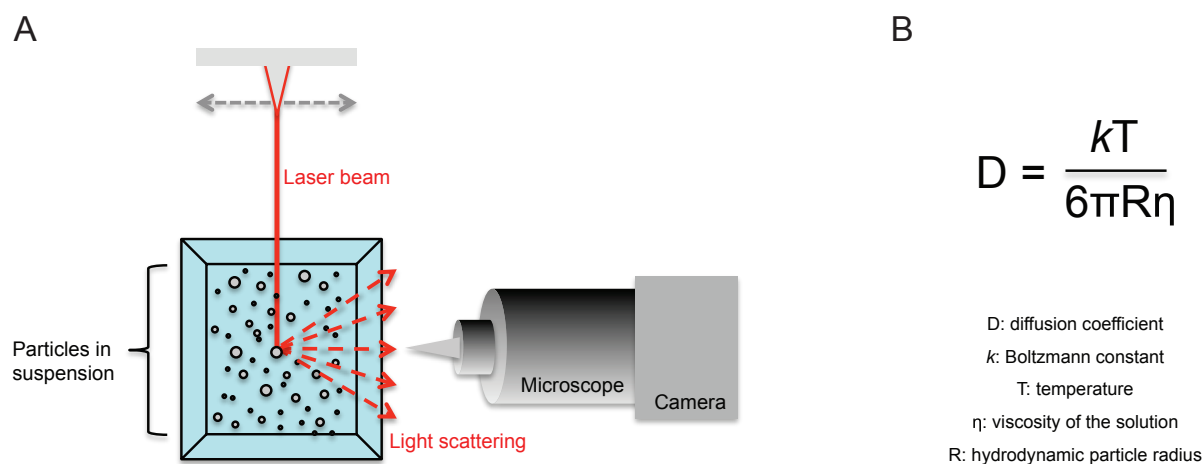


Fig. 5.25: The functional principle of the NTA technology

A: Schematic drawing showing the setup of an NTA instrument consisting of a sample chamber, a laser beam and a CCD camera associated to a light microscope. B: The Stokes-Einstein equation describing the relation between viscosity and diffusion of spherical particles in liquids.

5.6.1 Evaluation of NTA performance

Size measurements of nanoparticles by NTA can only be precise and reproducible when the appropriate video capture and analysis settings are used. Furthermore the samples have to be of sufficient quality and, if possible, free of contaminating precipitates. Therefore the first measurements aimed at the establishment of optimal parameter settings for routine measurement of particles. Generally speaking, the NTA measurements are sensitive to external vibration, insufficient sample mixing or presence of air bubbles. Furthermore the nanoparticles need to be diluted to an appropriate concentration. To verify the accuracy of the ZetaView NTA instrument and to establish adequate acquisition settings, 100 nm and 300 nm polystyrene (PS) standard beads were used. Before measuring the camera sensitivity and the shutter, which defines the reverse exposure time, need to be determined manually. In general, nanoparticles of different sizes require different settings: small monodisperse particles, such as 100 nm beads, need to be measured at a higher sensitivity and longer exposure time than large particles with the same refractive index. First, the influence of increasing sensitivity levels on bead concentrations and size distribution was investigated, while the shutter was kept constant at 70 (Fig. 5.26). By increasing the camera sensitivity level from 50 to 90 approximately 2.5x more standard beads with a size of 100 nm (Fig.

5.26A) and 1.46x more 300 nm beads (Fig. 5.26B) were detected. By contrast, the size distributions were not significantly affected and the average peak was 93.3 ± 2.7 nm (median 86.1 ± 4.2 nm) for 100 nm beads and 267.3 ± 18.3 nm (median 229 ± 37.5 nm) for 300 nm beads (Fig. 5.27B,C, right panels). However, higher sensitivity levels resulted in a broader size distribution. These investigations showed that changing settings have a strong influence especially on concentration measurements. The higher the camera sensitivity, the more particles are tracked by the software.

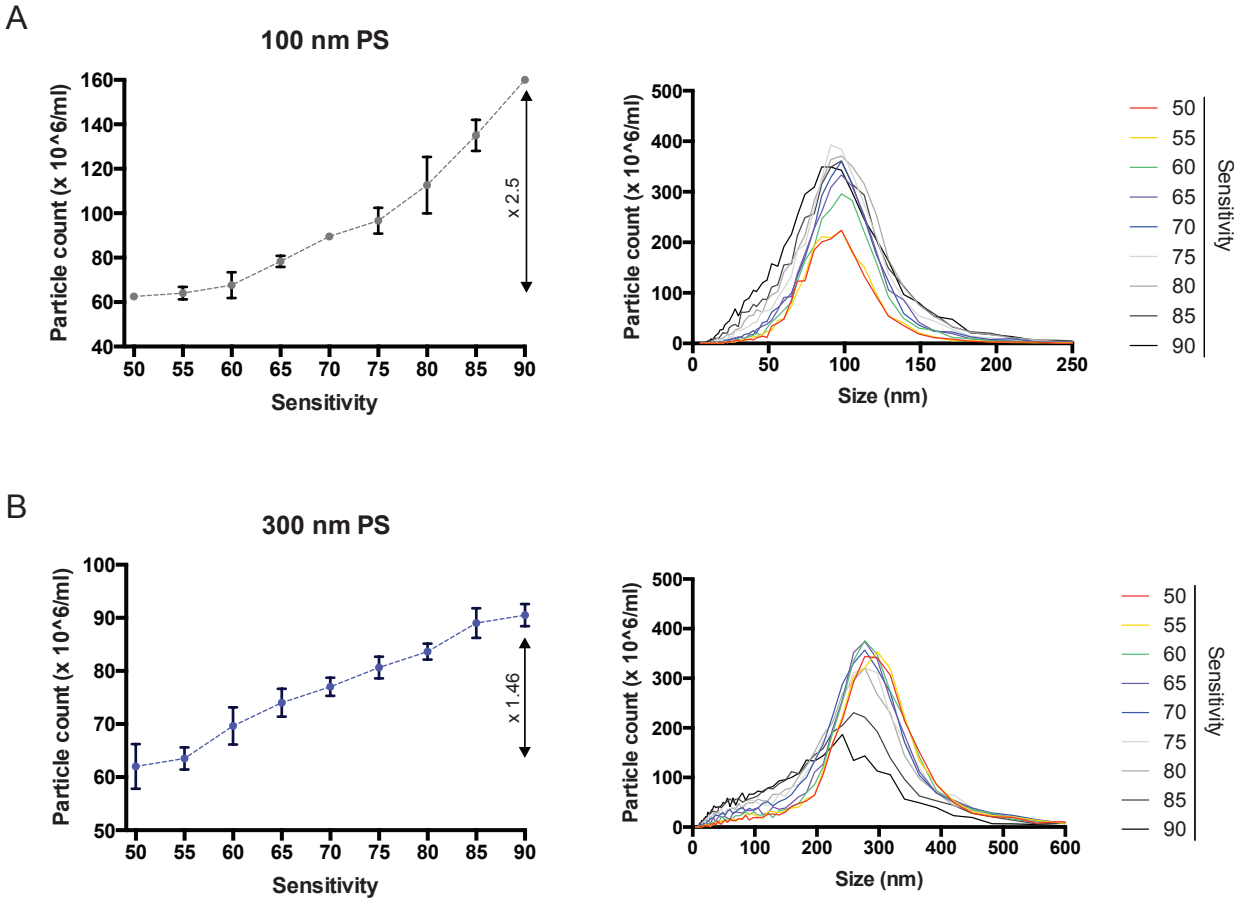


Fig. 5.26: Different camera sensitivity settings influence concentration and size measurements of 100 and 300 nm PS standard beads

100 nm (A) and 300 nm (B) PS beads were measured at different sensitivity levels. Left diagrams show the detected particle concentrations; mean \pm SD of three replicates is shown. Histograms display the corresponding size distributions.

Hence, parameters for measuring 100 nm and 300 nm were therefore chosen as indicated in Table 1 and were kept constant in all further experiments. Besides sensitivity and shutter several other parameters can be changed manually in the ZetaView acquisition software.

The camera records a grey scale image of each sample, which is afterwards converted into a digital image by the software. This image only consists of white and black pixels, which define the particles and the background. The post acquisition parameters listed in Table 1 are filter settings, which determine to what extent a grey value is recognized as white pixel and thus regarded as a nanoparticle. The minimum and maximum size describe the area of particles in pixel, whereas noise and large particle agglomerates are filtered out. The minimum brightness defines the threshold that distinguishes between background noise and information. Generally speaking, small particles (e.g. 100 nm) require a lower minimum brightness and size value, since the detected spots are small and light scattering is weaker in comparison to large 300 nm particles.

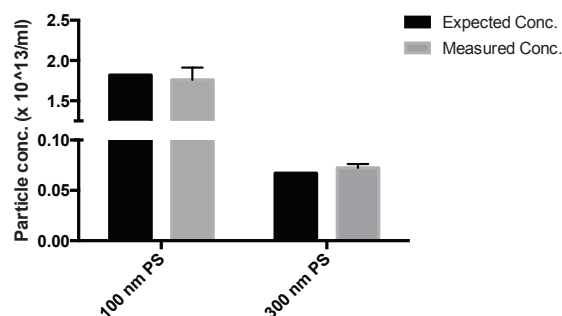
Table 1: Recommended parameter settings for measuring 100 nm and 300 nm PS beads.

Parameter settings	100 nm PS	300 nm PS	
Sensitivity	65	60	
Shutter	70	70	
Min. /max. particle size	5/ 1000	40/ 1000	Post acquisition parameters
Min. brightness	20	80	

By using the indicated set of parameters, the standard PS beads were measured in five independent replicates to verify the accuracy and reproducibility of NTA measurements (Fig. 5.27). The measured particle concentrations matched the calculated original concentration of the stock solutions (Fig. 5.27A). Serial dilution of 100 nm standard beads showed furthermore a linear correlation between the actual concentration and the measured data (Fig. 5.27B).

A

Beads	Expected concentration	Measured concentration (SD) n=5
100 nm PS	$1.82 \times 10^{13} \text{ cm}^{-3}$	$1.76 \times 10^{13} (0.15) \text{ cm}^{-3}$
300 nm PS	$6.7 \times 10^{11} \text{ cm}^{-3}$	$7.24 \times 10^{11} (0.38) \text{ cm}^{-3}$



B

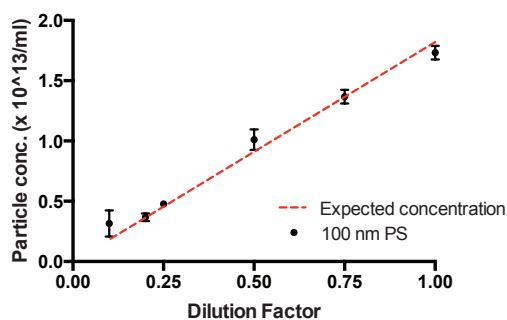


Fig. 5.27: Accuracy of size and concentration measurements of homogeneous PS standard beads

A: Concentration measurement of 100 nm and 300 nm standard beads in comparison to the given concentration of the stock solution. Measured concentrations represent mean and standard deviation of 5 measurements. B: 100 nm PS beads were diluted in a range of 1.82×10^{12} to 18.2×10^{12} particles per ml, mean \pm SD of three replicates are shown. The red line represents the expected concentration.

In contrast to standard beads, biological nanoparticles, such as cell-derived EVs, usually comprise a heterogeneous mixture of differently sized particles. Therefore to evaluate the resolution of NTA, 100 nm and 300 nm PS beads were mixed in different ratios. The size distributions and the corresponding video frames are shown in Fig. 5.28. Moreover, 3D density graphs were generated with the particle explorer (PEX) analysis software, an additional program, which enables in-depth analysis of recorded data.

Generally speaking, the measurement of particle concentrations in heterogeneous samples is less precise, because differently sized particles with similar refractive index display different scattering intensities. When the used settings are optimal for small particles (e.g. 100 nm), larger particles (e.g. 300 nm) may be over-exposed at the same time and consequently their number will be overestimated. On the contrary, when the camera settings are suitable for analysis of large beads, not all small particles are included in the tracking, since they display lower scattering intensities. Especially

detection of small amounts of particles of a certain size currently remains therefore one of the major limitations of the NTA technology.

For the measurements shown in Fig. 5.28, sensitivity and shutter levels were kept constant at 70. The NTA was able to distinguish the two size populations in a 1:1 mixture. However, it became apparent that higher numbers of large 300 nm particles have a negative influence on the peak resolution. The NTA was not able to clearly distinguish between the two bead populations when the number ratio of 100 nm beads to 300 nm was 1:4 (second row) or higher (not shown). On the other hand, small amounts of 300 nm beads did not particularly influence the detection of 100 nm beads. However, as depicted in Table 2, the peak representing the 300 nm beads shifted to the right and the estimated size was therefore higher than expected.

Table 2: Size distributions and peak resolution of mixed 100 nm and 300 nm PS beads (n = 2 measurements). n.d.: not detectable.

100 nm : 300 nm ratio	Mean (nm)	Peak 1 (nm)	Peak 2 (nm)
1:1	166.1 ± 7.8	128.2 ± 2.6	303.6 ± 6.4
1:4	187.5 ± 5.6	n.d.	348.3 ± 9.8
4:1	156.6 ± 4.6	133.7 ± 10.4	326.7 ± 16.5
10:1	179.8 ± 2.6	141.5 ± 7.1	349.2 ± 1.1
100:1	115 ± 7.35	141.5 ± 7.1	n.d.

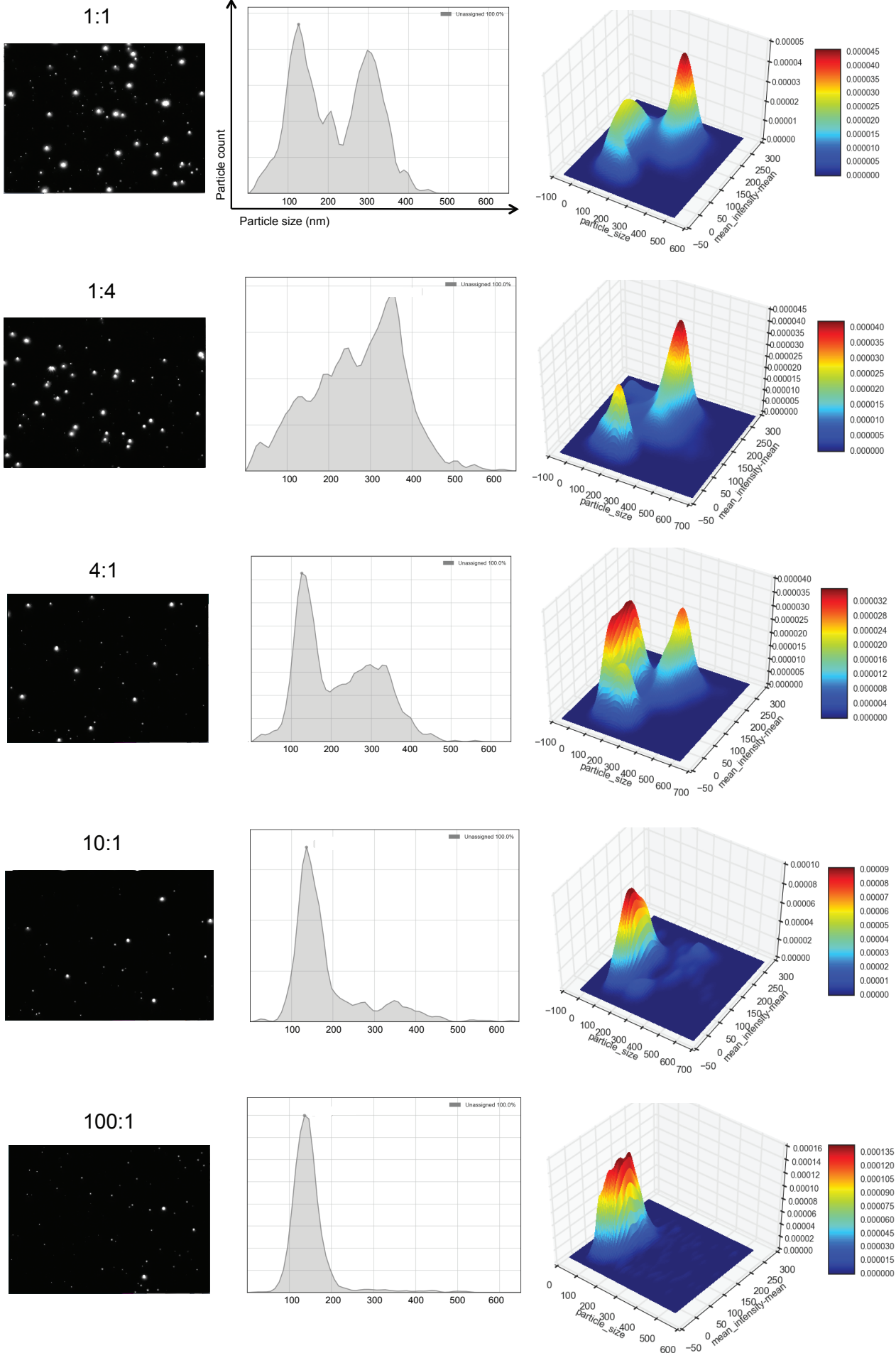


Fig. 5.28: Evaluation of mixtures of 100 nm and 300 nm PS beads

Monodisperse 100 nm and 300 nm PS standard beads were mixed in different number ratios. A representative NTA video frame (left panels), the measured size distribution (middle panels) and 3D surface plots (right panels) are shown.

5.6.2 Detection of fluorescent PS beads

The Zetaview NTA instrument is equipped with a 488 nm laser and an appropriate long pass filter (500 nm), which allows light above a defined wavelength to pass. By using the filter the scattering light from the laser is blocked and only the fluorescence is recorded by the camera. This allows specific tracking of fluorescently labeled EVs and thus the detection of specific EV subpopulations.

To assess the principle of fluorescence NTA, fluorescent 100 nm PS standard beads were recorded in the scattering mode and, by applying the filter, in the fluorescent mode in three independent replicates (Fig. 5.29). It is important to notice that the camera settings need to be adjusted for both modes individually. In the fluorescent mode a higher sensitivity level is required for optimal particle detection. The parameter settings were used as indicated in Table 3. Although 100% of the standard particles are fluorescent, the particle concentration measured in the fluorescent mode was always lower compared to the scattering mode. For this reason a calibration factor was determined and used for concentration measurements. In both modes the number versus sensitivity plot was recorded and compared in Fig. 5.30A. By dividing the particle numbers detected with the indicated sensitivities a calibration factor of 1.49 was calculated.

Table 3: Parameter settings for measuring 100 nm PS fluoresbrite® microspheres

Parameter settings	Scattering mode	Fluorescent mode
Sensitivity	60	95
Shutter	70	70
Min. /max. particle size	5/1000	5/1000
Min. brightness	20	20

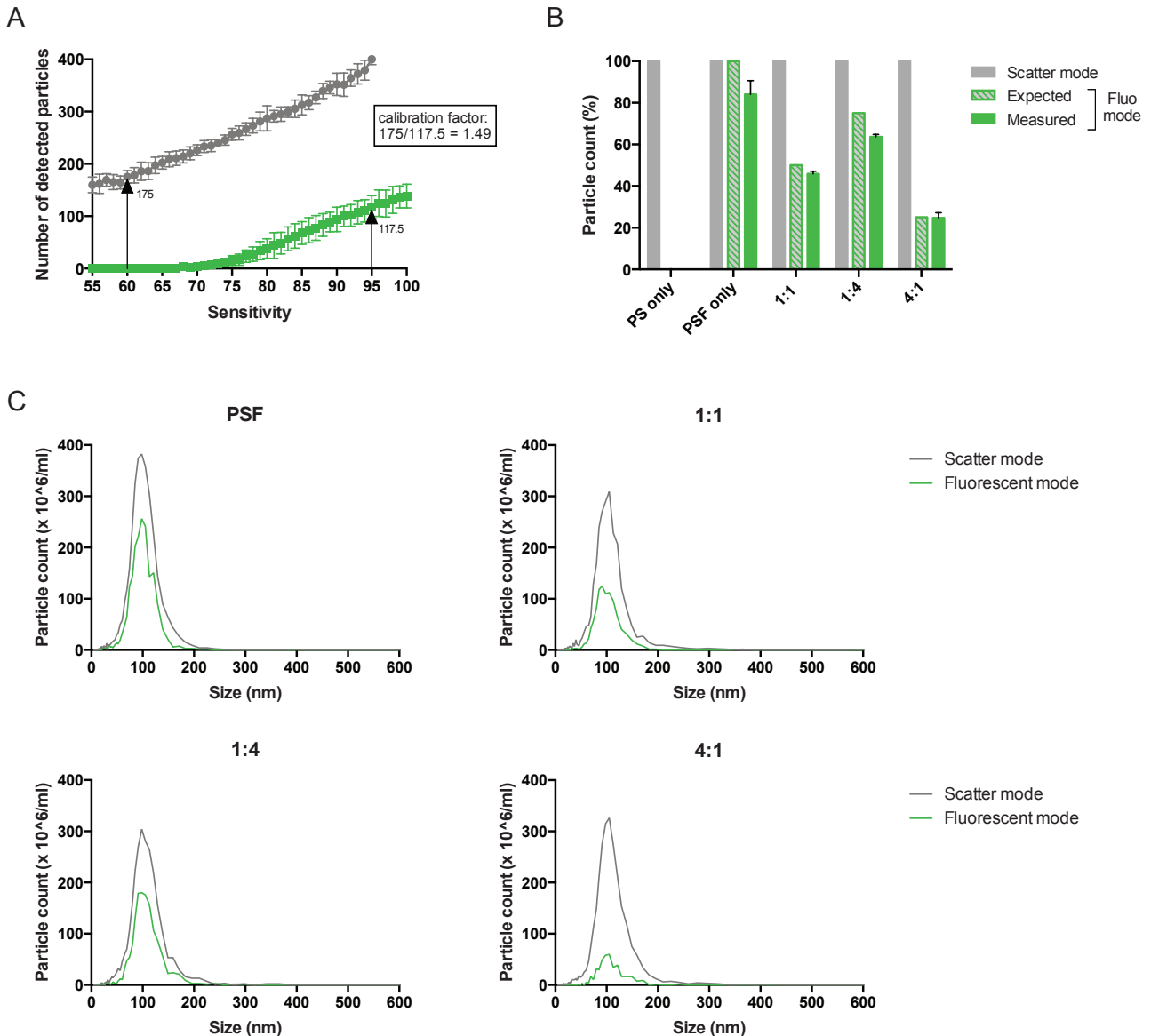


Fig. 5.29: Evaluation of detection of fluorescent 100 nm PS beads by NTA

A: Number versus sensitivity plot of 100 nm fluoresbrite® beads (PSF) measured in scatter mode (grey line) and fluorescent mode (green line). The numbers of detected particles at sensitivity level 60 and 95 were used for the calculation of the calibration factor. Mean \pm SD of three measurements are shown. B: Particle concentrations of non-fluorescent 100 nm PS beads and PSF beads were measured in scatter and fluorescent mode. The beads were furthermore mixed in different ratios. The measured concentration of fluorescent particles was multiplied by the calibration factor 1.49 and normalized against the particle amount measured in the scatter mode. Striped bars represent the expected particle count. Mean and SD of three measurements are shown. C: Size distributions of PSF beads measured in scatter and fluorescent mode. The beads were mixed in different ratios with non-fluorescent PS beads.

Next, the particle concentration of fluorescent beads (PSF) or mixtures of PSF and non-fluorescent PS beads was measured and the data determined in the fluorescent mode were adjusted by multiplication by the calibration factor 1.49 (Fig. 5.29B). The measured proportions of fluorescent and non-fluorescent beads were matching with expected values, confirming the accuracy of the measurements and thus qualifying PSF beads as suitable tools for the calibration of fluorescent measurements. The size distributions recorded in the scatter mode (grey lines) and the fluorescent mode (green lines) appeared to be overlapping, as expected (Fig. 5.29C).

5.6.3 Characterization of HEK293-derived EVs by NTA

The NTA technology holds a lot of promise for the rapid characterization of extracellular vesicles derived from human body fluids or cell culture supernatants. The following investigations therefore aimed at the evaluation of NTA for detection and quantification of HEK293-derived EVs. Membrane-enclosed vesicles have in general a lower refractive index than polystyrene beads. For this reason EVs usually need to be measured with higher sensitivity and exposure time than polystyrene beads of similar size, thus the following measurements were performed at a sensitivity level of 75 and a shutter of 70. EVs were isolated from HEK293 supernatants by serial centrifugation and subsequent density gradient as described in chapter 5.1. The frequency of particle populations in different gradient fractions was verified with NTA by measuring each of the eight fractions individually (Fig. 5.30). In line with the dotblot analysis for CD63, by far the highest concentrations of particles were detected in fractions 2 and 3 (Fig. 5.30A). EV-containing fractions were pooled, washed in PBS and measured by NTA in three independent dilutions (Fig. 5.30B). The mean size was 120 ± 3.7 nm. Moreover, repetitive measurement over three days confirmed stability of the EVs and reproducibility of the concentration measurements (Fig. 5.30C).

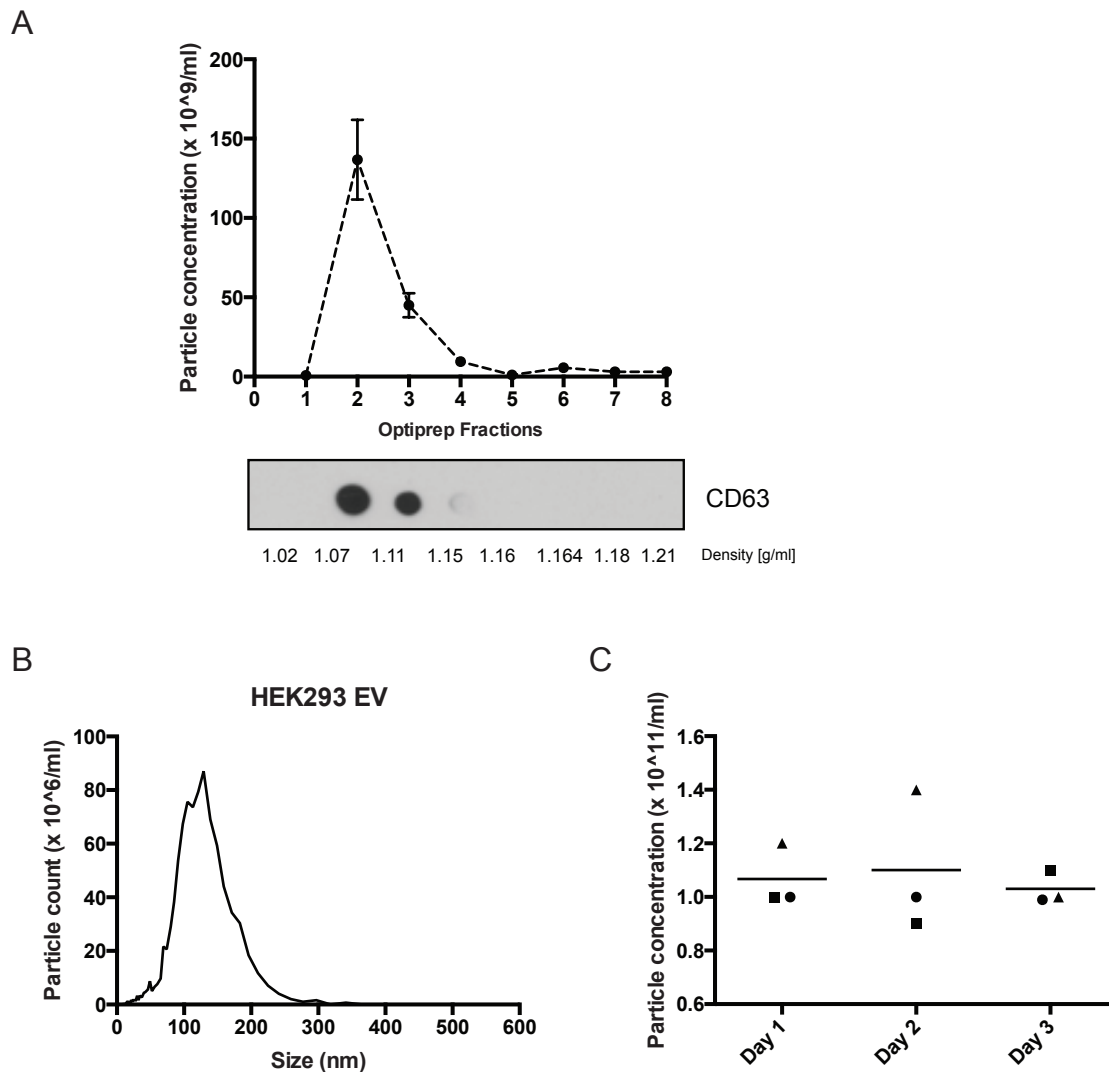


Fig. 5.30: Measurement of HEK293-derived EVs by NTA

HEK293 cell culture supernatant was applied to serial centrifugation, ultracentrifugation and subsequently loaded on an iodixanol gradient. Eight fractions of 500 μ l each were collected after gradient centrifugation. A: Particle concentration was measured in each fraction by NTA. Mean of three measurements is shown. 2 μ l of each fraction were furthermore spotted on a nitrocellulose membrane and CD63 was detected by immunoblotting. The density of each fraction was determined by using a refractometer. B: EV-containing fractions were pooled and washed in PBS. The size distribution was measured in three replicates. Mean is shown. C: Repetitive concentration measurements over three days. The horizontal line represents the mean concentration.

5.6.4 Fluorescent labeling of CD40L+ EVs

Detection of particular EV subpopulations labeled with specific antibodies by NTA represents a promising tool for diagnostic applications, such as the detection of disease-specific EVs in patient samples. One major challenge here is the achievement of the optimal labeling efficiency, which requires titration of the labeled antibody and maximal

reduction of fluorescent background. Furthermore the fluorophores coupled to the antibodies must be sufficiently photostable and of high brightness, since they are exposed to excitation for several seconds.

To detect specific vesicle populations by fluorescent NTA, EVs were isolated from HEK293 cells stably expressing the membrane protein CD40L and subsequently labeled with an Alexa488 coupled anti-CD40L antibody. As a control, EVs derived from CD40L-negative HEK293 cells were treated in the same way. The EVs were stained with an excess of antibody in a small volume, subsequently diluted in 1 ml of PBS and directly applied to NTA. The EVs were measured with the parameters indicated in Table 4.

Table 4: Settings for measuring HEK293 EVs labeled with an Alexa488-coupled antibody

Parameter settings	Scattering mode	Fluorescent mode
Sensitivity	75	95
Shutter	70	50
Min. /max. particle size	5/1000	5/1000
Min. brightness	20	20

With the 488 nm laser in place labeled CD40L+ EVs were detected in the fluorescent NTA mode, whereas no CD40L-negative control EVs were visible, as expected. The number of detected CD40L+ particles was recorded over a timespan of 1000 frames (approx. 30 sec, Fig. 5.31A). Within this time, no significant photobleaching of the fluorophore was observed. In three independent measurements, the particle number detected in each frame was ranging steadily from 8 to 19 particles on average, therefore qualifying Alexa488 as a photostable fluorophore. Measuring size and concentration of labeled EVs in scatter and fluorescent mode showed that only approximately 25.7% of the EVs tracked in the scatter mode were also visible in the fluorescence mode and decorated with the CD40L-specific antibody (Fig. 5.31B). However, evaluation of immunoelectron microscopy images indicated a higher proportion of approximately 75% of CD40L+ EVs (Fig. 5.31C, 65 vesicles were enumerated in total). These results suggest that NTA in principle is able to detect specific fluorescently labeled EVs, but tends to underrate their numbers. Most likely, the amount of CD40L molecules present on the surface of EVs is heterogeneous and NTA may not be able to detect CD40L^{low}

particles, which display a low fluorescent intensity. Electron microscopy is more sensitive and also allows identification of EVs that were bound by only a few gold particles. Detection of certain EV subpopulations therefore remains challenging and further investigations on optimal labeling efficiency are needed. Washing of stained EVs by ultracentrifugation did not improve the results (not shown). Staining with lower amounts of anti-CD40L antibody led to a slight reduction of particle numbers measured in the fluorescent mode.

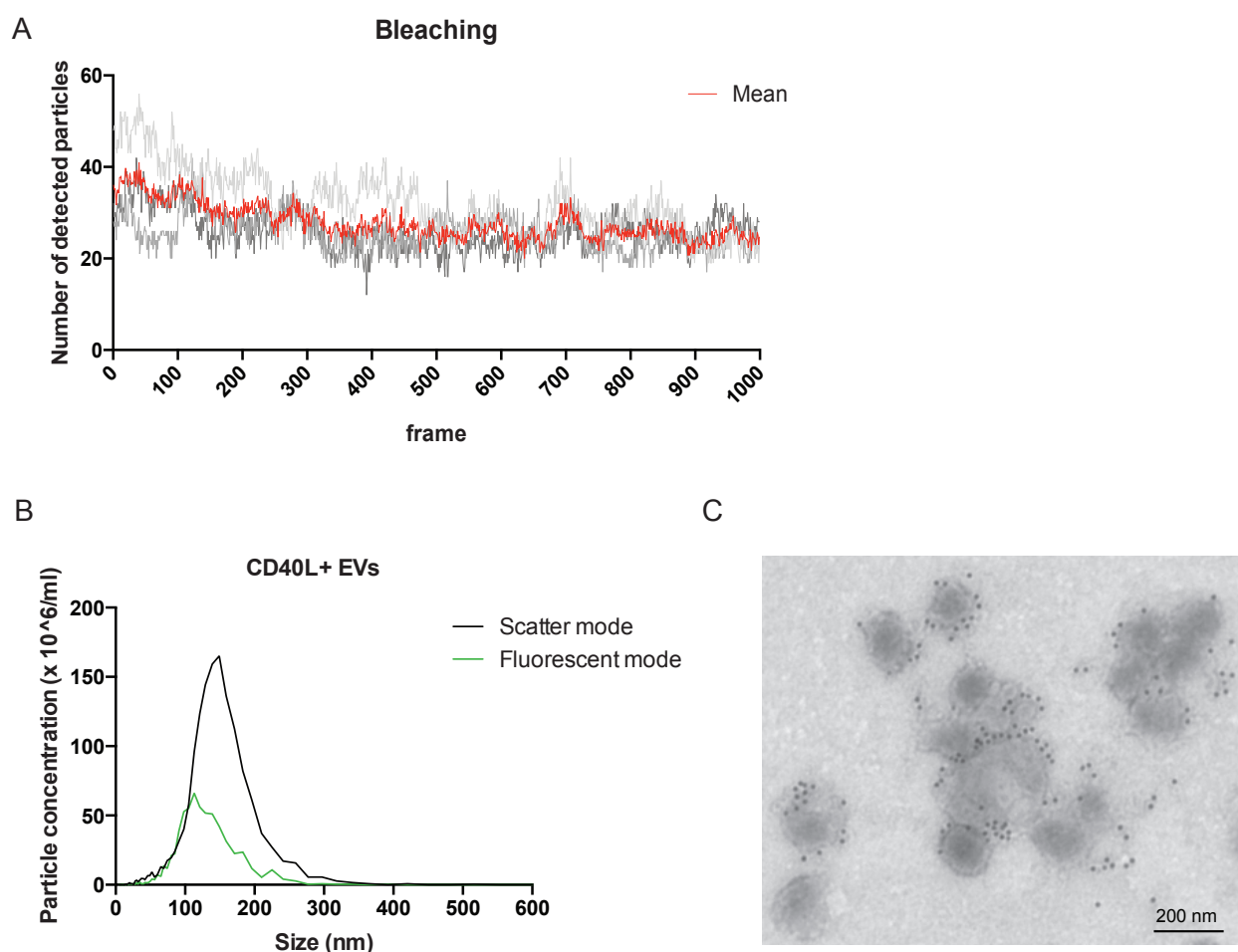


Fig. 5.31: Detection of fluorescently labeled CD40L-positive EVs

EVs isolated from HEK293 cells stably expressing CD40L were labeled with a CD40L-specific antibody coupled to Alexa488 and measured by NTA. A: Number of detected particles in the fluorescent mode tracked over time. Each data point on the x-axis corresponds to 1/30 sec. The red line represents the mean of three independent measurements. B: Size distribution measured in the scatter (black line) and fluorescent mode (green line). C: Immunoelectron microscopy of EVs stained with an anti-CD40L antibody and a gold-conjugated secondary antibody.

All in all, the performed experiments qualify nanoparticle tracking as a unique technique to characterize EVs in complementation to other methods. The ZetaView instrument enables reproducible quantification and sizing of PS standard beads and HEK293-derived EVs under specified and constant parameter settings. NTA already became a widely used method for EV characterization, but it also implicates several disadvantages. Its performance therefore needs to be assessed and monitored thoroughly.

6 Discussion

For several decades extracellular vesicles did not capture much attention because they were considered to be mainly responsible for the recycling of cellular material. Only since 25 years it is known that cells actually use EVs to actively communicate with neighboring or distant cells in both healthy and pathological conditions. Since then EVs have been extensively studied and the number of reports about EVs is growing rapidly. EVs can be isolated from a variety of biological fluids and have a great diagnostic and therapeutic value. Yet, EV research is still in its infancy and many mechanisms underlying EV biogenesis and EV-mediated cell-cell communication remain to be elucidated. The aim of this work was to develop and evaluate an immunotherapeutic approach based on engineered EVs for the treatment of chronic lymphocytic leukemia. This was achieved by isolating EVs from transfected HEK293 producer cells and investigating their effect on the immune system. The data showed that the EVs designed in this context were directed to specific target cells and transferred functional protein and nucleic acids, thus stimulating specific immune responses and demonstrating the great potential of EVs as therapeutic tools. These findings and their relevance for future research will be discussed on the following pages.

6.1. Isolation and characterization of EVs

The definition of consensus methods for EV purification and characterization remains a major challenge for the EV field. A variety of different techniques for EV isolation has been described, but standardization is still lacking. In the present study EVs were isolated from HEK293 cell culture supernatants by differential centrifugation and density gradient fractionation, where EVs were floating according to their buoyant density to an equilibrium of around 1.05 – 1.13 g/ml. This workflow represents one of the most commonly used methods and it enables isolation of EVs of high purity. As shown in 5.1, the iodixanol gradient efficiently separated contaminating soluble proteins from EVs. However this isolation procedure is time-consuming and requires special equipment, such as costly ultracentrifuges, and is therefore not applicable for clinical use or diagnostics, e.g. for the isolation of EVs from human body fluids as circulating biomarkers of disease. Alternative and particularly faster isolation methods are currently under investigation, such as size-exclusion chromatography (SEC),

immunoaffinity columns or precipitating agents, e.g. Polyethylene glycol (PEG) [28,30,185]. Although EV-precipitating agents are easy to handle and allow fast isolation, they suffer from impurities from co-precipitating proteins [32,185]. In contrast, SEC results in a similar purity like density gradient centrifugation and seems to be a suitable method for EV purification and potentially also for clinical applications [186,187]. There is evidence that the isolation technique directly influences the purity and composition of EV preparations, even when derived from the same cell type [185]. Furthermore, culture conditions, the producer cell type, its physiological state or presence of cell stress affect quality and yield of EV samples [188]. Bovine EVs present in fetal calf serum can contaminate EV preparations and therefore the HEK293 producer cells used in this study were grown in medium that had been depleted from EVs by ultracentrifugation.

Characterization of EV preparations comprises a combination of several methods and usually EVs are characterized by their size, density, their protein and nucleic acid content and their morphology. In the context of the present study electron microscopy showed that EVs isolated from HEK293 cells have a round, cup-shaped morphology and a size of 120-150 nm. Immunoblotting confirmed that these EVs, furthermore, contain the tetraspanin CD63, as well as the exosome-associated proteins TSG101 and Alix. In contrast, Calnexin, a protein of the endoplasmatic reticulum, was not detected. Thus, the isolation of EVs by ultracentrifugation and density gradient fractionation was demonstrated to be a reliable method for the isolation of pure EVs.

It should be mentioned that none of the currently existing isolation techniques are able to separate different EV subtypes, e.g. exosomes and microvesicles, or EVs secreted by different cell types. EV samples therefore always consist of a mixture of different EVs. Identification of novel unique EV markers may help to overcome this obstacle, e.g. by immunoprecipitation. Efforts to improve existing methods and develop new technologies are currently ongoing. Nanoparticle tracking analysis (NTA) is a novel tool that may facilitate distinguishing of EV subpopulations. It's potential will be critically discussed in the next section.

6.1.1 NTA technology: A reliable method for EV characterization?

Nanoparticle tracking analysis is a novel technique based on the light-scattering capacity of nanoparticles. It is more sensitive than conventional dynamic light scattering (DLS) and frequently used in the EV field for sizing and quantification of EVs [33,34,189]. Evaluation of the ZetaView instrument showed that concentration measurements of polystyrene standard beads and HEK293-derived EVs with optimal parameter settings are reliable and reproducible (5.6). However these experiments also identified several drawbacks of the NTA technology. One substantial disadvantage is that different parameters in data acquisition and analysis can significantly affect the results, such as the absolute particle count. Thus, it is mandatory to keep parameter settings constant, in order to achieve precise and reproducible measurements. However, the search for the most suitable settings and the correct sample concentration can be very time-consuming. It is, therefore, recommended to establish a set of fixed standardized parameters for each individual sample type (e.g. HEK293-derived EVs, polystyrene beads), in order to facilitate reproducibility. In fact, a skilled operator is required who chooses the optimal parameters manually. He therefore has the power to influence NTA results substantially, both wittingly and unwittingly. All in all, it remains questionable whether NTA data produced by different research groups can be directly compared and reproduced because description of parameter settings in publications is often incomplete. Beyond that, different NTA instruments are found on the market, which are equipped with different hardware components (e.g. camera type) and software, thus making comparison of results difficult.

In addition to this, measuring of polydisperse nanoparticle samples by NTA is still challenging and requires further technical improvement. Chapter 5.6.1 showed that heterogeneous mixtures of 100 nm and 300 nm PS beads are difficult to detect. The peak resolution of the ZetaView instrument was particularly low when small amounts of 100 nm particles were mixed with high numbers of 300 nm particles. Mainly the large particles were captured. This can be explained by the fact that small faint particles are eclipsed by the intense light scattering of large particles, thereby preventing some of them from being traced. This phenomenon may lead to misinterpretation of the recorded data. However, it is probably one of the most intriguing future applications of the NTA technology to detect and characterize particular EV types, e.g. disease-associated EVs in body fluids. Especially the possibility to measure fluorescently labeled

EVs is promising. In this respect, it was demonstrated that measurement of fluorescent PS beads or antibody-labeled EVs is possible, but that the absolute particle counts were underestimated, most likely due to a lack of detection sensitivity or a suboptimal labeling efficiency of the antibody (5.6.4). More sensitive cameras may improve the detection of fluorescent particles. Optimal calibration methods for NTA are still lacking and until now most calibration has been performed with polystyrene microspheres. However, these standard beads are homogeneous in size and show a light scattering behavior that is different from that of EVs. For this reason we are currently aiming to generate cell-derived standard EVs for a more reliable calibration of NTA measurements.

Cell culture supernatants, human plasma, urine or ascites samples each contain a heterogeneous mixture of different vesicles and NTA, in combination with other methods, is a useful tool to further identify the different features and phenotypes of EVs. Although improvement of the existing NTA instruments and the corresponding analysis software are mandatory, the NTA technology holds promise for future research and may be even applicable for diagnostics or clinical vesicle samples.

6.2 EV-based therapeutics

Development of novel EV-based therapeutic approaches, including anti-tumor therapy, immune-modulatory therapies, drug delivery and pathogen vaccination, is currently a major task of the EV research field. In principle, EVs are ideal, well-tolerated cell-free delivery vehicles and can transfer therapeutic biomolecules, such as proteins, RNAs or small molecules, to recipient cells. Thus, controlled design of modified EVs with increased overall immunogenicity may facilitate the development of novel vaccines, immunotherapeutics or drug delivery systems. In the present study immune accessory CD40L, as well as the herpesviral proteins gp350 and pp65 were successfully incorporated into EVs by overexpression in HEK293 producer cells. Because CD40L and gp350 are membrane-anchored proteins, they were detected on the surface of purified vesicles by immunoelectron microscopy and flow cytometry (5.2; 5.3.1). However, the electron microscopy analysis also demonstrated that transfected HEK293 cells release an EV population that is heterogeneous in their enrichment of surface CD40L or gp350; some vesicles were bound by multiple gold-conjugated antibody molecules, whereas

others were completely negative. Gp350 mediated binding of EVs exclusively to B cells expressing the receptor molecule for gp350, CD21. Loading of B cells with EVs carrying gp350 and pp65 led to reactivation of HLA-matched gp350- and pp65-specific CD4⁺ T cells, respectively (5.3.6; 5.4.1). It has been already shown previously, that vesicle-associated antigens are actually more immunogenic than soluble proteins [190]. Therefore EV-mediated transfer of viral proteins is an efficient strategy for the induction of specific immune responses. However, EVs do not stimulate T cells directly but rather depend on uptake and further processing by APCs to induce specific immune responses against EV-associated antigens. This can be explained by the fact that HEK293 cells do not express MHC class II molecules and only very low amounts of MHC class I molecules. Thus, EVs derived from these cells naturally have a low intrinsic immunogenic profile. EV-associated CD40L also retained its functionality and efficient interaction between CD40L⁺ EVs and the CD40 receptor on B lymphocytes resulted in B-cell activation and proliferation (5.2). This observation led to the hypothesis that CD40 stimulation could promote the *in vitro* infection of primary B cells by EBV and, therefore, the effect of CD40L⁺ EVs on EBV infection of B cells and transformation efficiency was investigated (5.2.1). FACS analysis demonstrated that already in the first days after infection B-cell proliferation was clearly enhanced through costimulation of CD40. In general, only a small proportion of infected B cells becomes finally transformed into lymphoblastoid cell lines (LCLs) [191,192]. Pretreatment of B cells with CD40L⁺ EVs resulted in an increased frequency of EBV-mediated transformation *in vitro*, as shown by limiting dilution assays (5.2.1). Treatment with CD40L⁺ EVs was advantageous for the infection efficiency, especially when the titer of infectious virus, or the numbers of B cells per well, were low. Control EVs isolated from CD40L-negative HEK293 cells had no influence on the number of EBV growth-transformed B cells. Transfer of CD40L via EVs is, therefore, a useful tool to improve EBV-mediated transformation with low titer virus stocks. CD40L⁺ EVs together with IL-4 may also be suitable to replace CD40L-expressing feeder cells for B-cell cultivation, but this hypothesis still needs to be tested. In general, CD40-activated B cells represent an attractive source of highly efficient antigen-presenting cells for immunotherapy [172]. Transfer of CD40L is also a promising strategy to restore the poor antigen-presenting capacity of malignant B cells derived from chronic lymphocytic leukemia (CLL), as discussed in 6.2.1.

There is now an urgent need for standardized EV-based methods and regulations to enable safe translation of EV therapies into clinical practice [86]. Many open questions remain: How can clinical-grade EVs be produced? How should dosing of EVs be evaluated? What is the half-life of EVs and how is their biodistribution? Although EV-based therapies are already making their way into clinics and several Phase I clinical trials are currently evaluating their safety, further investigations are urgently needed to fully understand biogenesis and fate of therapeutic vesicles [87]. However, *in vivo* monitoring of EV trafficking remains challenging. A few sensitive reporter systems to demonstrate EV transfer between cells have been developed, e.g. based on the transfer of EV-associated *Cre* mRNA to reporter cells. The Cre/loxP reporter system was also used successfully in this study, demonstrating that EVs derived from Cre-overexpressing HEK293 cells deliver *Cre* mRNA to target cells (5.3.3). This mRNA was translated in recipient BJAB cells and RAW264.7 macrophages expressing a Cre/loxP reporter plasmid. Excision of a stop signal by the Cre enzyme led to a detectable shift from mBFP to GFP expression in these cells. However, numbers of GFP-positive cells were low, most likely because HEK293-derived gp350+ EVs mostly bind to the surface of target cells rather than actively entering the cell (5.3.2). Therefore uptake of a sufficient amount of EV-associated *Cre* mRNA, translation into functional protein and subsequent Cre/loxP recombination appeared to be a rather rare event, at least *in vitro*.

The Cre/loxP system has already been used successfully in transgenic mice expressing Cre recombinase in immune cells and a LacZ reporter gene in target cells [193]. Interaction with EVs and consequent LacZ expression was detected in some neurons and other non-immune cells in the whole animal. Also other reporter systems based on fluorescently labeled mRNA or EV-associated luciferase protein have been introduced recently, but so far were only used in cell culture (*reviewed in* [194]). Taken together, such visualization systems allow identification of EV target cells and will be important for future *in vivo* investigations in order to understand EV fate and biodistribution, thus facilitating development of EV-based therapeutics.

6.2.1 Engineered EVs for immunotherapy of CLL

Currently no curative therapy for CLL exists, but its slow progression and the long median survival of CLL cells *in vivo* make the disease an attractive indication for immunotherapeutic approaches. CD40L is known to be a promising candidate molecule

for CLL immunotherapy and has already been used in recombinant viral vectors in clinical trials [160,166]. However, there are several biosafety concerns that emerge with the use of viral vectors. By contrast, the present study indicates that engineered EVs represent an efficient and virus-free tool for the delivery of functional CD40L to CLL cells. CD40L+/gp350+ EVs interacted with CD40 on the cell surface and promoted survival of CLL cells *in vitro* (5.3.4). Even more important, these EVs activated downstream signaling: phosphorylation of ERK1/2 and JNK kinases was observed in CLL cells already after 20 minutes upon stimulation with CD40L+ EVs. Furthermore, they clearly stimulated upregulation of the immunomodulatory surface molecules CD54, CD80, CD86 and CD95, thus enhancing the antigen-presenting capacity of CLL cells (5.3.5). As a consequence, gp350-specific T cells were successfully stimulated by HLA-matched CLL cells loaded with CD40L+/gp350 EVs (5.3.6). EVs lacking CD40L did not induce T-cell activation, thus demonstrating the crucial role of CD40L for the immunogenicity of CLL cells.

6.2.2 Activation of CMV-specific T cells as effector cells in CLL

The immunotherapeutic strategy for CLL treatment that was described in the present study aimed at the one hand at transferring functional CD40L to CLL cells, and on the other hand at redirecting the pre-existing CMV-specific immunity towards CLL cells. Although CLL is generally characterized by T-cell dysfunction, CMV-specific T cells are functionally intact and their numbers are even augmented in comparison to healthy age-matched individuals [139,140,142]. Pp65 is one of the major targets of CMV-specific CD8+ T cells and these cells have been associated with the control of viral replication in both healthy individuals and CLL patients [195,196]. To target full-length pp65 into EVs, the protein was overexpressed in HEK293 producer cells and the incorporation into vesicles was confirmed by immunoblotting (5.4). LCLs loaded with pp65+ EVs successfully stimulated IFN γ secretion of pp65-specific CD4+ T cells (5.4.1). In fact, internalization of EVs by recipient cells favors the presentation of EV-derived antigens on MHC class II molecules. However, pp65+ EVs processed and presented by LCLs also activated the cytotoxic activity of pp65-specific CD8+ T cells, as demonstrated by measuring IFN γ and granzyme B induction. Since EVs purified from pp65-expressing HEK293 cells did not only contain pp65 protein, but also *pp65* mRNA, it is tempting to speculate that these mRNA molecules are translated in recipient cells, processed and

presented on MHC class I molecules. However, a valid proof of this theory is still lacking. As described in chapter 5.3.3, usage of a Cre reporter system showed that EV-mediated transfer of *Cre* mRNA to B cells and translation into functional Cre proteins is possible. More likely, stimulation of CD8⁺ T-cell responses may be ascribed to cross-presentation of EV-associated antigens by MHC class I molecules. This mechanism is mainly used by dendritic cells, which present endogenous antigens that are normally presented in association with MHC class II molecules to CTLs in the lymph nodes [197]. Especially in response to vaccines, cross-presentation and subsequent activation of CD8⁺ T cell responses is crucial. To what extent B cells are able to cross-present extracellular proteins in association with MHC class I molecules is still a matter of debate. Previous investigations in our group already showed that EBV-derived virus-like particles (VLPs) stimulate virus-specific CD8⁺ T-cell responses efficiently [198]. In fact, VLPs and EVs share similar biogenesis pathways and morphological features. VLPs carry a full set of different viral proteins and are therefore promising vaccine candidates, but they also represent potential pathogenic agents and might induce adverse immune responses. In contrast, in EVs potentially dangerous viral material is absent. They can be modified in a controlled manner and the fact that they are able to trigger specific CD8⁺ T-cell responses qualifies EVs as potentially safe vaccine candidates and immunotherapeutic agents. Furthermore, incorporation of full-length antigens into EVs enables a MHC class I-unrestricted usage.

In line with this, primary CLL cells effectively stimulated allogeneic HLA-matched pp65-specific CD8⁺ T cells after loading with CD40L⁺/gp350⁺/pp65⁺ EVs (5.4.1). Furthermore autologous T cells were expanded by co-incubation of CLL-derived PBMCs with these vesicles and IL-2, so that after 20 days of incubation, cultures almost exclusively consisted of antigen-specific CD4⁺ and CD8⁺ T cells (5.4.3). In contrast, no viable cells were detectable in those cultures that were treated with control EVs derived from non-transfected HEK293 cells. Flow cytometry analysis showed that CD4⁺ T cells represented the major effector cell population. However also numbers of pp65-specific CD8⁺ T cells were enhanced, as demonstrated by pentamer staining of the HLA-A2-restricted pp65-derived epitope NLV (5.4.3). Coincubation with autologous peptide- or EV-loaded CLL cells, furthermore, confirmed that the enriched cells contained functional pp65-specific T cells. Thus, stimulation of T cells with EV-loaded CLL cells is a powerful

option to selectively expand specific T cells from CLL cells *in vitro* in an HLA-independent manner.

In summary it can be said that these data demonstrate a strong immunogenic effect of EV-associated pp65. In principle, also T cells specific for other immunogenic CMV proteins, e.g. the immediate-early 1 (IE-1) protein, are abundantly found in CMV-positive adults. Therefore, these proteins may also be suitable for EV-mediated delivery. EVs carrying a set of different immunogenic CMV proteins are possibly able to induce particularly strong immune responses by stimulating T cells of different specificities.

The events causing the distinctive CMV-specific immunity in CLL patients are still unclear. Conceivably, expanded T-cell numbers in CLL are compensating for other defects in anti-CMV immune defense, such as NK cell dysfunction or defective humoral immunity. Because cytotoxic CMV-specific T cells show a lower expression of inhibitory molecules in comparison to other CLL-derived CD8⁺ T cells, they potentially exhibit an enhanced proliferative capacity or an extended lifespan [142]. Further investigations on the mechanisms that cause expansion of CMV-specific T cell in CLL may contribute to the development of novel strategies to restore the functionality of other T-cell subpopulations. It remains unclear whether other T-cell subpopulations within the tumor microenvironment are also functionally intact or whether CMV-specific T cells in CLL are a rare exception. It is for example currently speculated that even T cells specific for immunodominant EBV proteins are functionally impaired in CLL and, in contrast to CMV-specific T cells, express high levels of exhaustion markers (*A. Kater, unpublished data*). In conclusion, the immunotherapeutic strategy based on taking advantage of autologous virus-specific cytotoxic T cells (CTLs) for targeting and killing of CLL cells is currently confined to CMV-specific T cells. Luckily, the majority of CLL patients is seropositive for CMV (approx. 65%), so that this immunotherapeutic approach is, in principle, suitable for many patients.

6.2.3 Preliminary *in vivo* evaluation of an EV-based immunotherapy for CLL

Genetically engineered mouse models of CLL are indispensable tools for understanding the molecular mechanisms underlying the disease pathogenesis. However, CLL is a very heterogeneous disease, comprising different genetic aberrations and variably regulated leukemia-associated genes, thus making *in vivo* studies challenging. Several genetically

engineered CLL mouse models have been described that develop lymphoproliferations late in life and simulate an indolent course of the disease [199]. The E μ -TCL-1 transgenic mouse was the first one developing a CLL-like disease and ever since has been widely used and studied [182]. Since the *TCL1* gene is highly expressed also in the majority of CLL patients, this transgenic mouse represents a convenient preclinical model and was also used in the context of this study.

The model system described in 5.5. introduced for the first time a potential *in vivo* model for the evaluation of an EV-based CLL treatment strategy. C57BL/6 mice were immunized with EVs containing murine CD40L and gp350 or pp65, in order to induce specific immune responses against these antigens. High titers of gp350-specific antibodies were detected 15 weeks later in the serum of all mice immunized with mCD40L+/gp350+ EVs. A humoral response against pp65 was only detected in one mouse out of three, indicating that this protein is predominately located within EVs, thus less accessible for immune recognition. Malignant CD19+/CD5+ cells were isolated from the spleen of an E μ -TCL-1 mouse, loaded *ex vivo* with gp350 and pp65 peptide pools and injected into the pre-immunized C57BL/6 mice. Tracking of the CLL cells in blood samples by flow cytometry indicated that cell proliferation was transiently hampered in mice immunized with mCD40L+/gp350+ EVs or mCD40L+/pp65+ EVs. However, after 10 weeks, this delay was compensated and all tested mice had a load of 65-75% of TCL-1 cells in their blood stream and around 90% in the spleen. This can most likely be ascribed to the only transient presentation of peptides on the surface of TCL-1 cells. Since these cells do not stably express gp350 or pp65, the peptides are only presented for a short period of time. One possible solution to overcome this limitation may be the transduction of TCL-1 cells with a lentivirus to induce stable antigen expression. Since mice immunized with EVs also indicated specific cellular immune responses, it can be assumed that in those mice the engraftment of gp350- or pp65-expressing CLL cells is significantly hindered. All in all, repetition of these experiments with a larger number of mice will enable to validate the observed results.

6.3 Concluding remarks and outlook

The present study represents the first detailed description and evaluation of an unique immunotherapeutic approach for CLL based on engineered extracellular vesicles. My experiments demonstrated that controlled manipulation of EV composition and function represents an efficient strategy for the generation of EVs with specific features. Transfer of CD40L to B cells via EVs was shown to be a valuable tool that induced survival and proliferation of normal and malignant B lymphocytes, and furthermore, significantly enhanced the antigen-presenting capacity of CLL cells. Additional incorporation of herpesviral proteins increased the immunogenicity of these EVs and redirected specific immune responses towards the EV-loaded cells. Especially the induction of CTL immune responses is of therapeutic relevance for the treatment of malignant diseases, and engineered EVs represent a flexible and effective system that elicits CD8+ T cell-specific immunity. Next, further *in vivo* investigations will be required to confirm the enhanced immune recognition of CLL cells reactivated by EVs.

CLL remains the most common leukemia in western countries and due to demographic changes in society it is believed that the prevalence and mortality of CLL will further increase [116,200]. Beyond doubt, an improved therapy for CLL is urgently needed and according to my data engineered EVs may be suitable tools to substantially improve the immune status of CLL patients.

7 References

- [1] S. Keller, M. P. Sanderson, A. Stoeck, and P. Altevogt, "Exosomes: from biogenesis and secretion to biological function," *Immunol. Lett.*, vol. 107, no. 2, pp. 102–8, Nov. 2006.
- [2] M. Simons and G. Raposo, "Exosomes--vesicular carriers for intercellular communication," *Curr. Opin. Cell Biol.*, vol. 21, no. 4, pp. 575–81, Aug. 2009.
- [3] M. Colombo, G. Raposo, and C. Théry, "Biogenesis, Secretion, and Intercellular Interactions of Exosomes and Other Extracellular Vesicles," *Annu. Rev. Cell Dev. Biol.*, vol. 30, pp. 255–89, 2014.
- [4] M. Yáñez-Mó, P. R.-M. Siljander, Z. Andreu, A. B. Zavec, F. E. Borràs, E. I. Buzas, K. Buzas, E. Casal, F. Cappello, J. Carvalho, E. Colás, A. Cordeiro-da Silva, et al., "Biological properties of extracellular vesicles and their physiological functions," *J. Extracell. vesicles*, vol. 4, p. 27066, 2015.
- [5] S. J. Gould and G. Raposo, "As we wait: coping with an imperfect nomenclature for extracellular vesicles," *J. Extracell. vesicles*, vol. 2, pp. 3–5, 2013.
- [6] C. Théry, A. Regnault, J. Garin, J. Wolfers, L. Zitvogel, P. Ricciardi-Castagnoli, G. Raposo, and S. Amigorena, "Molecular characterization of dendritic cell-derived exosomes: Selective accumulation of the heat shock protein hsc73," *J. Cell Biol.*, vol. 147, no. 3, pp. 599–610, 1999.
- [7] C. Thery, M. Boussac, P. Veron, P. Ricciardi-Castagnoli, G. Raposo, J. Garin, and S. Amigorena, "Proteomic Analysis of Dendritic Cell-Derived Exosomes: A Secreted Subcellular Compartment Distinct from Apoptotic Vesicles," *J. Immunol.*, vol. 166, no. 12, pp. 7309–7318, 2001.
- [8] P. D. Robbins and A. E. Morelli, "Regulation of immune responses by extracellular vesicles," *Nat. Rev. Immunol.*, vol. 14, no. 3, pp. 195–208, 2014.
- [9] C. Théry, L. Zitvogel, and S. Amigorena, "Exosomes: composition, biogenesis and function," *Nat. Rev. Immunol.*, vol. 2, no. 8, pp. 569–79, Aug. 2002.
- [10] A. V. Vlassov, S. Magdaleno, R. Setterquist, and R. Conrad, "Exosomes: Current knowledge of their composition, biological functions, and diagnostic and therapeutic potentials," *Biochim. Biophys. Acta - Gen. Subj.*, vol. 1820, no. 7, pp. 940–948, 2012.
- [11] J. Conde-Vancells, E. Rodriguez-Suarez, N. Embade, D. Gil, R. Matthiesen, M. Valle, F. Elortza, S. C. Lu, J. M. Mato, and J. M. Falcon-Perez, "Characterization and comprehensive proteome profiling of exosomes secreted by hepatocytes," *J. Proteome Res.*, vol. 7, no. 12, pp. 5157–5166, 2008.
- [12] G. Van Niel, I. Porto-Carreiro, S. Simoes, and G. Raposo, "Exosomes: A common pathway for a specialized function," *J. Biochem.*, vol. 140, no. 1, pp. 13–21, 2006.
- [13] J. C. Gross, V. Chaudhary, K. Bartscherer, and M. Boutros, "Active Wnt proteins are secreted on exosomes," *Nat. Cell Biol.*, vol. 14, no. 10, pp. 1036–1045, 2012.
- [14] H. Sheldon, E. Heikamp, H. Turley, R. Dragovic, P. Thomas, C. E. Oon, R. Leek, M. Edelmann, B. Kessler, R. C. A. Sainson, I. Sargent, J. L. Li, and A. L. Harris, "New mechanism for Notch signaling to endothelium at a distance by delta-like 4 incorporation into exosomes," *Blood*, vol. 116, no. 13, pp. 2385–2394, 2010.
- [15] H. Hasegawa, H. J. Thomas, K. Schooley, and T. L. Born, "Native IL-32 is released from intestinal epithelial cells via a non-classical secretory pathway as a membrane-associated protein," *Cytokine*, vol. 53, no. 1, pp. 74–83, 2011.
- [16] M. A. Kovach, B. H. Singer, M. W. Newstead, X. Zeng, T. A. Moore, E. S. White, S. L. Kunkel, M. Peters-Golden, and T. J. Standiford, "IL-36 γ is secreted in microparticles and exosomes by lung macrophages in response to bacteria and bacterial components," *J. Leukoc. Biol.*, 2016.
- [17] S. Mathivanan, H. Ji, and R. J. Simpson, "Exosomes: extracellular organelles important in intercellular communication," *J. Proteomics*, vol. 73, no. 10, pp. 1907–20, Sep. 2010.

-
- [18] J. Wolfers, a Lozier, G. Raposo, a Regnault, C. Théry, C. Masurier, C. Flament, S. Pouzieux, F. Faure, T. Tursz, E. Angevin, S. Amigorena, and L. Zitvogel, "Tumor-derived exosomes are a source of shared tumor rejection antigens for CTL cross-priming," *Nat. Med.*, vol. 7, no. 3, pp. 297–303, 2001.
- [19] R. Wubbolts, R. S. Leckie, P. T. M. Veenhuizen, G. Schwarzmann, W. Möbius, J. Hoernschmeyer, J. W. Slot, H. J. Geuze, and W. Stoorvogel, "Proteomic and biochemical analyses of human B cell-derived exosomes: Potential implications for their function and multivesicular body formation," *J. Biol. Chem.*, vol. 278, no. 13, pp. 10963–10972, 2003.
- [20] K. Laulagnier, C. Motta, S. Hamdi, S. Roy, F. Fauvelle, J.-F. Pageaux, T. Kobayashi, J.-P. Salles, B. Perret, C. Bonnerot, and M. Record, "Mast cell- and dendritic cell-derived exosomes display a specific lipid composition and an unusual membrane organization," *Biochem. J.*, vol. 380, no. Pt 1, pp. 161–71, 2004.
- [21] A. Llorente, T. Skotland, T. Sylvänne, D. Kauhanen, T. Róg, A. Orłowski, I. Vattulainen, K. Ekroos, K. Sandvig, "Molecular lipidomics of exosomes released by PC-3 prostate cancer cells," *Biochim. Biophys. Acta - Mol. Cell Biol. Lipids*, vol. 1831, no. 7, pp. 1302–1309, 2013.
- [22] M. Record, K. Carayon, M. Poirot, and S. Silvente-Poirot, "Exosomes as new vesicular lipid transporters involved in cell-cell communication and various pathophysiologicals," *Biochim. Biophys. Acta - Mol. Cell Biol. Lipids*, vol. 1841, no. 1, pp. 108–120, 2014.
- [23] H. Valadi, K. Ekström, A. Bossios, M. Sjöstrand, J. J. Lee, and J. O. Lötvall, "Exosome-mediated transfer of mRNAs and microRNAs is a novel mechanism of genetic exchange between cells," *Nat. Cell Biol.*, vol. 9, no. 6, pp. 654–9, Jun. 2007.
- [24] O. G. de Jong, M. C. Verhaar, Y. Chen, P. Vader, H. Gremmels, G. Posthuma, R. M. Schiffelers, M. Gucek, and B. W. M. van Balkom, "Cellular stress conditions are reflected in the protein and RNA content of endothelial cell-derived exosomes," *J. Extracell. Vesicles*, vol. 1, no. 0, pp. 1–12, 2012.
- [25] X. Yu, S. L. Harris, and A. J. Levine, "The regulation of exosome secretion: A novel function of the p53 protein," *Cancer Res.*, vol. 66, no. 9, pp. 4795–4801, 2006.
- [26] C. Théry, A. Clayton, S. Amigorena, and G. Raposo, "Isolation and Characterization of Exosomes from Cell Culture Supernatants," pp. 1–29, 2006.
- [27] J. Schageman, E. Zeringer, M. Li, T. Barta, K. Lea, J. Gu, S. Magdaleno, R. Setterquist, A. V. Vlassov, J. Schageman, et al., "The Complete Exosome Workflow Solution: From Isolation to Characterization of RNA Cargo," *Biomed Res. Int.*, vol. 2013, pp. 1–15, 2013.
- [28] B. J. Tauro, D. W. Greening, R. A. Mathias, H. Ji, S. Mathivanan, A. M. Scott, and R. J. Simpson, "Comparison of ultracentrifugation, density gradient separation, and immunoaffinity capture methods for isolating human colon cancer cell line LIM1863-derived exosomes," *Methods*, vol. 56, no. 2, pp. 293–304, 2012.
- [29] J. Webber and A. Clayton, "How pure are your vesicles?," *J. Extracell. Vesicles*, vol. 2, no. 7, pp. 1–6, 2013.
- [30] K. W. Witwer, E. I. Buzás, L. T. Bemis, A. Bora, C. Lässer, J. Lötvall, E. N. Nolte-'t Hoen, M. G. Piper, S. Sivaraman, J. Skog, C. Théry, M. H. Wauben, and F. Hochberg, "Standardization of sample collection, isolation and analysis methods in extracellular vesicle research," *J. Extracell. vesicles*, vol. 2, pp. 1–25, 2013.
- [31] E. Willms, H. J. Johansson, I. Mäger, Y. Lee, K. E. M. Blomberg, M. Sadik, A. Alaarg, C. I. E. Smith, J. Lehtiö, S. El Andaloussi, M. J. A. Wood, and P. Vader, "Cells release subpopulations of exosomes with distinct molecular and biological properties," *Sci. Rep.*, vol. 6, no. February, p. 22519, 2016.
- [32] J. Van Deun, P. Mestdagh, R. Sormunen, V. Cocquyt, K. Vermaelen, J. Vandesompele, M. Bracke, O. De Wever, et al., "The impact of disparate isolation methods for extra-cellular vesicles on downstream RNA profiling," *J. Extracell. Vesicles*, vol. 3, pp. 1–14, 2014.
- [33] R. A. Dragovic, C. Gardiner, A. S. Brooks, D. S. Tannetta, D. J. P. Ferguson, P. Hole, B. Carr, C. W. G. Redman, A. L. Harris, et al., "Sizing and phenotyping of cellular vesicles using Nanoparticle Tracking Analysis," *Nanomedicine Nanotechnology, Biol. Med.*, vol. 7, no. 6, pp. 780–788, 2011.

-
- [34] C. Gardiner, Y. J. Ferreira, R. a Dragovic, C. W. G. Redman, and I. L. Sargent, "Extracellular vesicle sizing and enumeration by nanoparticle tracking analysis," *J. Extracell. vesicles*, vol. 2, no. 1, pp. 1–11, 2013.
- [35] R. Nieuwland, R. Berckmans, R. Rotteveel-Eijkman, K. Maquelin, K. Roozendaal, P. Jansen, K. ten Have, L. Eijnsman, C. Hack, and A. Sturk, "Cell-Derived Microparticles Generated in Patients During Cardiopulmonary Bypass Are Highly Procoagulant," *Circulation*, vol. 96, no. 10, pp. 3534–3541, 1997.
- [36] S. Robert, R. Lacroix, P. Poncelet, K. Harhour, T. Bouriche, C. Judicone, J. Wischhusen, L. Arnaud, and F. Dignat-George, "High-sensitivity flow cytometry provides access to standardized measurement of small-size microparticles-brief report," *Arterioscler. Thromb. Vasc. Biol.*, vol. 32, no. 4, pp. 1054–1058, 2012.
- [37] V. Pospichalova, J. Svoboda, Z. Dave, A. Kotrbova, K. Kaiser, D. Klemova, L. Ilkovics, A. Hampl, I. Crha, E. Jandakova, et al., "Simplified protocol for flow cytometry analysis of fluorescently labeled exosomes and microvesicles using dedicated flow cytometer.," *J. Extracell. vesicles*, vol. 4, p. 25530, 2015.
- [38] E. J. van der Vlist, E. N. M. Nolte-t Hoen, W. Stoorvogel, G. J. a Arkesteijn, and M. H. M. Wauben, "Fluorescent labeling of nano-sized vesicles released by cells and subsequent quantitative and qualitative analysis by high-resolution flow cytometry.," *Nat. Protoc.*, vol. 7, no. 7, pp. 1311–26, 2012.
- [39] H. C. Anderson, "Vesicles associated with calcification in the matrix of epiphyseal cartilage.," *J. Cell Biol.*, vol. 41, no. 1, pp. 59–72, 1969.
- [40] N. Crawford, "The Presence of Contractile Proteins in Platelet Microparticles Isolated from Human and Animal Platelet-free Plasma," *Br. J. Haematol.*, vol. 21, no. 1, pp. 53–69, Jul. 1971.
- [41] H. F. Dvorak, S. C. Quay, N. S. Orenstein, a M. Dvorak, P. Hahn, a M. Bitzer, and a C. Carvalho, "Tumor shedding and coagulation.," *Science*, vol. 212, no. 4497, pp. 923–4, 1981.
- [42] B. T. Pan and R. M. Johnstone, "Fate of the transferrin receptor during maturation of sheep reticulocytes in vitro: Selective externalization of the receptor," *Cell*, vol. 33, no. 3, pp. 967–978, 1983.
- [43] R. M. Johnstone, M. Adam, J. R. Hammond, L. Orr, and C. Turbide, "Vesicle formation during reticulocyte maturation. Association of plasma membrane activities with released vesicles (exosomes).," *J. Biol. Chem.*, vol. 262, no. 19, pp. 9412–9420, 1987.
- [44] G. Raposo, H. W. Nijman, W. Stoorvogel, R. Liejendekker, C. V Harding, C. J. Melief, and H. J. Geuze, "B lymphocytes secrete antigen-presenting vesicles.," *J. Exp. Med.*, vol. 183, no. 3, pp. 1161–72, 1996.
- [45] L. Zitvogel, A. Regnault, A. Lozier, J. Wolfers, C. Flament, D. Tenza, P. Ricciardi-Castagnoli, G. Raposo, and S. Amigorena, "Eradication of established murine tumors using a novel cell-free vaccine: dendritic cell-derived exosomes.," *Nat. Med.*, vol. 4, no. 5, pp. 594–600, 1998.
- [46] T. Tian, Y. L. Zhu, Y. Y. Zhou, G. F. Liang, Y. Y. Wang, F. H. Hu, and Z. D. Xiao, "Exosome uptake through clathrin-mediated endocytosis and macropinocytosis and mediating miR-21 delivery," *J. Biol. Chem.*, vol. 289, no. 32, pp. 22258–22267, 2014.
- [47] K. J. Svensson, H. C. Christianson, A. Wittrup, E. Bourseau-Guilmain, E. Lindqvist, L. M. Svensson, M. Mörgelin, and M. Belting, "Exosome uptake depends on ERK1/2-heat shock protein 27 signaling and lipid raft-mediated endocytosis negatively regulated by caveolin-1," *J. Biol. Chem.*, vol. 288, no. 24, pp. 17713–17724, 2013.
- [48] K. J. McKelvey, K. L. Powell, A. W. Ashton, J. M. Morris, and S. a. McCracken, "Exosomes: Mechanisms of Uptake," *J. Circ. Biomarkers*, vol. 4, no. 7, p. 1, 2015.
- [49] L. A. Mulcahy, R. C. Pink, and D. R. F. Carter, "Routes and mechanisms of extracellular vesicle uptake," *J. Extracell. vesicles*, vol. 3, pp. 1–14, 2014.
- [50] E. N. M. N.- Hoen, S. I. Buschow, S. M. Anderton, W. Stoorvogel, H. Marca, and M. Wauben, "Activated T cells recruit exosomes secreted by dendritic cells via LFA-1," *Cell*, vol. 113, no. 9, pp. 1977–1981, 2009.

-
- [51] C. Admyre, B. Bohle, S. M. Johansson, M. Focke-Tejkl, R. Valenta, A. Scheynius, and S. Gabrielsson, "B cell-derived exosomes can present allergen peptides and activate allergen-specific T cells to proliferate and produce TH2-like cytokines," *J. Allergy Clin. Immunol.*, vol. 120, no. 6, pp. 1418–1424, 2007.
- [52] H. G. Lamparski, A. Metha-Damani, J. Y. Yao, S. Patel, D. H. Hsu, C. Ruegg, and J. B. Le Pecq, "Production and characterization of clinical grade exosomes derived from dendritic cells," *J. Immunol. Methods*, vol. 270, no. 2, pp. 211–226, 2002.
- [53] D.-H. Hsu, P. Paz, G. Villaflor, A. Rivas, A. Mehta-Damani, E. Angevin, L. Zitvogel, and J.-B. Le Pecq, "Exosomes as a tumor vaccine: enhancing potency through direct loading of antigenic peptides.," *J. Immunother.*, vol. 26, no. 5, pp. 440–50.
- [54] C. Théry, L. Duban, E. Segura, P. Véron, O. Lantz, and S. Amigorena, "Indirect activation of naïve CD4+ T cells by dendritic cell-derived exosomes.," *Nat. Immunol.*, vol. 3, no. 12, pp. 1156–1162, 2002.
- [55] M. Kovar, O. Boyman, X. Shen, I. Hwang, R. Kohler, and J. Sprent, "Direct stimulation of T cells by membrane vesicles from antigen-presenting cells," *Proc Natl Acad Sci U S A*, vol. 103, no. 31, pp. 11671–11676, 2006.
- [56] A. Montecalvo, W. J. Shufesky, D. B. Stolz, M. G. Sullivan, Z. Wang, S. J. Divito, G. D. Papworth, S. C. Watkins, P. D. Robbins, A. T. Larregina, and A. E. Morelli, "Exosomes as a short-range mechanism to spread alloantigen between dendritic cells during T cell allorecognition.," *J. Immunol.*, vol. 180, pp. 3081–3090, 2008.
- [57] D. Feng, W. L. Zhao, Y. Y. Ye, X. C. Bai, R. Q. Liu, L. F. Chang, Q. Zhou, and S. F. Sui, "Cellular internalization of exosomes occurs through phagocytosis," *Traffic*, vol. 11, no. 5, pp. 675–687, 2010.
- [58] D. Fitzner, M. Schnaars, D. van Rossum, G. Krishnamoorthy, P. Dibaj, M. Bakhti, T. Regen, U.-K. Hanisch, and M. Simons, "Selective transfer of exosomes from oligodendrocytes to microglia by macropinocytosis.," *J. Cell Sci.*, vol. 124, no. Pt 3, pp. 447–458, 2011.
- [59] L. M. Wakim and M. J. Bevan, "Cross-dressed dendritic cells drive memory CD8+ T-cell activation after viral infection," *Nature*, vol. 471, no. 7340, pp. 629–632, 2011.
- [60] Q. Liu, D. M. Rojas-canales, S. J. Divito, W. J. Shufesky, D. B. Stolz, G. Erdos, M. L. G. Sullivan, G. A. Gibson, S. C. Watkins, A. T. Larregina, and A. E. Morelli, "Donor dendritic cell - derived exosomes promote allograft-targeting immune response," vol. 126, no. 8, pp. 1–16, 2016.
- [61] F. André, N. E. C. Scharz, N. Chaput, C. Flament, G. Raposo, S. Amigorena, E. Angevin, and L. Zitvogel, "Tumor-derived exosomes: A new source of tumor rejection antigens," *Vaccine*, vol. 20, no. SUPPL. 4, pp. 28–31, 2002.
- [62] A. Sobo-Vujanovic, S. Munich, and N. L. Vujanovic, "Dendritic-cell exosomes cross-present Toll-like receptor-ligands and activate bystander dendritic cells," *Cell. Immunol.*, vol. 289, no. 1–2, pp. 119–127, 2014.
- [63] A. Fleming, G. Sampey, M. C. Chung, C. Bailey, M. L. van Hoek, F. Kashanchi, and R. M. Hakami, "The carrying pigeons of the cell: exosomes and their role in infectious diseases caused by human pathogens," *Pathog. Dis.*, vol. 71, no. 2, pp. 109–120, 2014.
- [64] S. J. Gould, A. M. Booth, and J. E. K. Hildreth, "The Trojan exosome hypothesis.," *Proc. Natl. Acad. Sci. U. S. A.*, vol. 100, no. 19, pp. 10592–7, Sep. 2003.
- [65] D. D. Taylor, C. Gerçel-Taylor, K. S. Lyons, J. Stanson, and T. L. Whiteside, "T-cell apoptosis and suppression of T-cell receptor/CD3-zeta by Fas ligand-containing membrane vesicles shed from ovarian tumors.," *Clin. Cancer Res.*, vol. 9, no. 14, pp. 5113–9, Nov. 2003.
- [66] A. J. Abusamra, Z. Zhong, X. Zheng, M. Li, T. E. Ichim, J. L. Chin, and W.-P. Min, "Tumor exosomes expressing Fas ligand mediate CD8+ T-cell apoptosis.," *Blood Cells. Mol. Dis.*, vol. 35, no. 2, pp. 169–73.
- [67] R. Alonso, C. Mazzeo, I. Mérida, and M. Izquierdo, "A new role of diacylglycerol kinase alpha on the secretion of lethal exosomes bearing Fas ligand during activation-induced cell death of T lymphocytes.," *Biochimie*, vol. 89, no. 2, pp. 213–21, Feb. 2007.

-
- [68] L. Frängsmyr, V. Baranov, O. Nagaeva, U. Stendahl, L. Kjellberg, and L. Mincheva-Nilsson, "Cytoplasmic microvesicular form of Fas ligand in human early placenta: Switching the tissue immune privilege hypothesis from cellular to vesicular level," *Mol. Hum. Reprod.*, vol. 11, no. 1, pp. 35–41, 2005.
- [69] L. Mincheva-Nilsson, O. Nagaeva, T. Chen, U. Stendahl, J. Antsiferova, I. Mogren, J. Hernestal, and V. Baranov, "Placenta-Derived Soluble MHC Class I Chain-Related Molecules Down-Regulate NKG2D Receptor on Peripheral Blood Mononuclear Cells during Human Pregnancy: A Possible Novel Immune Escape Mechanism for Fetal Survival," *J. Immunol.*, vol. 176, no. 6, pp. 3585–3592, 2006.
- [70] L. A. Burnett and R. A. Nowak, "Exosomes mediate embryo and maternal interactions at implantation and during pregnancy," *Front. in Bioscience*, vol. 8, pp. 79–96, 2016.
- [71] F. R. Balkwill, M. Capasso, and T. Hagemann, "The tumor microenvironment at a glance," *J. Cell Sci.*, vol. 125, no. 23, pp. 5591–5596, 2012.
- [72] D. Quail and J. Joyce, "Microenvironmental regulation of tumor progression and metastasis," *Nat. Med.*, vol. 19, no. 11, pp. 1423–1437, 2013.
- [73] C. Grange, M. Tapparo, F. Collino, L. Vitillo, C. Damasco, M. C. Deregibus, C. Tetta, B. Bussolati, and G. Camussi, "Microvesicles released from human renal cancer stem cells stimulate angiogenesis and formation of lung premetastatic niche," *Cancer Res.*, vol. 71, no. 15, pp. 5346–5356, 2011.
- [74] and F. H. S. Asfar S. Azmi¹, Bin Bao, "NIH Public Access," vol. 32, no. 0, pp. 1–33, 2014.
- [75] D. Di Vizio, M. Morello, A. C. Dudley, P. W. Schow, R. M. Adam, S. Morley, D. Mulholland, M. Rotinen, et al., "Large oncosomes in human prostate cancer tissues and in the circulation of mice with metastatic disease," *Am. J. Pathol.*, vol. 181, no. 5, pp. 1573–1584, 2012.
- [76] S. Rana, K. Malinowska, and M. Zöller, "Exosomal tumor microRNA modulates premetastatic organ cells.," *Neoplasia*, vol. 15, no. 3, pp. 281–95, 2013.
- [77] T. E. Ichim, Z. Zhong, S. Kaushal, X. Zheng, X. Ren, X. Hao, J. a Joyce, H. H. Hanley, N. H. Riordan, J. Koropatnick, V. Bogin, B. R. Minev, W.-P. Min, and R. H. Tullis, "Exosomes as a tumor immune escape mechanism: possible therapeutic implications.," *J. Transl. Med.*, vol. 6, p. 37, 2008.
- [78] V. Huber, P. Filipazzi, M. Iero, S. Fais, and L. Rivoltini, "More insights into the immunosuppressive potential of tumor exosomes.," *J. Transl. Med.*, vol. 6, p. 63, 2008.
- [79] S. Khan, J. M. S. Jutzy, J. R. Aspe, D. W. McGregor, J. W. Neidigh, and N. R. Wall, "Survivin is released from cancer cells via exosomes," *Apoptosis*, vol. 16, no. 1, pp. 1–12, 2011.
- [80] A. Lisco, C. Vanpouille, and L. Margolis, "War and Peace between Microbes: HIV-1 Interactions with Coinfecting Viruses," *Cell Host Microbe*, vol. 6, no. 5, pp. 403–408, 2009.
- [81] T. Wurdinger, N. N. Gatson, L. Balaj, B. Kaur, X. O. Breakefield, and D. M. Pegtel, "Extracellular vesicles and their convergence with viral pathways.," *Adv. Virol.*, vol. 2012, no. 1, ID 767694, Jan. 2012.
- [82] E. Nolte-’t Hoen, T. Cremer, R. C. Gallo, and L. B. Margolis, "Extracellular vesicles and viruses: Are they close relatives?," *Proc. Natl. Acad. Sci.*, vol. 113, no. 33, p. 201605146, 2016.
- [83] F. Properzi, M. Logozzi, and S. Fais, "Exosomes: the future of biomarkers in medicine.," *Biomark. Med.*, vol. 7, no. 5, pp. 769–78, 2013.
- [84] J. Lin, J. Li, B. Huang, J. Liu, X. Chen, X.-M. Chen, Y.-M. Xu, L.-F. Huang, and X.-Z. Wang, "Exosomes: novel biomarkers for clinical diagnosis.," *ScientificWorldJournal.*, vol. 2015, p. 657086, 2015.
- [85] L. Belov, K. J. Matic, S. Hallal, O. G. Best, S. P. Mulligan, and R. I. Christopherson, "Extensive surface protein profiles of extracellular vesicles from cancer cells may provide diagnostic signatures from blood samples.," *J. Extracell. vesicles*, vol. 5, no. 17, p. 25355, 2016.
- [86] T. Lener, M. Gioma, L. Aigner, V. Börger, E. Buzas, G. Camussi, N. Chaput, D. Chatterjee, F. A. Court, H. A. del Portillo, L. O’Driscoll, S. Fais, J. M. Falcon-Perez, U. Felderhoff-Mueser, L. Fraile, Y. S. Ghos, et al., "Applying extracellular vesicles based therapeutics in clinical trials - an ISEV position paper," *J. Extracell. Vesicles*, vol. 4, no. January 2016, pp. 1–31, 2015.

-
- [87] B. György, M. E. Hung, X. O. Breakefield, and J. N. Leonard, "Therapeutic applications of extracellular vesicles: clinical promise and open questions.," *Annu. Rev. Pharmacol. Toxicol.*, vol. 55, pp. 439–64, 2015.
- [88] Z. E. Suntres, M. G. Smith, F. Momen-heravi, J. Hu, X. Zhang, Y. Wu, H. Zhu, J. Wang, J. Zhou, and W. P. Kuo, "Therapeutic Uses of Exosomes," *Exosomes Microvesicles*, vol. 1, pp. 1–8, 2013.
- [89] F. Arslan, R. C. Lai, M. B. Smeets, L. Akeroyd, A. Choo, E. N. E. Aguur, L. Timmers, H. V. van Rijen, P. A. Doevendans, G. Pasterkamp, S. K. Lim, and D. P. de Kleijn, "Mesenchymal stem cell-derived exosomes increase ATP levels, decrease oxidative stress and activate PI3K/Akt pathway to enhance myocardial viability and prevent adverse remodeling after myocardial ischemia/reperfusion injury," *Stem Cell Res.*, vol. 10, no. 3, pp. 301–312, 2013.
- [90] H. Xin, Y. Li, B. Buller, M. Katakowski, Y. Zhang, X. Wang, X. Shang, Z. Zhang, and M. Chopp, "Exosome-Mediated Transfer of miR-133b from Multipotent Mesenchymal Stromal Cells to Neural Cells Contributes to Neurite Outgrowth," ... *Cells*, vol. 30, no. 7, pp. 1556–1564, 2012.
- [91] M. E. Gaillard, D. Bottero, A. Errea, M. Ormazábal, M. E. Zurita, G. Moreno, M. Rumbo, C. Castuma, E. Bartel, et al., "Acellular pertussis vaccine based on outer membrane vesicles capable of conferring both long-lasting immunity and protection against different strain genotypes," *Vaccine*, vol. 32, no. 8, pp. 931–937, 2014.
- [92] M. Ormazábal, E. Bartel, M. E. Gaillard, D. Bottero, A. Errea, M. E. Zurita, G. Moreno, M. Rumbo, C. Castuma, D. Flores, M. J. Martín, and D. Hozbor, "Characterization of the key antigenic components of pertussis vaccine based on outer membrane vesicles," *Vaccine*, vol. 32, no. 46, pp. 6084–6090, 2014.
- [93] G. Mignot, S. Roux, C. Théry, E. Ségura, and L. Zitvogel, "Prospects for exosomes in immunotherapy of cancer," *J. Cell. Mol. Med.*, vol. 10, no. 2, pp. 376–388, 2006.
- [94] C. Beauvillain, M. O. Juste, S. Dion, J. Pierre, and I. Dimier-Poisson, "Exosomes are an effective vaccine against congenital toxoplasmosis in mice," *Vaccine*, vol. 27, no. 11, pp. 1750–1757, 2009.
- [95] J. Colino and C. M. Snapper, "Exosomes from bone marrow dendritic cells pulsed with diphtheria toxoid preferentially induce type 1 antigen-specific IgG responses in naive recipients in the absence of free antigen.," *J. Immunol.*, vol. 177, no. 6, pp. 3757–62, Sep. 2006.
- [96] A. Delcayre, A. Estelles, J. Sperinde, T. Roulon, P. Paz, B. Aguilar, J. Villanueva, S. Khine, and J. B. Le Pecq, "Exosome Display technology: Applications to the development of new diagnostics and therapeutics," *Blood Cells, Mol. Dis.*, vol. 35, no. 2, pp. 158–168, 2005.
- [97] Y. T. Sato, K. Umezaki, S. Sawada, S.-A. Mukai, Y. Sasaki, N. Harada, H. Shiku, and K. Akiyoshi, "Engineering hybrid exosomes by membrane fusion with liposomes.," *Sci. Rep.*, vol. 6, no. February, p. 21933, 2016.
- [98] R. B. Rountree, S. J. Mandl, J. M. Nachtwey, K. Dalpozzo, L. Do, J. R. Lombardo, P. L. Schoonmaker, K. Brinkmann, U. Dirmeier, R. Laus, and A. Delcayre, "Exosome targeting of tumor antigens expressed by cancer vaccines can improve antigen immunogenicity and therapeutic efficacy," *Cancer Res.*, vol. 71, no. 15, pp. 5235–5244, 2011.
- [99] R. Ruiss, S. Jochum, R. Mocikat, W. Hammerschmidt, and R. Zeidler, "EBV-gp350 confers B-cell tropism to tailored exosomes and is a neo-antigen in normal and malignant B cells--a new option for the treatment of B-CLL.," *PLoS One*, vol. 6, no. 10, p. e25294, Jan. 2011.
- [100] M. a Morse, J. Garst, T. Osada, S. Khan, A. Hobeika, T. M. Clay, N. Valente, R. Shreeniwas, M. A. Sutton, A. Delcayre, D.-H. Hsu, J.-B. Le Pecq, and H. K. Lyerly, "A phase I study of dexosome immunotherapy in patients with advanced non-small cell lung cancer.," *J. Transl. Med.*, vol. 3, no. 1, p. 9, 2005.
- [101] B. Escudier, T. Dorval, N. Chaput, F. André, M.-P. Caby, S. Novault, C. Flament, C. Leboulaire, C. Borg, et al., "Vaccination of metastatic melanoma patients with autologous dendritic cell (DC) derived-exosomes: results of the first phase I clinical trial.," *J. Transl. Med.*, vol. 3, no. 1, p. 10, 2005.

-
- [102] S. Dai, D. Wei, Z. Wu, X. Zhou, X. Wei, H. Huang, and G. Li, "Phase I clinical trial of autologous ascites-derived exosomes combined with GM-CSF for colorectal cancer.," *Mol. Ther.*, vol. 16, no. 4, pp. 782–790, 2008.
- [103] D. Sun, X. Zhuang, X. Xiang, Y. Liu, S. Zhang, C. Liu, S. Barnes, W. Grizzle, D. Miller, and H.-G. Zhang, "A novel nanoparticle drug delivery system: the anti-inflammatory activity of curcumin is enhanced when encapsulated in exosomes.," *Mol. Ther.*, vol. 18, no. 9, pp. 1606–1614, 2010.
- [104] B. Besse, M. Charrier, V. Lapierre, E. Dansin, O. Lantz, D. Planchard, T. Le Chevalier, A. Livartoski, F. Barlesi, et al., "Dendritic cell-derived exosomes as maintenance immunotherapy after first line chemotherapy in NSCLC.," *Oncoimmunology*, vol. 5, no. 4, p. e1071008, 2016.
- [105] N. Chiorazzi, K. R. Rai, and M. Ferrarini, "Chronic lymphocytic leukemia.," *N. Engl. J. Med.*, vol. 352, no. 8, pp. 804–15, Feb. 2005.
- [106] S. Zhang and T. J. Kipps, "The pathogenesis of chronic lymphocytic leukemia.," *Annu. Rev. Pathol.*, vol. 9, pp. 103–18, 2014.
- [107] G. Gaidano, R. Foà, and R. Dalla-favera, "Review series Molecular pathogenesis of chronic lymphocytic leukemia.," vol. 122, no. 10, 2012.
- [108] H. Ghamlouch, H. Ouled-Haddou, G. Damaj, B. Royer, B. Gubler, and J. P. Marolleau, "A Combination of Cytokines Rescues Highly Purified Leukemic CLL B-Cells from Spontaneous Apoptosis In Vitro.," *PLoS One*, vol. 8, no. 3, pp. 1–9, 2013.
- [109] J. A. Burger, P. Ghia, A. Rosenwald, and F. Caligaris-Cappio, "The microenvironment in mature B-cell malignancies: a target for new treatment strategies.," *Blood*, vol. 114, no. 16, pp. 3367–75, Oct. 2009.
- [110] M. Seifert, L. Sellmann, J. Bloehdorn, F. Wein, S. Stilgenbauer, J. Dürig, and R. Küppers, "Cellular origin and pathophysiology of chronic lymphocytic leukemia.," *J. Exp. Med.*, vol. 209, no. 12, pp. 2183–98, Nov. 2012.
- [111] R. García-Muñoz, V. R. Galiacho, and L. Llorente, "Immunological aspects in chronic lymphocytic leukemia development.," *Ann. Hematol.*, vol. 91, no. 7, pp. 981–996, 2012.
- [112] R. Damle, "Ig V gene mutation status and CD38 expression as novel prognostic indicators in chronic lymphocytic leukemia.," *Blood*, vol. 94, no. 6, pp. 1840 – 1847, 1999.
- [113] H. Dohner, "Genomic aberrations and survival in chronic lymphocytic leukemia.," *N. Engl. J. Med.*, vol. 343, pp. 1910–1916, 2000.
- [114] N. Caporaso, L. Goldin, C. Plass, G. Calin, G. Marti, S. Bauer, E. Raveche, M. Lou McMaster, D. Ng, O. Landgren, and S. Slager, "Chronic lymphocytic leukaemia genetics overview.," *Br. J. Haematol.*, vol. 139, no. 5, pp. 630–4, Dec. 2007.
- [115] S. Stilgenbauer, A. Schnaiter, P. Paschka, T. Zenz, M. Rossi, K. Döhner, A. Bühler, S. Böttcher, M. Ritgen, et al., "Gene Mutations and Treatment Outcome in Chronic Lymphocytic Leukemia.," *Blood*, vol. 123, no. 21, pp. 3247–3255, 2014.
- [116] M. Hallek, "Chronic lymphocytic leukemia: 2015 Update on diagnosis, risk stratification, and treatment.," *Am. J. Hematol.*, vol. 90, no. 5, pp. 446 – 60, 2015.
- [117] I. Hus and J. Roliński, "Current concepts in diagnosis and treatment of chronic lymphocytic leukemia.," *Contemp. Oncol. (Poznań, Poland)*, vol. 19, no. 5, pp. 361–7, 2015.
- [118] a D. Hamblin and T. J. Hamblin, "The immunodeficiency of chronic lymphocytic leukaemia.," *Br. Med. Bull.*, vol. 87, pp. 49–62, Jan. 2008.
- [119] A. Nosari, "Infectious complications in chronic lymphocytic leukemia.," *Mediterr. J. Hematol. Infect. Dis.*, vol. 4, no. 1, 2012.
- [120] S. A. Parikh, J. F. Leis, K. G. Chaffee, T. G. Call, C. A. Hanson, W. Ding, A. A. Chanan-Khan, D. Bowen, M. Conte, et al., "Hypogammaglobulinemia in newly diagnosed chronic lymphocytic leukemia: Natural history, clinical correlates, and outcomes.," *Cancer*, vol. 121, no. 17, pp. 2883–91, Sep. 2015.
- [121] M. Schlesinger, I. Broman, and G. Lugassy, "The complement system is defective in chronic lymphatic leukemia patients and in their healthy relatives.," *Leukemia*, vol. 10, no. 9, pp. 1509–13, Sep. 1996.

-
- [122] M. E. Heath and B. D. Cheson, "Defective complement activity in chronic lymphocytic leukemia," *Am. J. Hematol.*, vol. 19, no. 1, pp. 63–73, May 1985.
- [123] L. Fayad, M. J. Keating, J. M. Reuben, S. O'Brien, B. N. Lee, S. Lerner, and R. Kurzrock, "Interleukin-6 and interleukin-10 levels in chronic lymphocytic leukemia: correlation with phenotypic characteristics and outcome," *Blood*, vol. 97, no. 1, pp. 256–263, 2001.
- [124] M. Lotz, E. Ranheim, and T. J. Kipps, "Transforming growth factor beta as endogenous growth inhibitor of chronic lymphocytic leukemia B cells," *J. Exp. Med.*, vol. 179, no. 3, pp. 999–1004, Mar. 1994.
- [125] K. Kato, M. J. Cantwell, S. Sharma, and T. J. Kipps, "Gene transfer of CD40-ligand induces autologous immune recognition of chronic lymphocytic leukemia B cells," *J. Clin. Invest.*, vol. 101, no. 5, pp. 1133–1141, 1998.
- [126] K. C. Howland, L. J. Ausubel, C. A. London, and A. K. Abbas, "The roles of CD28 and CD40 ligand in T cell activation and tolerance," *J. Immunol.*, vol. 164, no. 9, pp. 4465–70, 2000.
- [127] C. D. Gimmi, G. J. Freeman, J. G. Gribben, G. Gray, and L. M. Nadler, "Human T-cell clonal anergy is induced by antigen presentation in the absence of B7 costimulation," *Proc. Natl. Acad. Sci. U. S. A.*, vol. 90, no. 14, pp. 6586–6590, 1993.
- [128] J. Banchereau, D. Blanchard, J. P. Galizzi, C. Van Kooten, F. Rousset, S. Saeland, and P. Alto, "The CD40 antigen and its ligand," *Annu. Rev. Immunol.*, vol. 12, pp. 881–922, 1994.
- [129] S. Néron, P. J. Nadeau, A. Darveau, and J. F. Leblanc, "Tuning of CD40-CD154 interactions in human B-lymphocyte activation: A broad array of in vitro models for a complex in vivo situation," *Arch. Immunol. Ther. Exp. (Warsz.)*, vol. 59, no. 1, pp. 25–40, 2011.
- [130] I. S. Grewal and R. a Flavell, "CD40 and CD154 in cell-mediated immunity," *Annu. Rev. Immunol.*, vol. 16, pp. 111–35, Jan. 1998.
- [131] R. E. Callard, R. J. Armitage, W. C. Fanslow, M. K. Spriggs, R. Jo, W. C. Fanslow, and M. K. Spriggs, "CD40 ligand and its role in X-linked hyper-IgM syndrome," *Immunol. Today*, vol. 14, no. 11, pp. 559–564, 1993.
- [132] J. B. a G. Haanen and T. N. M. Schumacher, "Vaccine leads to memory loss," *Nat. Med.*, vol. 13, no. 3, pp. 248–250, 2007.
- [133] E. A. Ranheim and T. J. Kipps, "Activated T cells induce expression of B7/BB1 on normal or leukemic B cells through a CD40-dependent signal," *J. Exp. Med.*, vol. 177, no. 4, pp. 925–35, 1993.
- [134] L. E. Van den Hove, S. W. Van Gool, P. Vandenberghe, M. Bakkus, K. Thielemans, M. A. Boogaerts, and J. L. Ceuppens, "CD40 triggering of chronic lymphocytic leukemia B cells results in efficient alloantigen presentation and cytotoxic T lymphocyte induction by up-regulation of CD80 and CD86 costimulatory molecules," *Leukemia*, vol. 11, no. 4, pp. 572–580, 1997.
- [135] M. Cantwell, T. Hua, J. Pappas, and T. J. Kipps, "Acquired CD40-ligand deficiency in chronic lymphocytic leukemia," *Nat. Med.*, vol. 3, no. 9, pp. 984–989, 1997.
- [136] T. Melchardt, L. Weiss, R. Greil, and A. Egle, "Viral infections and their management in patients with chronic lymphocytic leukemia," *Leuk. Lymphoma*, vol. 54, no. 8, pp. 1602–13, 2013.
- [137] B. Pourgheysari, N. Khan, D. Best, R. Bruton, L. Nayak, and P. a H. Moss, "The cytomegalovirus-specific CD4+ T-cell response expands with age and markedly alters the CD4+ T-cell repertoire," *J. Virol.*, vol. 81, no. 14, pp. 7759–65, Jul. 2007.
- [138] S. Koch, A. Larbi, D. Ozcelik, R. Solana, C. Gouttefangeas, S. Attig, A. Wikby, J. Strindhall, C. Franceschi, and G. Pawelec, "Cytomegalovirus infection: a driving force in human T cell immunosenescence," *Ann. N. Y. Acad. Sci.*, vol. 1114, pp. 23–35, Oct. 2007.
- [139] W. J. M. Mackus, F. N. J. Frakking, A. Grummels, L. E. Gamadia, G. J. De Bree, D. Hamann, R. a W. Van Lier, and M. H. J. Van Oers, "Expansion of CMV-specific CD8+CD45RA+CD27- T cells in B-cell chronic lymphocytic leukemia," *Blood*, vol. 102, no. 3, pp. 1057–63, Aug. 2003.

-
- [140] B. Pourgheysari, R. Bruton, H. Parry, L. Billingham, C. Fegan, J. Murray, and P. Moss, "The number of cytomegalovirus-specific CD4+ T cells is markedly expanded in patients with B-cell chronic lymphocytic leukemia and determines the total CD4+ T-cell repertoire," *Blood*, vol. 116, no. 16, pp. 2968–74, Oct. 2010.
- [141] J. C. Riches and J. G. Gribben, "Hanging tough: CMV-specific CD81 T cells in CLL," *Blood*, vol. 123, no. 5, pp. 608–609, 2014.
- [142] G. D. Te Raa, M. F. Pascutti, J. J. García-Vallejo, E. Reinen, E. B. M. Remmerswaal, I. J. M. Ten Berge, R. A. W. Van Lier, E. Eldering, M. H. J. Van Oers, S. H. Tonino, and A. P. Kater, "CMV-specific CD8+ T-cell function is not impaired in chronic lymphocytic leukemia," *Blood*, vol. 123, no. 5, pp. 717–724, 2014.
- [143] I. Messaoudi, J. Lemaoult, J. A. Guevara-Patino, B. M. Metzner, and J. Nikolich-Zugich, "Age-related CD8 T cell clonal expansions constrict CD8 T cell repertoire and have the potential to impair immune defense," *J. Exp. Med.*, vol. 200, no. 10, pp. 1347–58, Nov. 2004.
- [144] N. Khan, A. Hislop, N. Gudgeon, M. Cobbold, R. Khanna, L. Nayak, A. B. Rickinson, and P. A. H. Moss, "Herpesvirus-specific CD8 T cell immunity in old age: cytomegalovirus impairs the response to a coresident EBV infection," *J. Immunol.*, vol. 173, no. 12, pp. 7481–9, Dec. 2004.
- [145] A. P. Kater, E. B. M. Remmerswaal, M. a Nolte, E. Eldering, M. H. J. van Oers, and R. a W. van Lier, "Autologous cytomegalovirus-specific T cells as effector cells in immunotherapy of B cell chronic lymphocytic leukaemia," *Br. J. Haematol.*, vol. 126, no. 4, pp. 512–6, Aug. 2004.
- [146] R. Mous, P. Savage, E. B. M. Remmerswaal, R. a W. van Lier, E. Eldering, and M. H. J. van Oers, "Redirection of CMV-specific CTL towards B-CLL via CD20-targeted HLA/CMV complexes," *Leuk. Off. J. Leuk. Soc. Am. Leuk. Res. Fund, U.K.*, vol. 20, no. 6, pp. 1096–102, Jun. 2006.
- [147] T. Zenz, J. G. Gribben, M. Hallek, H. Döhner, M. J. Keating, and S. Stilgenbauer, "Risk categories and refractory CLL in the era of chemoimmunotherapy," *Blood*, vol. 119, no. 18, pp. 4101–4107, 2012.
- [148] M. N. Richter, "Generalized Reticular Cell Sarcoma of Lymph Nodes Associated with Lymphatic Leukemia*," *Am. J. Pathol.*, vol. 4, no. 4, pp. 285–292.7, 1928.
- [149] A. M. Tsimberidou and M. J. Keating, "Richter syndrome: Biology, incidence, and therapeutic strategies," *Cancer*, vol. 103, no. 2, pp. 216–228, 2005.
- [150] S. D. Scott, "Rituximab: a new therapeutic monoclonal antibody for non-Hodgkin's lymphoma," *Cancer Pract.*, vol. 6, no. 3, pp. 195–7.
- [151] M. Hallek, "Signaling the end of chronic lymphocytic leukemia: new frontline treatment strategies," *Hematology Am. Soc. Hematol. Educ. Program*, vol. 2013, pp. 138–50, 2013.
- [152] R. J. Brentjens, I. Rivière, J. H. Park, M. L. Davila, X. Wang, J. Stefanski, C. Taylor, R. Yeh, S. Bartido, O. Borquez-Ojeda, et al., "Safety and persistence of adoptively transferred autologous CD19-targeted T cells in patients with relapsed or chemotherapy refractory B-cell leukemias," *Blood*, vol. 118, no. 18, pp. 4817–4828, 2011.
- [153] A. Mato and D. L. Porter, "A drive through cellular therapy for CLL in 2015: Allogeneic cell transplantation and CARs," *Blood*, vol. 126, no. 4, pp. 478–485, 2015.
- [154] N. Singh, N. V. Frey, S. A. Grupp, and S. L. Maude, "CAR T Cell Therapy in Acute Lymphoblastic Leukemia and Potential for Chronic Lymphocytic Leukemia," *Curr. Treat. Options Oncol.*, vol. 17, no. 6, 2016.
- [155] C. Porter, DL., Levine, B., Kalos, M., Bagg, A., and June, "Chimeric Antigen Receptor-Modified T Cells in Chronic Lymphoid Leukemia - NEJMoa1103849," *New Eng. J. Med.*, pp. 727–733, 2011.
- [156] J. N. Kochenderfer, M. E. Dudley, S. H. Kassim, R. P. T. Somerville, R. O. Carpenter, S. S. Maryalice, J. C. Yang, et al., "Chemotherapy-refractory diffuse large B-cell lymphoma and indolent B-cell malignancies can be effectively treated with autologous T cells expressing an anti-CD19 chimeric antigen receptor," *J. Clin. Oncol.*, vol. 33, no. 6, pp. 540–549, 2015.

-
- [157] A. P. Kater, M. H. J. Van Oers, and T. J. Kipps, "Review article Cellular immune therapy for chronic lymphocytic leukemia," *Blood*, vol. 110, no. 8, pp. 2811–2818, 2007.
- [158] E. Biagi, R. Rousseau, E. Yvon, M. Schwartz, G. Dotti, A. Foster, D. Havlik-Cooper, B. Grilley, A. Gee, K. Baker, G. Carrum, L. Rice, M. Andreeff, U. Popat, and M. Brenner, "Responses to human CD40 ligand/human interleukin-2 autologous cell vaccine in patients with B-cell chronic lymphocytic leukemia," *Clin. Cancer Res.*, vol. 11, no. 19 I, pp. 6916–6923, 2005.
- [159] D. Messmer and T. J. Kipps, "CD154 gene therapy for human B-cell malignancies," *Ann. N. Y. Acad. Sci.*, vol. 1062, pp. 51–60, Dec. 2005.
- [160] W. G. Wierda, M. J. Cantwell, S. J. Woods, L. Z. Rassenti, C. E. Prussak, and T. J. Kipps, "CD40-ligand (CD154) gene therapy for chronic lymphocytic leukemia," *Blood*, vol. 96, no. 9, pp. 2917–24, Nov. 2000.
- [161] P. Chu, D. Deforce, I. M. Pedersen, Y. Kim, S. Kitada, J. C. Reed, and T. J. Kipps, "Latent sensitivity to Fas-mediated apoptosis after CD40 ligation may explain activity of CD154 gene therapy in chronic lymphocytic leukemia," *Proc. Natl. Acad. Sci. U. S. A.*, vol. 99, no. 6, pp. 3854–9, 2002.
- [162] C. M. Wendtner, D. M. Kofler, C. Mayr, D. Bund, and M. Hallek, "The potential of gene transfer into primary B-CLL cells using recombinant virus vectors," *Leuk. Lymphoma*, vol. 45, no. 5, pp. 897–904, 2004.
- [163] K. a Tolba, W. J. Bowers, S. P. Hilchey, M. W. Halterman, D. F. Howard, E. Rita, H. J. Federoff, J. D. Rosenblatt, and R. E. Giuliano, "chronic lymphocytic leukemia Development of herpes simplex virus-1 amplicon – based immunotherapy for chronic lymphocytic leukemia," *Gene Ther.*, vol. 98, no. 2, pp. 287–295, 2011.
- [164] M. Bonamino, M. Serafini, G. D'Amico, G. Gaipa, E. Todisco, S. Bernasconi, J. Golay, A. Biondi, and M. Introna, "Functional transfer of CD40L gene in human B-cell precursor ALL blasts by second-generation SIN lentivectors," *Gene Ther.*, vol. 11, no. 1, pp. 85–93, 2004.
- [165] C. Mayr, D. M. Kofler, H. Büning, D. Bund, M. Hallek, and C. M. Wendtner, "Transduction of CLL cells by CD40 ligand enhances an antigen-specific immune recognition by autologous T cells," *Blood*, vol. 106, no. 9, pp. 3223–3226, 2005.
- [166] J. E. Castro, J. Melo-Cardenas, M. Urquiza, J. S. Barajas-Gamboa, R. S. Pakbaz, and T. J. Kipps, "Gene immunotherapy of chronic lymphocytic leukemia: a phase I study of intranodally injected adenovirus expressing a chimeric CD154 molecule," *Cancer Res.*, vol. 72, no. 12, pp. 2937–48, Jun. 2012.
- [167] F. L. Graham, J. Smiley, W. C. Russell, and R. Nairn, "Characteristics of a human cell line transformed by DNA from human adenovirus type 5," *J. Gen. Virol.*, vol. 36, no. 1, pp. 59–74, Jul. 1977.
- [168] H. J. Delecluse, T. Hilsendegen, D. Pich, R. Zeidler, and W. Hammerschmidt, "Propagation and recovery of intact, infectious Epstein-Barr virus from prokaryotic to human cells," *Proc. Natl. Acad. Sci. U. S. A.*, vol. 95, no. 14, pp. 8245–50, Jul. 1998.
- [169] B. Kempkes, D. Pich, R. Zeidler, and W. Hammerschmidt, "Immortalization of human primary B lymphocytes in vitro with DNA," *Proc. Natl. Acad. Sci. U. S. A.*, vol. 92, no. 13, pp. 5875–9, 1995.
- [170] A. Moosmann, N. Khan, M. Cobbold, C. Zentz, H.-J. Delecluse, G. Hollweck, A. D. Hislop, N. W. Blake, D. Croom-Carter, et al., "B cells immortalized by a mini-Epstein-Barr virus encoding a foreign antigen efficiently reactivate specific cytotoxic T cells," *Blood*, vol. 100, no. 5, pp. 1755–1764, 2002.
- [171] A. Moosmann, I. Bigalke, J. Tischer, L. Schirrmann, J. Kasten, S. Tippmer, M. Leeping, D. Prevalšek, G. Jaeger, G. Ledderose, J. Mautner, W. Hammerschmidt, D. J. Schendel, and H. J. Kolb, "Effective and long-term control of EBV PTLD after transfer of peptide-selected T cells," *Blood*, vol. 115, no. 14, pp. 2960–2970, 2010.
- [172] J. L. Schultze, S. Michalak, M. J. Seamon, G. Dranoff, K. Jung, J. Daley, J. C. Delgado, J. G. Gribben, and L. M. Nadler, "CD40-activated human B cells: an alternative source of highly efficient antigen presenting cells to generate autologous antigen-specific T cells for adoptive immunotherapy," *J. Clin. Invest.*, vol. 100, no. 11, pp. 2757–2765, 1997.

-
- [173] C. Hömig-Hölzel, C. Hojer, J. Rastelli, S. Casola, L. J. Strobl, W. Müller, L. Quintanilla-Martinez, A. Gewies, J. Ruland, K. Rajewsky, and U. Zimmer-Strobl, "Constitutive CD40 signaling in B cells selectively activates the noncanonical NF-kappaB pathway and promotes lymphomagenesis," *J. Exp. Med.*, vol. 205, no. 6, pp. 1317–1329, 2008.
- [174] B. P. Garrone, E. Neidhardt, E. Garcia, L. Galibert, C. Van Kooten, and J. Banchereau, "Fas Ligation Induces Apoptosis of CD40- activated Human B Lymphocytes," vol. 182, no. November, 1995.
- [175] D. A. Thorley-lawson and K. Geilinger, "Monoclonal antibodies against the major glycoprotein (gp350/220) of Epstein-Barr virus neutralize infectivity," *Cloning*, vol. 77, no. 9, pp. 5307–5311, 1980.
- [176] E. M. Sokal, K. Hoppenbrouwers, C. Vandermeulen, M. Moutschen, P. Léonard, A. Moreels, M. Haumont, A. Bollen, F. Smets, and M. Denis, "Recombinant gp350 vaccine for infectious mononucleosis: a phase 2, randomized, double-blind, placebo-controlled trial to evaluate the safety, immunogenicity, and efficacy of an Epstein-Barr virus vaccine in healthy young adults," *J. Infect. Dis.*, vol. 196, no. 12, pp. 1749–53, Dec. 2007.
- [177] K. Ridder, A. Sevko, J. Heide, M. Dams, A.-K. Rupp, J. Macas, J. Starmann, M. Tjwa, K. H. Plate, H. Sülthmann, P. Altevogt, V. Umansky, and S. Momma, "Extracellular vesicle-mediated transfer of functional RNA in the tumor microenvironment," *Oncoimmunology*, vol. 4, no. 6, p. e1008371, 2015.
- [178] A. Zomer, C. Maynard, F. J. Verweij, A. Kamermans, R. Schäfer, E. Beerling, R. M. Schiffelers, E. De Wit, J. Berenguer, et al., "In vivo imaging reveals extracellular vesicle-mediated phenocopying of metastatic behavior," *Cell*, vol. 161, no. 5, pp. 1046–1057, 2015.
- [179] A. Zomer, S. C. Steenbeek, C. Maynard, and J. van Rheenen, "Studying extracellular vesicle transfer by a Cre-loxP method," *Nat. Protoc.*, vol. 11, no. 1, pp. 87–101, 2016.
- [180] T. Mizuno and T. L. Rothstein, "B cell receptor (BCR) cross-talk: CD40 engagement enhances BCR-induced ERK activation," *J. Immunol.*, vol. 174, pp. 3369–3376, 2005.
- [181] S. M. Salti, E. M. Hammelev, J. L. Grewal, S. T. Reddy, S. J. Zemple, W. J. Grossman, M. H. Grayson, and J. W. Verbsky, "Granzyme B regulates antiviral CD8+ T cell responses," *J. Immunol.*, vol. 187, no. 12, pp. 6301–9, 2011.
- [182] R. Bichi, S. A. Shinton, E. S. Martin, A. Koval, G. A. Calin, R. Cesari, G. Russo, R. R. Hardy, and C. M. Croce, "Human chronic lymphocytic leukemia modeled in mouse by targeted TCL1 expression," *Proc. Natl. Acad. Sci. U. S. A.*, vol. 99, no. 10, pp. 6955–60, 2002.
- [183] Y. Pekarsky, N. Zanesi, R. I. Aqeilan, and C. M. Croce, "Animal models for chronic lymphocytic leukemia," *J. Cell. Biochem.*, vol. 100, no. 5, pp. 1109–1118, 2007.
- [184] G. Pérez-chacón, J. M. Zapata, I. De Investigaciones, B. Alberto, and C. Uam, "Mouse Models of Chronic Lymphocytic Leukemia," 2011.
- [185] A. Gámez-Valero, M. Monguió-Tortajada, L. Carreras-Planella, M. Franquesa, K. Beyer, and F. E. Borràs, "Size-Exclusion Chromatography-based isolation minimally alters Extracellular Vesicles' characteristics compared to precipitating agents," *Sci. Rep.*, vol. 6, no. September, p. 33641, 2016.
- [186] A. N. Böing, E. Van Der Pol, A. E. Grootemaat, F. a. Coumans, A. Sturk, and R. Nieuwland, "Single-step isolation of extracellular vesicles from plasma by size-exclusion chromatography," *Int. Meet. ISEV Rotterdam*, vol. 3, p. 118, 2014.
- [187] R. J. Lobb, M. Becker, S. W. Wen, C. S. F. Wong, A. P. Wiegman, A. Leimgruber, and A. Möller, "Optimized exosome isolation protocol for cell culture supernatant and human plasma," *J. Extracell. Vesicles*, vol. 1, no. 27031, pp. 1–11, 2015.
- [188] J. M. Gudbergsson, K. B. Johnsen, M. N. Skov, and M. Duroux, "Systematic review of factors influencing extracellular vesicle yield from cell cultures," *Cytotechnology*, 2015.
- [189] V. Filipe, A. Hawe, and W. Jiskoot, "Critical evaluation of nanoparticle tracking analysis (NTA) by NanoSight for the measurement of nanoparticles and protein aggregates," *Pharm. Res.*, vol. 27, no. 5, pp. 796–810, 2010.

-
- [190] I. S. Zeelenberg, M. Ostrowski, S. Krumeich, A. Bobrie, C. Jancic, A. Boissonnas, A. Delcayre, J. B. Le Pecq, B. Combadière, S. Amigorena, and C. Théry, "Targeting tumor antigens to secreted membrane vesicles in vivo induces efficient antitumor immune responses," *Cancer Res.*, vol. 68, no. 4, pp. 1228–1235, 2008.
- [191] M. A. Shokrgozar and F. Shokri, "Enumeration of hepatitis B surface antigen-specific B lymphocytes in responder and non-responder normal individuals vaccinated with recombinant hepatitis B surface antigen," *Immunology*, vol. 104, no. 1, pp. 75–79, 2001.
- [192] V. Younesi, F. G. Shirazi, A. Memarian, A. Amanzadeh, M. Jeddi-Tehrani, and F. Shokri, "Assessment of the effect of TLR7/8, TLR9 agonists and CD40 ligand on the transformation efficiency of Epstein-Barr virus in human B lymphocytes by limiting dilution assay," *Cytotechnology*, vol. 66, no. 1, pp. 95–105, 2014.
- [193] K. Ridder, S. Keller, M. Dams, A. K. Rupp, J. Schlaudraff, D. Del Turco, J. Star mann, J. Macas, D. Karpova, K. Devraj, et al., "Extracellular Vesicle-Mediated Transfer of Genetic Information between the Hematopoietic System and the Brain in Response to Inflammation," *PLoS Biol.*, vol. 12, no. 6, 2014.
- [194] M. Tkach and C. Théry, "Communication by Extracellular Vesicles: Where We Are and Where We Need to Go," *Cell*, vol. 164, no. 6, pp. 1226–1232, 2016.
- [195] T. Bunde, A. Kirchner, B. Hoffmeister, D. Habedank, R. Hetzer, G. Cherepnev, S. Proesch, P. Reinke, H.-D. Volk, H. Lehmkuhl, and F. Kern, "Protection from cytomegalovirus after transplantation is correlated with immediate early 1-specific CD8 T cells," *J. Exp. Med.*, vol. 201, no. 7, pp. 1031–6, 2005.
- [196] L. Gibson, S. Dooley, S. Trzmielina, M. Somasundaran, D. Fisher, M. G. Revello, and K. Luzuriaga, "Cytomegalovirus (CMV) IE1- and pp65-specific CD8+ T cell responses broaden over time after primary CMV infection in infants," *J. Infect. Dis.*, vol. 195, no. 12, pp. 1789–1798, 2007.
- [197] T. a M. Groothuis and J. Neefjes, "The many roads to cross-presentation.," *J. Exp. Med.*, vol. 202, no. 10, pp. 1313–8, 2005.
- [198] R. Ruiss, S. Jochum, G. Wanner, G. Reisbach, W. Hammerschmidt, and R. Zeidler, "A Virus-Like Particle-Based Epstein-Barr Virus Vaccine," *J. Virol.*, vol. 85, no. 24, pp. 13105–13113, 2011.
- [199] G. Simonetti, M. Teresa, S. Bertilaccio, P. Ghia, and U. Klein, "Perspectives Mouse models in the study of chronic lymphocytic leukemia pathogenesis and therapy," *Blood*, vol. 124, no. 7, pp. 1010–1019, 2014.
- [200] L. Watson, P. Wyld, and D. Catovsky, "Disease burden of chronic lymphocytic leukaemia within the European Union.," *Eur. J. Haematol.*, vol. 81, no. 4, pp. 253–8, Oct. 2008.

8 Abbreviations

AP	alkaline phosphatase	MHC	major histocompatibility complex
APC	antigen-presenting cell	mRNA	messenger RNA
APS	ammonium persulfate	MTT	3-(4, 5-dimethylthiazolyl-2)-2, 5-diphenyltetrazolium bromide
BFP	blue fluorescent protein	MVB	multi-vesicular body
bp	base pair	NK cell	natural killer cell
BSA	bovine serum albumine	NTA	nanoparticle tracking analysis
CD	cluster of differentiation	NTP	nucleoside triphosphate
CD40L	CD40 ligand	OD	optical density
cDNA	complementary DNA	PAGE	polyacrylamide gelelectrophoresis
CFSE	carboxyfluorescein succinimidyl ester	PBMCs	peripheral bloo mono-nuclear cells
CLL	chronic lymphocytic leukemia	PBS	phosphate buffered saline
CMV	Cytomegalovirus	PCR	polymerase chain reaction
CR	complete remission	PEI	polyethylenimine
CTL	cytotoxic T-lymphocyte	PFA	paraformaldehyde
DAPI	4',6-diamidino-2-phenylindole	RIPA	paraformaldehyde
DC	dendritic cell	RNA	ribonucleic acid
DMSO	Dimethyl sulfoxide	rpm	rounds per minute
DNA	deoxyribonucleic acid	RS	Richter syndrome
e.g.	for example (<i>exempli gratia</i>)	RT	room temperature
EBV	Epstein-Barr virus	SD	standard deviation
ELISA	enzyme-linked immunosorbent assay	SDS	sodium dodecyl sulfate
ELISPOT	enzyme-linked immunospot assay	SEC	size-exclusion chromatography
EV	extracellular vesicle	TCL-1	T cell leukemia-1
FACS	fluorescence-activated cell sorting	TEMED	tetramethylethylenediamine
FCS	fetal calf serum	TPA	tetradecanoylphorbol acetate
GAPDH	glyceraldehyde 3-phosphate dehydrogenase	VLP	virus-like particle
GFP	green fluorescent protein		
GM-CSF	granulocyte-macrophage colony-stimulating factor		
GRU	green raji unit		
HLA	human leukocyte antigen		
HRP	horseradish peroxidase		
HLA	human leukocyte antigen		
IFN	interferon		
IL	interleukin		
kDa	kilodalton		
LCL	lymphoblastoid cell line		

9 Presentations

Parts of this work were presented in international conferences and meetings:

- | | |
|--|---|
| September 16 th – 18 th , 2016
Cologne, Germany | Xth International Workshop of the German CLL Study Group
<u>Poster</u> : “Engineered extracellular vesicles carrying CD40L and herpesviral proteins redirect antiviral immune responses towards CLL cells: An immunotherapeutic approach” |
| May 3 rd – 7 th , 2016
Rotterdam, the Netherlands | 5th Annual Meeting of the International Society of Extracellular Vesicles (ISEV)
<u>Poster</u> : “Recombinant exosomes carrying CD40L and herpesviral proteins redirect antiviral immune responses towards malignant B-CLL cells: An immunotherapeutic approach” |
| November 19 th – 21 th , 2015
Munich, Germany | Joint Annual Meeting (German Society of Infectious Diseases & Germany Center for Infection Research)
<u>Poster</u> : “Novel neutralizing antibody with clinical potential against Epstein-Barr virus infections in the immunocompromised host” |
| April 23 rd – 26 th , 2015
Washington DC, USA | 4th Annual Meeting of the International Society of Extracellular Vesicles (ISEV)
<u>Talk</u> : “Recombinant exosomes for immunotherapy of chronic lymphocytic leukemia (CLL)” |
| June 22 nd – 27 th , 2014
Dresden, Germany | Summer School on Infection Research
<u>Poster</u> : “Recombinant exosomes for immunotherapy of chronic lymphocytic leukemia (CLL)” |

10 Danksagung

Eine wissenschaftliche Arbeit ist nie das Werk einer einzelnen Person. Deshalb möchte ich mich an dieser Stelle bei allen bedanken, die zum Gelingen meiner Dissertation beigetragen haben:

- **Prof. Dr. Reinhard Zeidler** für die Bereitstellung dieses Projekts, die wissenschaftliche Betreuung meiner Arbeit, die Unterstützung bei all meinen Vorhaben, sowie die vielen Ideen und Diskussionen, die mich immer weitergebracht haben und mir trotzdem viele Freiheiten ließen.
- **PD Dr. Josef Mautner** für die Übernahme der offiziellen Betreuung meiner Promotion an der Fakultät für Biologie, die stete Hilfsbereitschaft bei fachlichen Fragen und die Unterstützung meiner Arbeit als Mitglied meines Thesis Komitees.
- **Prof. Dr. Rainer Glaß** für die Bereitschaft als Zweitgutachter dieser Arbeit zu fungieren.

Außerdem ein großes Dankeschön an:

- **Prof. Dr. Wolfgang Hammerschmidt** und **Dr. Andreas Moosmann**, die immer eine offene Tür und ein offenes Ohr für wissenschaftliche Fragestellungen hatten und meine Arbeit durch ihre Ideen stets bereicherten.
- **Prof. Dr. Clemens Wendtner** für das Interesse an meiner Arbeit als Mitglied meines Thesis Komitees, sowie die Vermittlung von CLL Blutproben.
- Das **Münchner Leukämie Labor**, insbesondere Frau Dr. Frauke Bellos, für die Kooperationsbereitschaft und die Bereitstellung von CLL Blutproben.
- Allen **CLL Patienten**, die sich bereit erklärten, unsere Forschung durch ihre Blutspende zu unterstützen.
- **Manja Luckner** für die Herstellung der Elektronenmikroskopie Bilder.
- **Dunja Baatout** und **Dr. Lukas Frenzel** für die Kooperationsbereitschaft und die Durchführung der Mausexperimente.

Allen meinen **Laborkollegen und -kolleginnen** der Abteilung für Genvektoren, insbesondere aus Labor 205, ein riesiges Dankeschön für die angenehme und freundschaftliche Arbeitsatmosphäre, die vielen unterhaltsamen Gespräche und Ablenkungen von ernüchternden Experimenten, sowie die gemeinsamen Unternehmungen.

Mein besonderer Dank gilt: **Rosi-** für die Hilfe und Unterstützung bei den bürokratischen Dingen des Doktorandendaseins. **Judith-** für deine Hilfsbereitschaft in allen möglichen Bereichen, deinen Humor und die Verbreitung urbayrischer Vokabeln. **Corinna** und **Bettina** für die sehr gute Zusammenarbeit und gegenseitige Unterstützung, sowie euren unermüdlichen Einsatz für Zucht und Ordnung im Labor. **Dagi-** für deine Hilfe bei allen technischen Zellkultur- und EBV-bezogenen Fragen, sowie den Austausch literarischer Schmankerl. **Manuel-** für deine Begeisterungsfähigkeit in allen möglichen wissenschaftlichen Fragestellungen und das Überlassen diverser T-Zellklone und LCLs. **Paula-** für die vielen schönen Stunden außerhalb des Labors und den unerschöpflichen Vorrat motivierender polnischer Süßigkeiten und Spirituosen.

Zu guter Letzt möchte ich meiner **Familie** und meinen **Freunden** danken, die mich immer bedingungslos unterstützt und motiviert haben.

